NASA TR R-66

NATIONAL AERONAUTICS AND SPACE ADMINISTRATION

TECHNICAL REPORT
R-66

A STUDY OF THE ASYMMETRIC TRANSONIC FLOW PAST A SHARP LEADING EDGE

By HOWARD A. STINE, CLEO B. WAGONER,
and ALVIN L. LUGN, Jr.

1960

For sale by the Superintendent of Documents, U.S. Government Printing Office, Washington 25, D.C. Yearly subscription, $15; foreign, $19; single copy price varies according to size --------- Price 60 cents

TECHNICAL REPORT R-66

A STUDY OF THE ASYMMETRIC TRANSONIC FLOW PAST A SHARP LEADING EDGE

By HOWARD A. STINE, CLEO B. WAGONER, and ALVIN L. LUGN, Jr.

Ames Research Center
Moffett Field, Calif.

CONTENTS

TECHNICAL REPORT R-66

A STUDY OF THE ASYMMETRIC TRANSONIC FLOW PAST A SHARP LEADING EDGE

By Howard A. Stine, Cleo B. Wagoner, and Alvin L. Lugn, Jr.

SUMMARY

An experimental and theoretical study has been made of the two-dimensional transonic flow past a 12° wedge airfoil with lower surface inclined 13° to the air stream. The experimental portion of the study consists of surveys of the flow field about the leading edge in a closed throat tunnel near choking Mach number by means of an X-ray densitometer. From these surveys various features have been determined; namely, the location of the stagnation point, the location of the sonic line, the size of the separation bubble on the upper surface, and the value of the Mach number at the bubble edge. These features were relatively insensitive to changes in Reynolds number in the range from 1×10^6 to 3×10^6 based on chord.

The theoretical portion of the study consists of the calculation by relaxation methods of an unbounded, inviscid, two-dimensional flow about a portion of the same body at a free-stream Mach number of exactly unity. The calculations yield a separation bubble on the upper surface which has a shape shown to be compatible with known theoretical conditions for viscous attachment to the upper surface of the body.

Agreement between the theoretically calculated and the experimentally determined features of the flow was good in regions where the local Mach number was 2 or less. In regions of higher local Mach number the agreement was fair. The theoretically determined Mach number on the bubble edge was 2.80 whereas the experimentally determined value was 2.30. The theoretically determined length of the separation bubble was 1.54-percent chord whereas the experimentally determined length was about 5-percent chord. The theoretically determined location of the stagnation point was 0.16-percent chord from the leading edge whereas the experimentally determined location was at 0.56-percent chord. The experience gained in studying the flow suggests the possibility that the solution obtained is not unique and that another solution in better agreement with experiment might exist.

INTRODUCTION

The asymmetric transonic flow about a lifting airfoil with sharp leading edge may be characterized by the type of flow which exists on the upper surface. The various types of flow possible on the upper surface can best be described by first specifying an airfoil of fixed nose angle and angle of attack and then considering the flow configurations which develop as the Mach number is varied. First, at low subsonic speeds, the characteristic pattern is that of complete separation of the flow from the upper surface. This separated pattern persists with little change until at some high subsonic Mach number (the value of which depends on the nose angle and angle of attack) the flow abruptly changes to a second type. This second flow pattern is typified by a small separation bubble on the upper surface at the leading edge. The flow bounding this bubble is supersonic as a result of overexpansion about the edge and thus leads to an oblique shock wave when it turns to the direction of the surface at the downstream end of the separation bubble. The flow then follows the surface, and its further history is determined by the shape of this surface. This attached flow pattern persists until a supersonic value of the free-stream Mach number is reached (the value again depending on nose angle and angle of attack) where it gives way finally to the familiar all-supersonic flow with attached leading-edge bow wave.

Since the second type of flow configuration described above persists over a fairly wide range of Mach numbers, these attached flows are of practical interest because of their effect on the aerodynamic force and moment parameters. They are also of interest theoretically because they are examples of transonic flows which yield to theoretical attack. An experimental and theoretical study of such a flow is the primary concern of the present paper.

The transition from the completely separated to the attached flow with bubble configuration was observed in the wind-tunnel tests described in reference 1. The flow bounding the bubble at the leading edge was clearly supersonic as evidenced by the attendant oblique shock wave. Qualitatively similar flows have also been observed buried in the supersonic flows past blunt plates and axisymmetric bodies of revolution (refs. 2 and 3) and in subsonic flow past sharp airfoils and a flat-faced cylinder (ref. 4).

A detailed quantitative picture of the flow structure in the vicinity of the leading edge is, however, lacking. The data presented in references 1, 2, 3, and 4 are limited to schlieren photographs which are subject to optical distortions and static-pressure distribution measurements which, for practical reasons, begin some distance back from the leading edge. Reference 5 presents quantitative flow field data about lifting wedges as obtained by interferometric methods. Here again, the flow near the leading edge is not clearly defined experimentally because of the decay of optical resolution in this region.

A theoretical model which approximates the observed flow is that of inviscid, irrotational flow past an inclined flat plate of infinite span at free-stream Mach number 1. Guderley, reference 6, obtained analytically a small-disturbance solution to this problem which, unfortunately, does not specify the true state of affairs at the leading edge. However, an exact solution to this same problem has been obtained numerically by Vincenti, Wagoner, and Fisher, reference 7, which does supply these features for an angle of attack of 13°. What is more important, the method lends itself to easy extension to a general class of flat-bottomed airfoil sections with sharp corners at leading and trailing edges. Within the scope of this inviscid theory the static pressure in the separation bubble is arbitrary. It is therefore possible to construct any one from an infinitude of flow patterns for given inclination of the flat lower surface. However, that particular pattern which corresponds most closely to flow in a real fluid must be selected to satisfy a boundary condition determined from viscous considerations.

The incorporation of viscosity can be achieved without empirical information, provided the boundary layer can be considered of negligible thickness at separation and the flow attachment can be considered a constant energy process. The necessary tools are furnished by theories for boundary-layer attachment recently developed by Chapman, Kuehn, and Larson for the laminar case (ref. 8), and by Korst, Page, and Childs for the turbulent case (ref. 9). Thus, it appears possible to select that particular one from the infinitude of inviscid, irrotational, mixed flow solutions which is compatible with restrictions imposed by the process of boundary-layer attachment.

The extent to which such a calculated flow pattern might agree with experimentally determined patterns cannot be decided from the data of references 1 through 5 because of the lack of sufficient detail very close to the leading edge, and especially in the neighborhood of the separation bubble. It may logically be anticipated, furthermore, that finite thickness of a real leading edge along with real viscous effects (in distinction to the theoretical viscous effects introduced by the theories of refs. 8 and 9) would produce departures from the theoretical picture in this region. The present work was initiated in an attempt to determine whether such disagreement was apt to be serious.

The experimental portion of the present work is a determination by means of X-ray densitometry of the density field characteristic of attached transonic flow past the leading edge of a wedge at angle of attack. Use of the X-ray densitometer permitted measurements free of aerodynamic interference somewhat closer to the leading edge, without loss of definition, than has been possible with other methods. These measurements provide information for a comparison with the results of the second portion of the investigation, which consists of an attempt to compute such a flow.

EXPERIMENTAL ARRANGEMENT AND APPARATUS

Marschner, reference 10, has studied theoretically the effect of chord-to-test-section-height ratio on the flow over a diamond airfoil for the

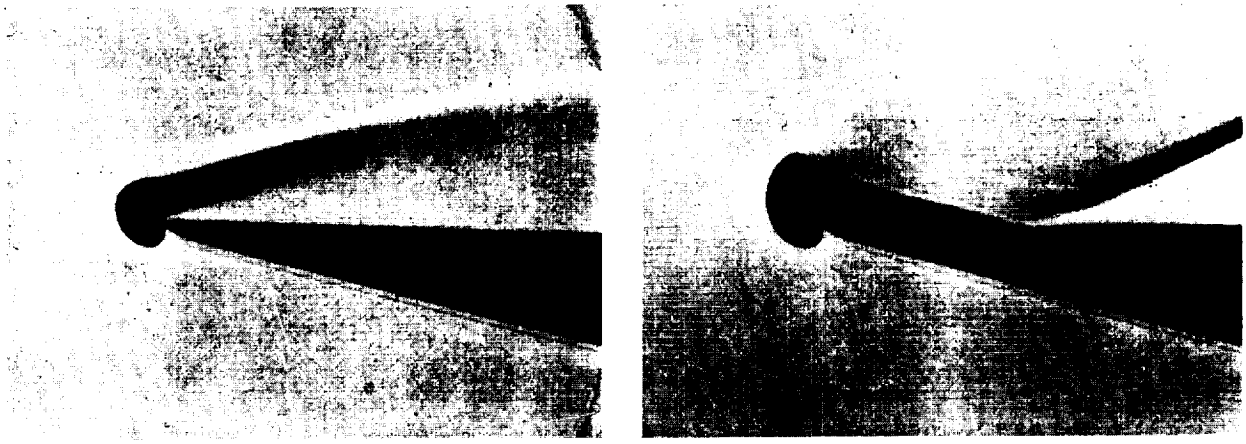

(a) Flow separation over suction surface; Mach number 0.69.

(b) Supersonic attached flow on suction surface; Mach number 0.70.

FIGURE 1. Shadow photographs showing optical distortion in two types of mixed flow about the leading edge of a 12° wedge at angle of attack of 7° and Reynolds number of 1.07×10^6.

case of choked flow in the wind tunnel. For moderate values of chord-to-height ratio he found that the pressure distribution over the forward surfaces of the nonlifting section was the same, for practical purposes, as the distribution over an identical body in unbounded flow at exactly sonic speed. Guderley (ref. 11) has obtained the same theoretical result for the asymmetric flow about a flat plate at small angle of attack. The decision to carry out the present experiments in a closed-throat wind tunnel was prompted by the expectation that this equivalence would apply also to a wedge at angle of attack.

Because of the tiny volume near the leading edge within which the interesting features of the flow are predicted to lie (ref. 7), because of the accompanying steep changes of density gradient which cause difficulty with optical methods (fig. 1), and because of the necessity to avoid disruption of the flow by insertion of probes, it appeared desirable to gather data with an X-ray densitometer. In one of the two arrangements used, relative movement was required between densitometer and test body. For structural as well as aerodynamic reasons, it was advantageous to move the densitometer with respect to the fixed test body. The avoidance of serious complication of the installation then rendered it infeasible either to bypass the side-wall boundary layers or to seal completely the narrow gaps between the tips of the airfoil and the wind-tunnel side walls. Thus, interpretation of the data required consideration of end effects.

WIND TUNNEL

The Ames 1- by 3-foot supersonic wind tunnel no. 1 is the closed-circuit, continuous-operation, variable-pressure type, and uses dried, filtered air as the working fluid. For subsonic operation, as in the present investigation, the flexible floor and ceiling of the 1-foot-wide nozzle are adjusted to form a smooth, symmetrical, two-dimensional contraction followed by a 6-foot-long test section having an approximately constant height of 34 inches. Speed is varied by changing the area of a sonic throat downstream of the test section.

Stagnation conditions in the wind-tunnel settling chamber are determined from pressure measurements, by means of manometers, and from temperature measurements, by means of iron-constantan thermocouples. A space-averaged value of stagnation density is determined from the average pressure and local temperature measurements by numerically averaging (across the settling chamber) the local densities as defined by the equation of state for an ideal gas. Nominal flow conditions at various axial locations through the contraction, test section, and diffuser are estimated from measurements of static pressure on the nozzle walls in the horizontal plane of symmetry. The probable relative errors in determining absolute values of pressure and temperature from the measurements are 0.5 and 0.4 percent, respectively, in the most uncertain cases.

TEST BODY AND SUPPORT SYSTEM

The test body, which spanned the width of the test section, was a wedge of 12° apex angle and of

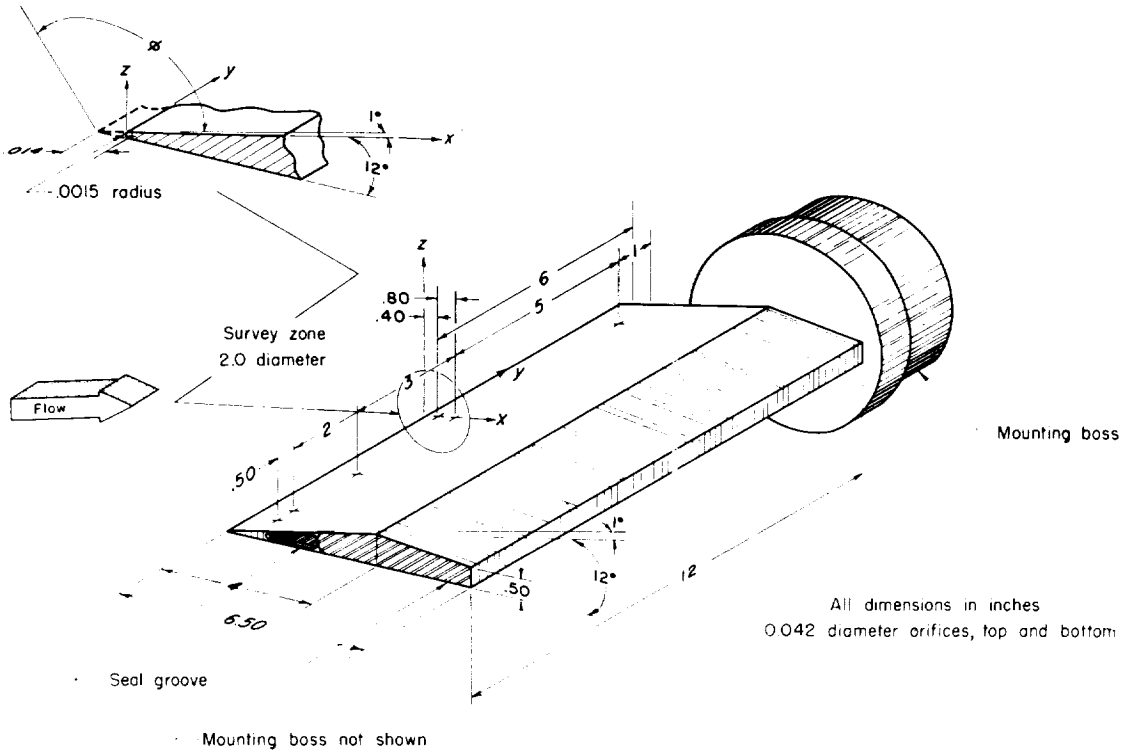

FIGURE 2.—Test body.

6½-inch chord having a boattailed upper (suction) surface and blunt trailing edge as shown in figure 2. The steel airfoil was hardened and the surfaces were ground and polished until the roughness was less than 16 microinches, root mean square. The lower (pressure) surface was positioned at an angle of 13° with respect to the longitudinal axis of the wind tunnel.

Static-pressure orifices were arranged on the upper and lower surfaces of the airfoil near the leading edge as shown in figure 2. The spanwise dimensions given in the figure are nominal; orifices at corresponding locations on upper and lower surfaces were displaced slightly from those quoted for structural reasons.

To reduce maintenance difficulties, the leading edge was provided with a radius of approximately 0.0015 inch. The projected leading edge (virtual wedge apex) was located in a plane 3 inches above the horizontal median plane of the wind tunnel, and this formed the axis for the cylindrical polar coordinates used to map the density field. Polar angles were measured relative to the free-stream direction, and increased in the counterclockwise sense when the flow approached from the left. The lower surface of the airfoil thus lay in the plane with angular coordinate 347°, and the upper surface from the leading edge to the ridge line occupied the plane with angular coordinate 359°. The Cartesian coordinate system shown in figure 2 is a right-hand system having the x-y plane in the forward portion of the upper surface and the y-z plane tangent to the leading edge.

The tips of the rear half of the airfoil were clamped to 4½-inch-thick steel plates which replaced the 2-foot-diameter wind-tunnel windows. The support plates had 3-inch inside diameter cylindrical holes bored concentric with the axis through the projected leading edge. These holes could be fitted as desired with windows for optically viewing the flow about the leading edge or with the X-ray densitometer equipment. When either the windows or the densitometer equipment were installed, gaps having a thickness of 0.001 inch and a length in the chordwise direction of 1¼ inches were present at the airfoil tips.

X-RAY EQUIPMENT

The X-ray densitometer is a device for measuring the density of a medium by the absorption of X-rays in that medium. For use in air, the

densitometer is designed to take advantage of two important properties of electromagnetic wave propagation through air. The first is the relative opacity of air to X-radiation at wave lengths greater than 1 Angstrom. The second is the negligible refraction and scattering of radiation at these wave lengths by inhomogeneous air over relatively short path lengths. Thus, air density as determined from the absorptive characteristics of an X-ray beam correspond uniquely to rectilinear propagation paths through the air. In the present investigation, two arrangements of the densitometer were employed: the so-called "narrow beam" arrangement (fig. 3(a)), and the "broad beam" arrangement (fig. 3(b)). A more detailed description of the densitometer equipment than that which follows is given in appendix A.

Narrow beam arrangement.—The narrow beam arrangement, hereafter called arrangement A (fig. 3(a)), had features which met the general requirements for X-ray densitometry in air discussed in reference 12. With arrangement A the density measurement was accomplished by comparing the intensities, as measured by Geiger-Mueller quantum counters, of two narrow X-ray beams from the same X-ray source (fig. 4). One beam was directed through the wind tunnel along a path parallel to a generating element of the two-dimensional test body, and the other through a reference chamber wherein a known air density could be maintained. Both beams had the same path length and passed through the same number of windows. Thus, in principle, the average density along the propagation path in the wind tunnel was the same as the known density in the reference chamber when the tunnel beam intensity was equal to the reference beam intensity.

Broad beam arrangement.—The second arrangement of the densitometer, arrangement B, is illustrated in figure 3(b). To minimize beam divergence and attenuation due to absorption outside the test air stream, the X-rays were passed through a 10-foot-long evacuated tube which was separated from the air stream by a membrane of organic synthetic material. Because of the pressure difference between the wind tunnel

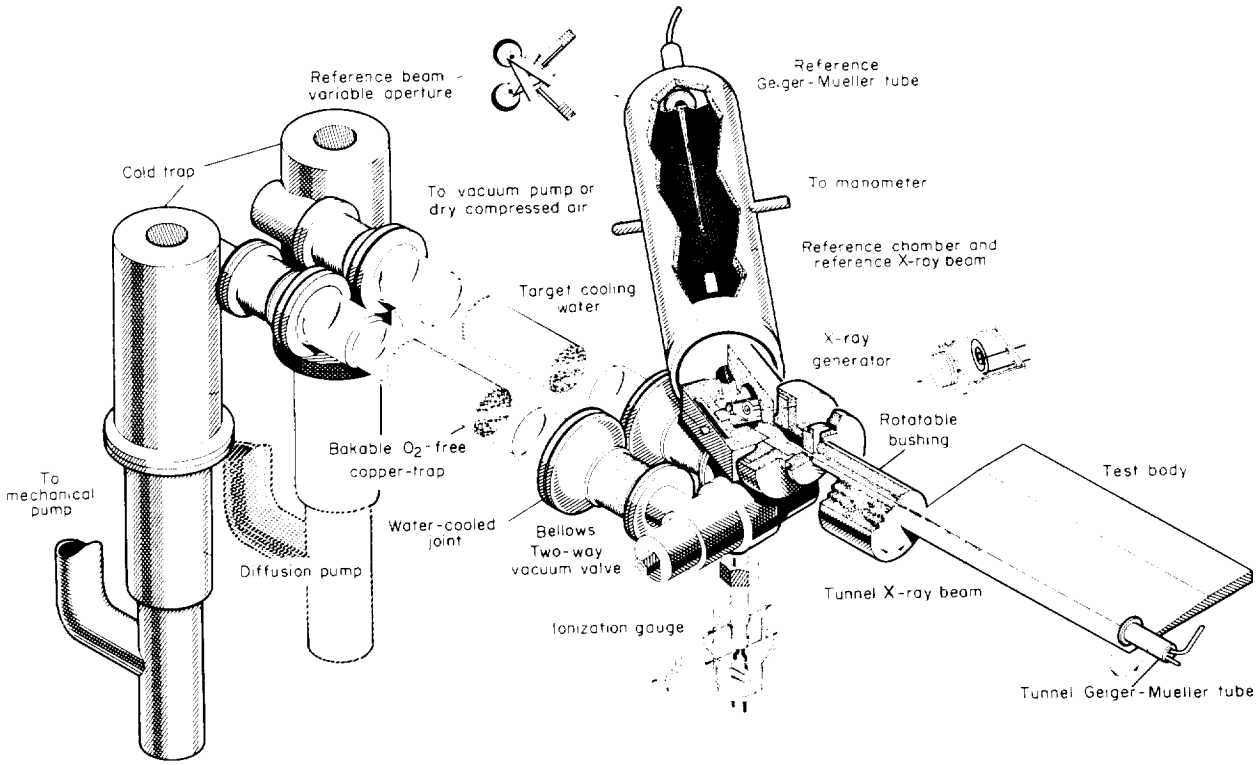

(a) Narrow-beam arrangement, arrangement A.

FIGURE 3.—Arrangements of X-ray densitometer.

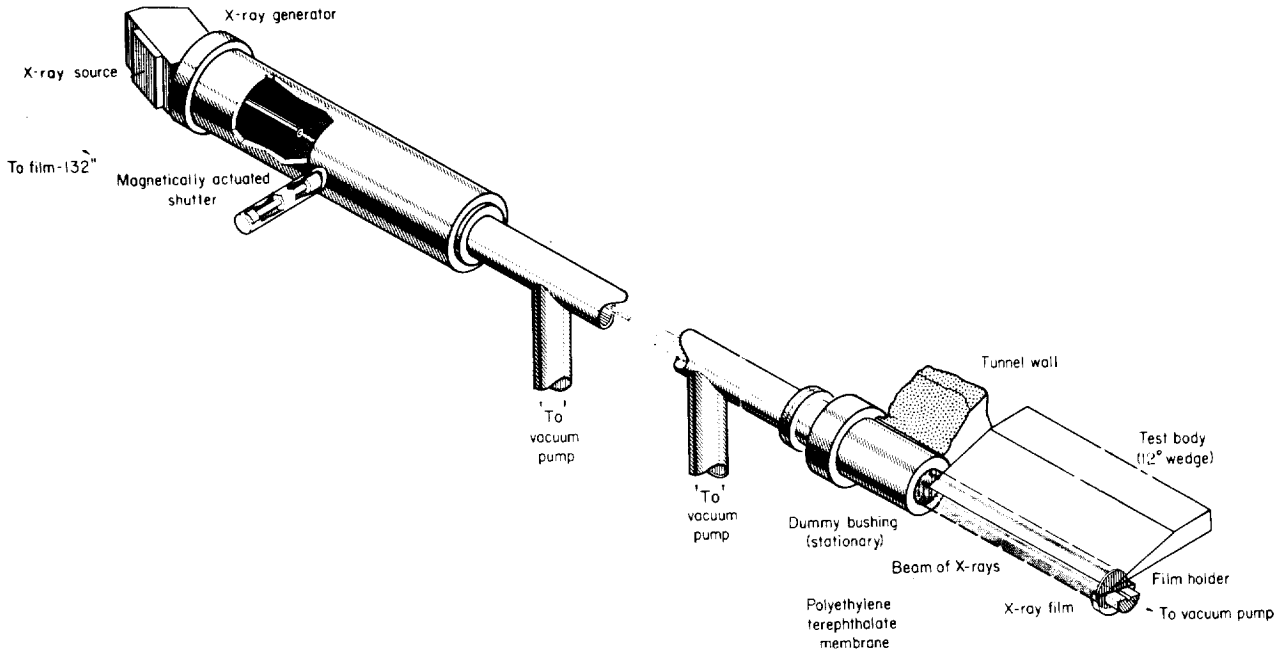

(b) Broad-beam arrangement, arrangement B.

FIGURE 3.—Concluded.

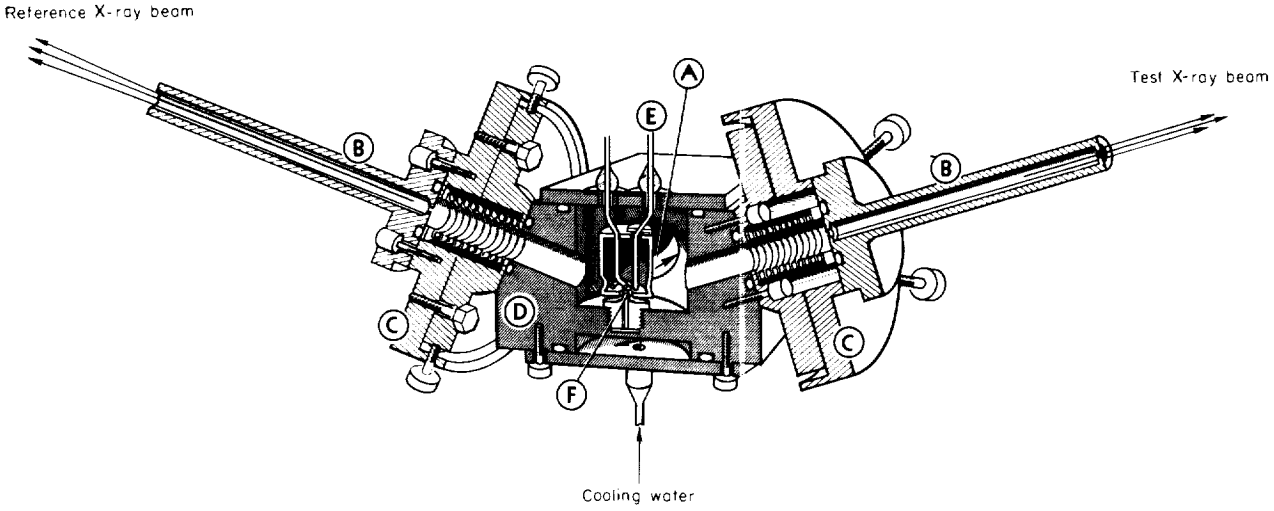

A To vacuum pumps
B Collimating tubes
C Adjustable mounts (showing interior bellows)
D Generator body
E Spiral pancake filament (surrounded by cylindrical focusing electrode)
F Target

FIGURE 4.—X-ray generator.

and tube, the membrane sagged into the tube and produced a ½-inch gap at the airfoil tip. The X-ray source (fig. 4 and appendix A) flooded the zone of interest in the wind tunnel with a nearly parallel beam of X-rays. As in usual industrial and medical radiological practice (see ref. 13), the X-rays that emerged from the zone of interest exposed a photosensitive emulsion, which was recessed 0.008 inch in the tunnel wall, and thus produced a radiograph of the flow field. Calibration information consisted of a series of exposures obtained with various known values of air density in the test section under static conditions. All negatives were exposed identically and processed concurrently. Analysis of the radiographs by means of an optical densitometer then led to the air density distribution.

TEST PROCEDURE AND EXPERIMENTAL RESULTS

Before X-ray intensity surveys were made in the mixed flow about the leading edge of the test body, certain preliminary experiments were carried out. These were initiated by calibrations of the air flow in the empty wind tunnel and by subsidiary operation and calibration of the X-ray densitometer on a test stand. Further preliminary tests involved operation of the tunnel with the test body in the absence of the densitometer, joint operation of densitometer and empty tunnel, and calibration of the densitometer in the presence of the test body with no flow in the tunnel. Those procedures which involved densitometer operation without flow and test body are detailed in appendix A.

CALIBRATION OF WIND TUNNEL

Experiments in empty tunnel.—Through the range of Mach numbers from 0.60 to 0.90 and Reynolds numbers per foot from 1×10^6 to 5×10^6, static-pressure distributions were measured on the side walls of the empty wind-tunnel test section. From these distributions, gradients were minimized by adjustment of the flexible floor and ceiling of the wind tunnel. The final adjustments yielded a uniform, slightly favorable pressure gradient through the test section as is shown in figure 5(a) for a Mach number of 0.75. As can be seen from figure 5(a), the reference orifice for this and all other citations of tunnel speed was 3.06 chord lengths upstream of the leading edge of the test body. The vertical position was at midheight on the wall of the wind tunnel.

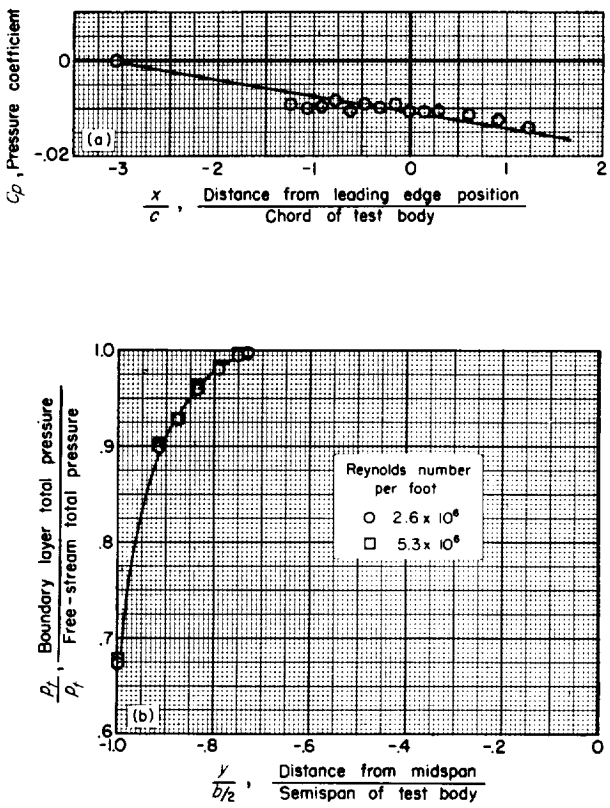

(a) Longitudinal static-pressure distribution through test section at mid-height on wind-tunnel wall; $Re/\text{ft}=3.8\times10^6$.

(b) Boundary-layer total-pressure profile on side wall at leading-edge position.

FIGURE 5.—Calibration of empty wind tunnel at Mach number 0.75.

Boundary-layer profiles on the side wall of the wind tunnel needed for evaluating end effects were determined by means of impact pressure surveys. Surveys were made at the example Mach number of 0.75 and Reynolds numbers per foot of 2.58×10^6 and 5.27×10^6. Figure 5(b) shows the impact pressure profiles so obtained. Little change in boundary-layer thickness due to doubling the Reynolds number per unit length is evident.

Experiments with test body in tunnel.—With the test body installed in the wind tunnel, wall pressures were measured in the vicinity of the leading edge at points where X-ray surveys were to be made. These measurements, typical examples of which are shown in figure 6(a), establish that the pressure distributions were

546395 60 —2

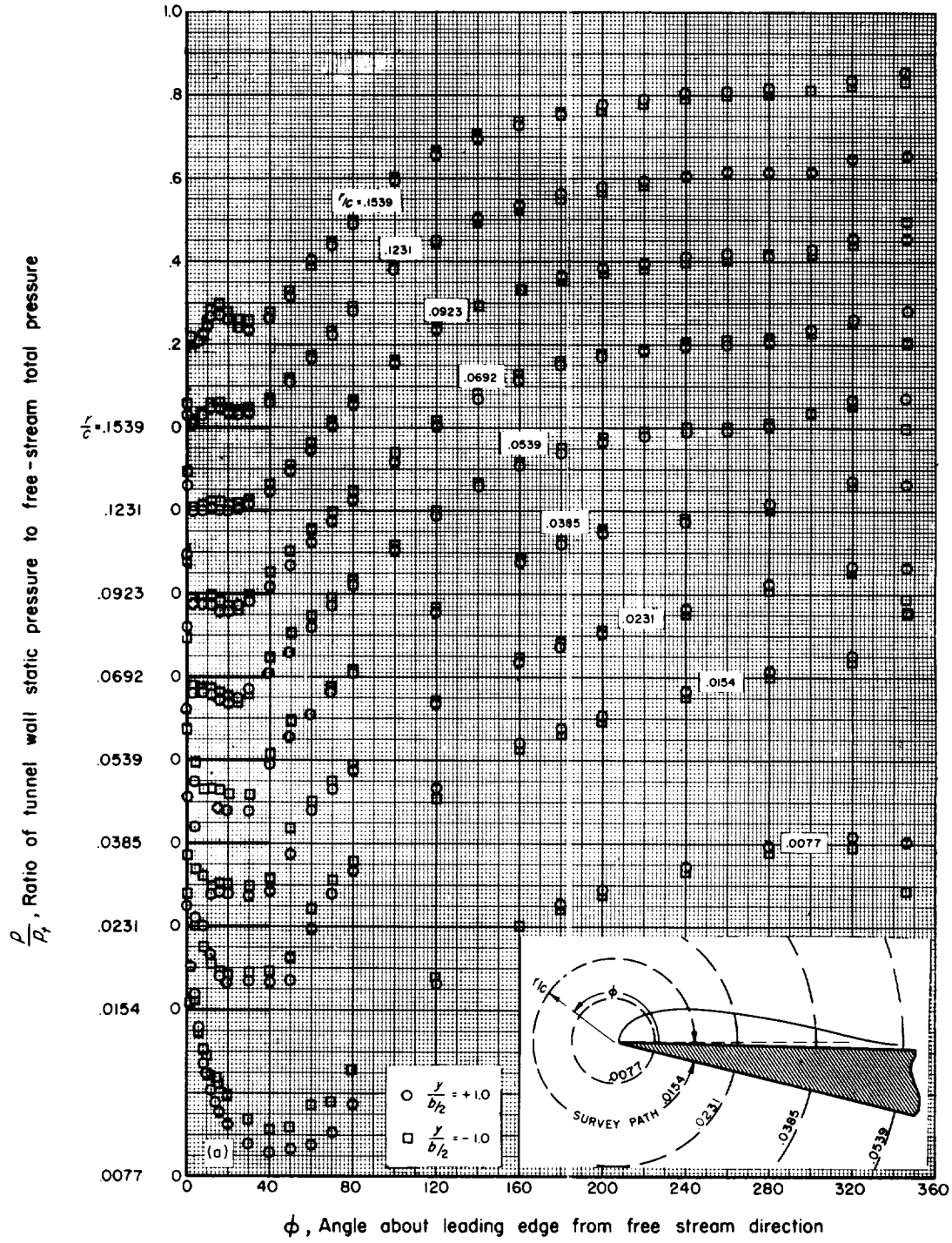

(a) Static-pressure distributions on wind-tunnel walls at various distances from leading edge.

FIGURE 6.—Pressure distributions near leading edge of test body; $M_\infty = 0.705$, $Re = 2.0 \times 10^6$.

substantially the same on both walls of the wind tunnel, except at distances of less than about $r/c=0.02$ from the leading edge where some asymmetry appeared. It may be noted that by means of the gas law these pressure distributions can be shown to be equivalent to local density distributions on the wall since, to a good approximation, the mean wall temperature is equal to the stagnation temperature.

Further, spanwise distributions of static pressure were obtained from the orifices on the upper and lower surfaces of the test body. Typical examples given in figure 6(b) show that the spanwise variations of pressure were not unduly large.

From shadowgraph and schlieren observations, the effects on the flow of changes in tunnel speed and stagnation conditions were qualitatively determined, and the wind-tunnel control parameters for steady occurrence of flow attachment were selected and checked for repeatability. As is illustrated by the shadowgraph pictures of figure 7, the flow attached at a Mach number of approximately 0.69, irrespective of a fivefold variation of Reynolds number. The lower Mach numbers listed represent the upper limit of Mach number for which the separated flow was stable. Simi-

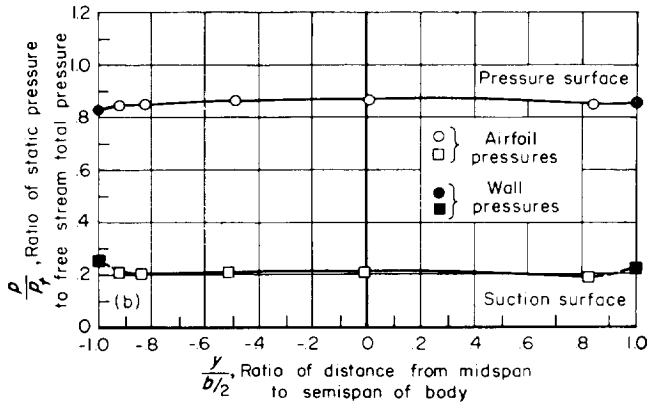

(b) Static-pressure distribution along span at fixed distance from leading edge, $r/c=0.1538$.

FIGURE 6.—Concluded.

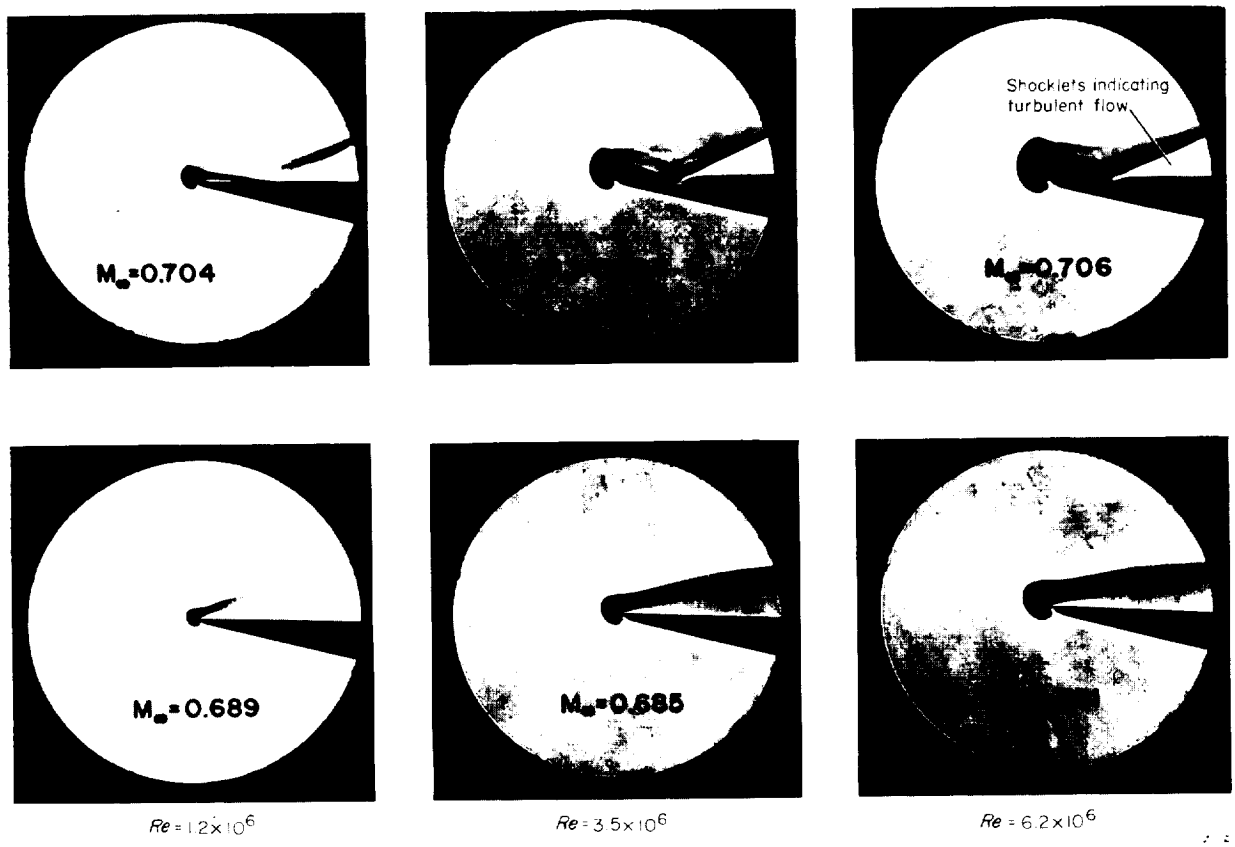

FIGURE 7.—Shadowgraphs showing limiting Mach numbers for stability of two types of flow as a function of Reynolds number.

larly, the higher values correspond to the lower limit of Mach number for stability of the attached flow.

DENSITY SURVEYS

Densitometer arrangement A. Point-by-point surveys through the flow field about the leading edge of the test body were made with densitometer arrangement A at Reynolds numbers of 1.08×10^6 and 2.03×10^6 and a Mach number of 0.705 ± 0.003. Spanwise-averaged values of density were deduced from the time-averaged X-ray intensity data by means of the procedure outlined in appendix A. These values appear in table I in ratio to values of the stagnation density in the wind-tunnel settling chamber numerically averaged over both space and time. They contain systematic errors due to end effects which arise both from the wind tunnel wall boundary layers and from the leakage through the 0.001-inch clearance gaps at the airfoil tips. It would be desirable to relate these average values to values which would be characteristic of an idealized two-dimensional test. Unfortunately this cannot be done with the available data. It is, however, possible to estimate the magnitude and direction of the discrepancies. As is shown in appendix A, the measured spanwise-averaged density values are all believed to be lower than the values characteristic of the flow at midspan. The discrepancy is at most less than 10 percent.

The density ratios at a Mach number of 0.705 given in table I are representative of the smallest opening of the sonic throat downstream of the test section (speed control choke) which would allow the steady occurrence of transonic attachment. Static-pressure distributions along the wind-tunnel wall show that the flow downstream of the body was subsonic, and a simple consideration involving the pertinent cross-sectional areas suggests that, for these data, choked flow could not exist at the location of the test body.

When the speed control choke was opened to its widest value, the tunnel Mach number rose from 0.705 ± 0.003 to 0.737 ± 0.003, and the corresponding ratio of minimum cross-sectional area at the speed control choke to the minimum cross-sectional area at the body location increased from 0.994 to 1.019. However, despite the fact that the over-all pressure ratio developed by the wind-tunnel drive was more than ample to produce supersonic flow downstream of the body, the downstream flow between the body and the speed control remained subsonic. Although it is possible that choking did not take place at the body location, it is conjectured that wind-tunnel operation then was characterized by the presence of two sonic throats, one at the body location, the other at the speed control choke. It is noted that the theory of Guderley (ref. 11) predicts a choking Mach number for the present arrangement of 0.726.

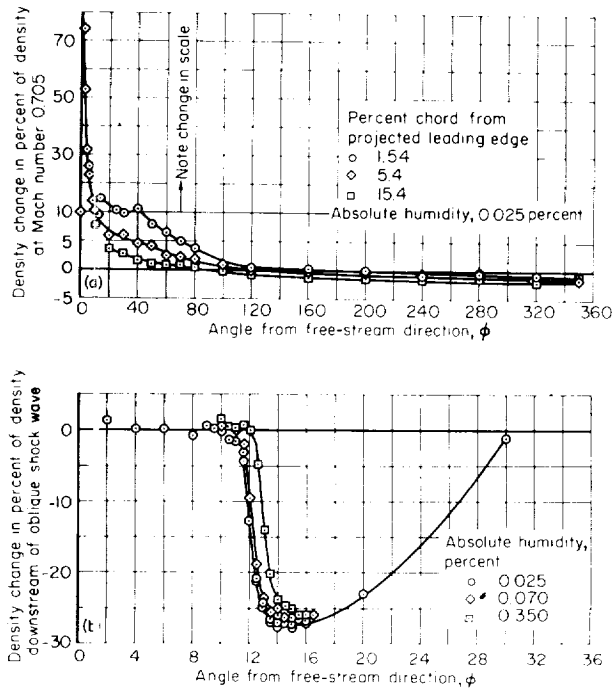

(a) Density change due to an increase of Mach number from 0.705 to 0.737.

(b) Density change through shock wave for various values of humidity; $M_\infty=0.705$, $r/c=0.1231$.

FIGURE 8.—Effect of Mach number and humidity on densities in the attached flow pattern; $Re=2.0\times10^6$.

With test conditions changed only by the opening of the speed control choke, small but systematic X-ray intensity changes were observed throughout the survey zone. These data, in terms of percentage change in density at a point in the flow due to opening the speed control choke, are shown in figure 8(a). Inspection of this graph reveals that the density at most survey points above the airfoil increased slightly when the choke was opened. On the other hand, the density at all survey points below the airfoil decreased when the choke was opened. The peaks very near the upper surface shown by the curves of figure 8(a)

can be traced to zones in the flow where the density gradients are very steep. The 75-percent density change, for example, occurs close to the foot of the attachment shock wave, and suggests that upstream movement of the attachment point took place when the choke was opened.

Tests were performed to determine the effects of humidity upon the flow pattern. For this purpose a detailed X-ray intensity survey was made along a circular arc which was approximately normal to, and passed through, the compression wave associated with the attachment process. This survey was repeated for various values of absolute humidity of the wind-tunnel air stream. As is shown in figure 8(b), an increase of humidity resulted in an upstream movement of the wave. It is indicated by the figure that a humidity level of 0.00025 pound of water per pound of dry air would, if doubled, cause negligible movement of the shock wave.

Meaningful values of density very near the surface of the test body could not be obtained with densitometer arrangement A because the surfaces of the model were deflected slightly by aerodynamic loads and thus introduced variations in angular intensity distribution of the reflected X-rays. Because of inability to calibrate accurately for this consistently, the surveys were normally terminated at distances from the body surface of 0.40-percent chord. In two tunnel runs it was possible to obtain what appeared to be successful calibrations and surveys into the reflection zone, and data were recorded for points closer to the surface.

Densitometer arrangement B. —In densitometer arrangement B the X-ray source was positioned very nearly on the axis through the projected leading edge of the test body. Because only minor reflection effects were encountered with this arrangement, it was possible to obtain interpretable results to within 0.10-percent chord of the surface. For this reason, surveys at the test conditions established for arrangement A were duplicated with arrangement B in order to gather additional information adjacent to the surface. Because of the speed with which radiographs could be taken, it was feasible to X-ray the separated flow pattern which preceded attachment. These radiographs and others taken at extremes of the wind-tunnel Reynolds number range provided much of the data for determining the effects of Reynolds number and Mach number on the flow pattern. They proved also to be indispensable in locating the stagnation zone on the lower surface of the body and in determining the size and shape of the separation bubble.

Positive prints of selected radiographs are illustrated in figure 9. In these illustrations, the whiter hues correspond to lower values of the density; the blacks, to higher. Because the density range covered by the film exceeds the latitude of the reproduction process, a detailed rendition of all portions of the flow field is impossible on a single print. Because of this difficulty, prints prepared from the same negative but having different exposure times are included for each of the illustrated flow conditions.

For reasons discussed in appendix A, the absolute density values deduced from the radio-

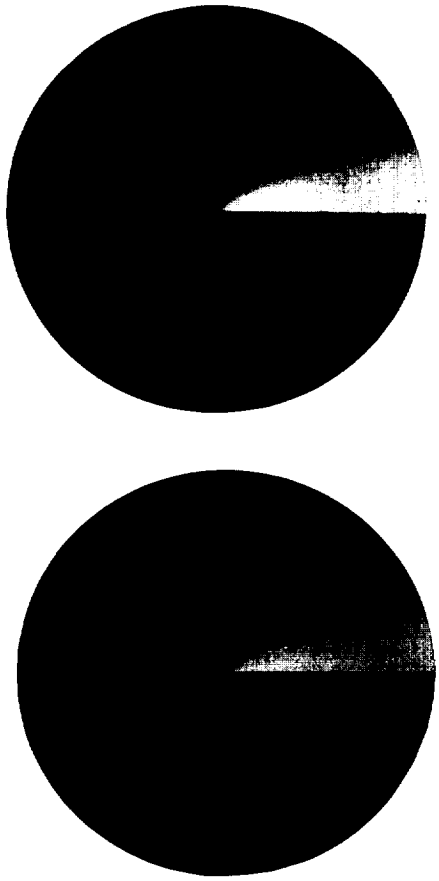

(a) Separated flow, $M_\infty = 0.681$.

FIGURE 9. —Radiographs showing two types of mixed flows about a sharp leading edge at a Reynolds number of 2.0×10^6.

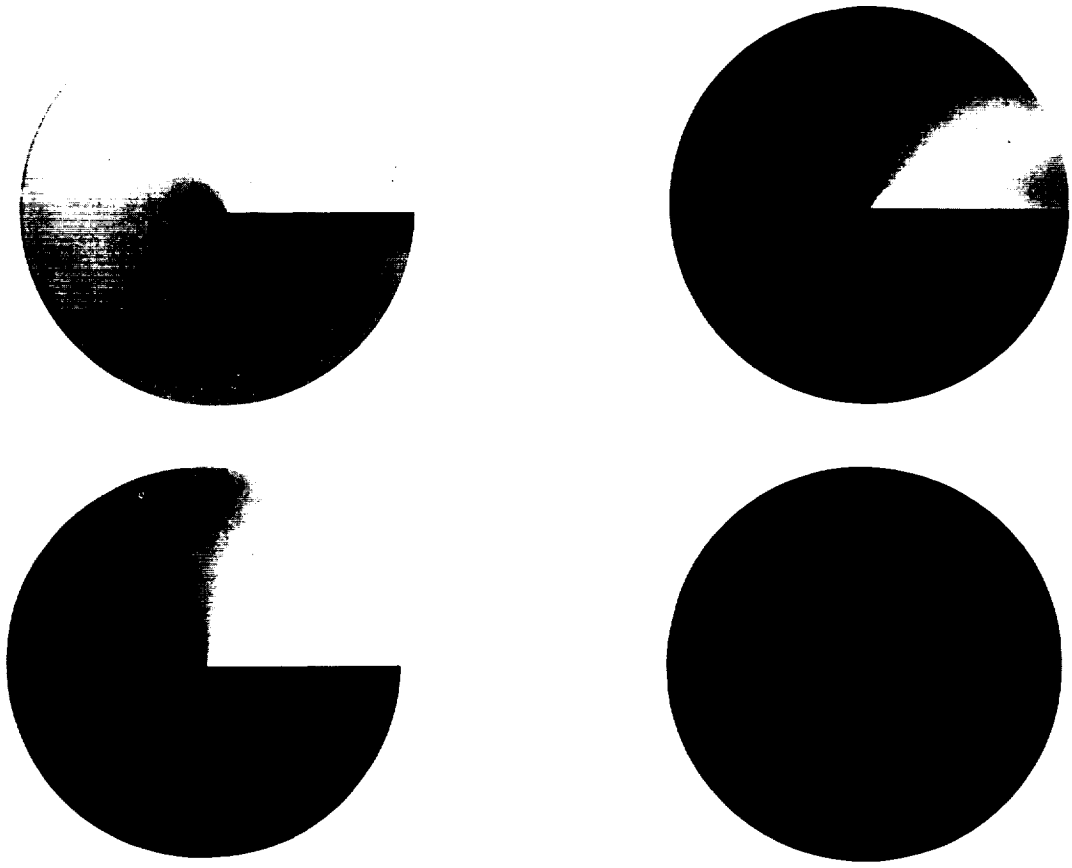

(b) Attached flow, $M_\infty = 0.737$.

FIGURE 9.– Concluded.

graphs are less reliable than those obtained with arrangement A and contain systematic errors of unknown magnitude. Because, however, of their utility in tracing constant-density lines in the flow field, especially in the neighborhood of the separation bubble, certain values have been included in table I.

RESULTS OF THEROETICAL CALCULATIONS

As was pointed out in the introduction, the inviscid solution to the problem of the inclined flat plate at Mach number 1 contains the static pressure in the separation bubble as an assignable parameter. Therefore, within the framework of the inviscid theory, an infinite family of solutions is possible at given angle of attack. Some viscous flow condition is consequently needed to render the problem unique. The present situation is completely analogous to the problem of the inviscid flow over a subsonic airfoil where the Kutta condition at the trailing edge is required. Fortunately, a similar condition in the form of a requirement on the process of attachment of the separated boundary layer has become available. Although the treatment which follows applies specifically to purely laminar attachment of the boundary layer, a similar treatment can readily be given to the process of turbulent-boundary-layer attachment (ref. 9).

CONDITIONS IN ATTACHMENT ZONE

Chapman, Kuehn, and Larson (ref. 8) have developed a theory of the mechanism which determines the static pressure in a separated region, and have established a corollary relation between the Mach number on the boundary of the separated region and the Mach number downstream of attachment. This criterion is based upon the assumptions that the boundary-layer thickness is negligible at separation, the flow is

adiabatic, and the separated boundary layer is laminar at least through the attachment zone. For the case of leading-edge separation under study, all these assumptions appear reasonable.

In supersonic flows the attachment criterion can be put into a form relating Mach number on the bubble boundary with the flow deflection which ensues as a result of the attachment process. Since specifying the Mach number implies fixing the static pressure, and since this pressure is assumed to exist throughout the bubble for the inviscid solution, these results, obviously, relate the bubble static pressure to the deflection angle at attachment. Unfortunately, this relation cannot be imposed on a given body a priori because the bubble shape, and thus the deflection angle, is not known until a bubble pressure has been assigned and an inviscid solution has been obtained on the basis of this pressure. To satisfy this requirement precisely therefore, iteration is, in general, required. Thus, the attack used here was simply that of selecting a bubble-edge Mach number of 2.80 for the initial trial value, calculating the inviscid flow by the method given in appendix B, and then comparing the resulting value of deflection angle with that required to satisfy the viscous attachment relations of reference 8. As will presently become evident, the agreement achieved was sufficiently good that further work was deemed unnecessary. These considerations are epitomized in figure 10.

Figure 10 shows, first, the relation between the flow deflection angle at attachment and the Mach number on the boundary of the separated layer as predicted by the laminar attachment theory of reference 8. Curves are shown both for deflections associated with an attached oblique shock wave and with a Prandtl-Meyer compression. The predicted flow deflection angles which accompany purely laminar attachment are seen to be moderate in magnitude whatever the supersonic Mach number on the bubble boundary. In fact, a maximum deflection of only about $12\frac{1}{2}°$ is predicted for a Mach number of approximately 3. Also, as is obvious from the figure, whether the attachment process takes place as a Prandtl-Meyer compression *beneath* the foot of the shock wave or as a turn *through* the oblique wave the predicted deflection angles are essentially the same.

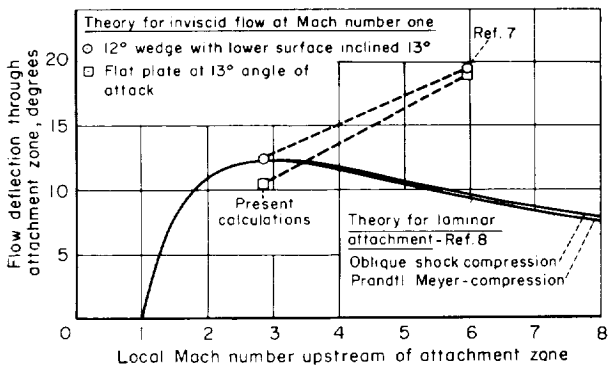

FIGURE 10. Relation between Mach number on separation streamline and flow deflection at attachment.

The deflection angles for the inviscid flow, which represent the results of the present calculations for a Mach number of 2.80 on the bubble boundary, and the calculations of reference 7, for a bubble boundary Mach number of 5.88, are also included in figure 10. Two values of deflection angle are plotted at each of the given Mach numbers. The lesser values corresponds to the flow impinging on the upper surface of the basic flat plate, whereas the greater values of deflection angle apply to attachment on a sharp wedge having a nose angle of 12°. These latter values were found by the addition of thickness to the basic flat plate, which does not alter the inviscid solutions provided the body slope remains discontinuous at the leading edge and the attachment shock wave does not influence the upstream zone of subsonic flow. The deflection angle in each case was then established by the intersection of the calculated separated streamline with the added upper surface. It is seen that the deflection angle for the wedge corresponding to the present solution compares very favorably with the value predicted by means of the attachment theory for a Mach number of 2.80.

It is perhaps worth noting that it has been indicated so far that the direct problem of finding the flow associated with a given shape of upper surface can be solved by these methods only by means of an iteration process. Almost trivial by comparison is the inverse problem of fitting a compatible upper surface to a given theoretical flow. All that need be done in principle is to arrange that the surface intersect the separated streamline of known Mach number at the angle specified by the curve of figure 10 and that the resulting attachment shock wave not affect the upstream subsonic flow.

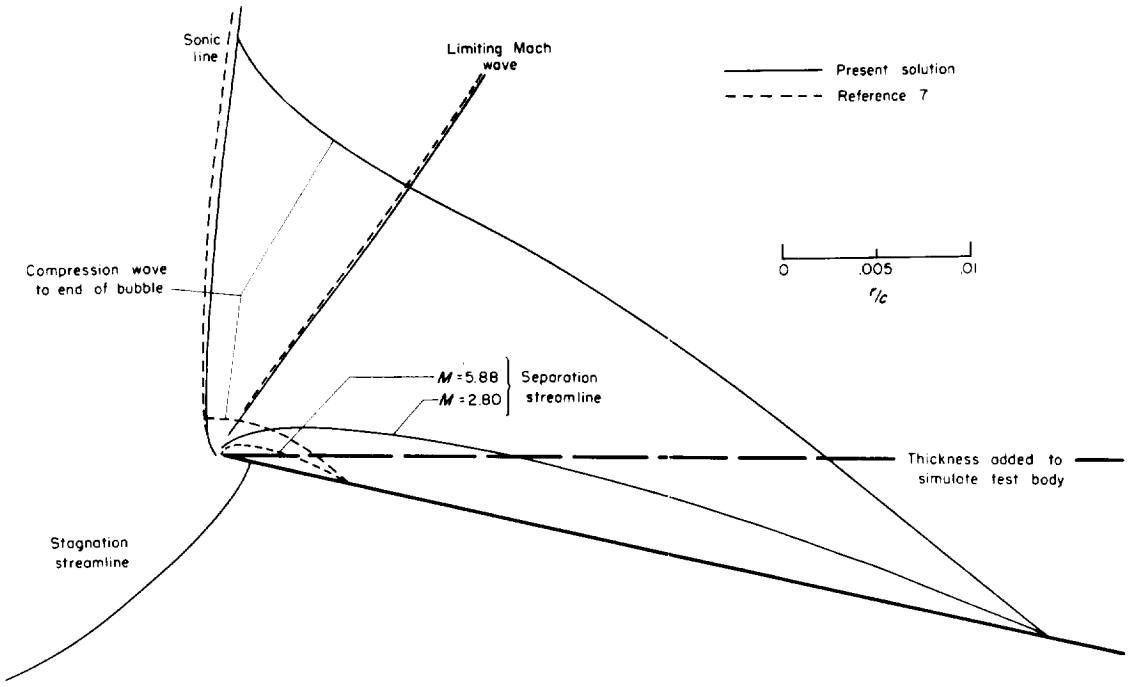

(a) Complete separation bubbles.

FIGURE 11.—Comparison of inviscid flow fields about a flat plate at angle of attack of 13° and free-stream Mach number 1 for two values of Mach number on the separation streamline.

A multitude of upper surface shapes, not necessarily flat, obviously can be so constructed for each of the two given inviscid flows.

CALCUATION OF INVISCID FLOW

The inviscid, irrotational flow about a flat plate airfoil at angle of attack of 13° was calculated for a free-stream Mach number of unity and for a Mach number of 2.80 on the separation streamline. The details of this calculation are given in appendix B and the stream function so calculated is presented in table II. Salient features of the flow field are compared in figure 11 with the features of the flow field given in reference 7. Specifically, the locations with respect to the airfoil of separation streamlines, limiting Mach waves, and sonic lines are compared. The flow field shown refers either to the basic flat plate or to the wedge. The flow lines stop at the "thickness added" line when the wedge is considered.

The Mach number assigned to the separation streamline in the calculations of reference 7 was 5.88, a value just high enough that the limiting Mach wave, which divides the interdependent mixed flow portion of the field from the independent all-supersonic portion on the upper surface, originated at the leading edge (fig. 11(b)). In contrast, the Mach number assigned to the separation streamline in the present case was 2.80, and the new calculations put the foot of the limiting Mach wave upon the separated streamline 0.045-percent chord back from the leading edge. Thus, as is explained in appendix B, the subsonic field becomes dependent upon the bubble pressure.

The most profound effect of decreasing the separation streamline Mach number from 5.88 to 2.80 is seen in figure 11(a) to be a growth of the separation bubble, in the case of the wedge, from a length of 0.38 to 1.59-percent chord, a factor of about 4. As a corollary effect, the portion of the sonic line which determines the shape of the bubble for the plate grows by a factor of about 10. This growth, however, does not also extend to the bubble thickness. Thus, the bubble of reference 7 for a separation Mach number of 5.88, although shorter actually is not as slender as that for the lower Mach number of 2.80. Consequently, the angles of intersection of this bubble boundary both with the top surface of the flat plate and with the top surface of the 12° wedge are greater than

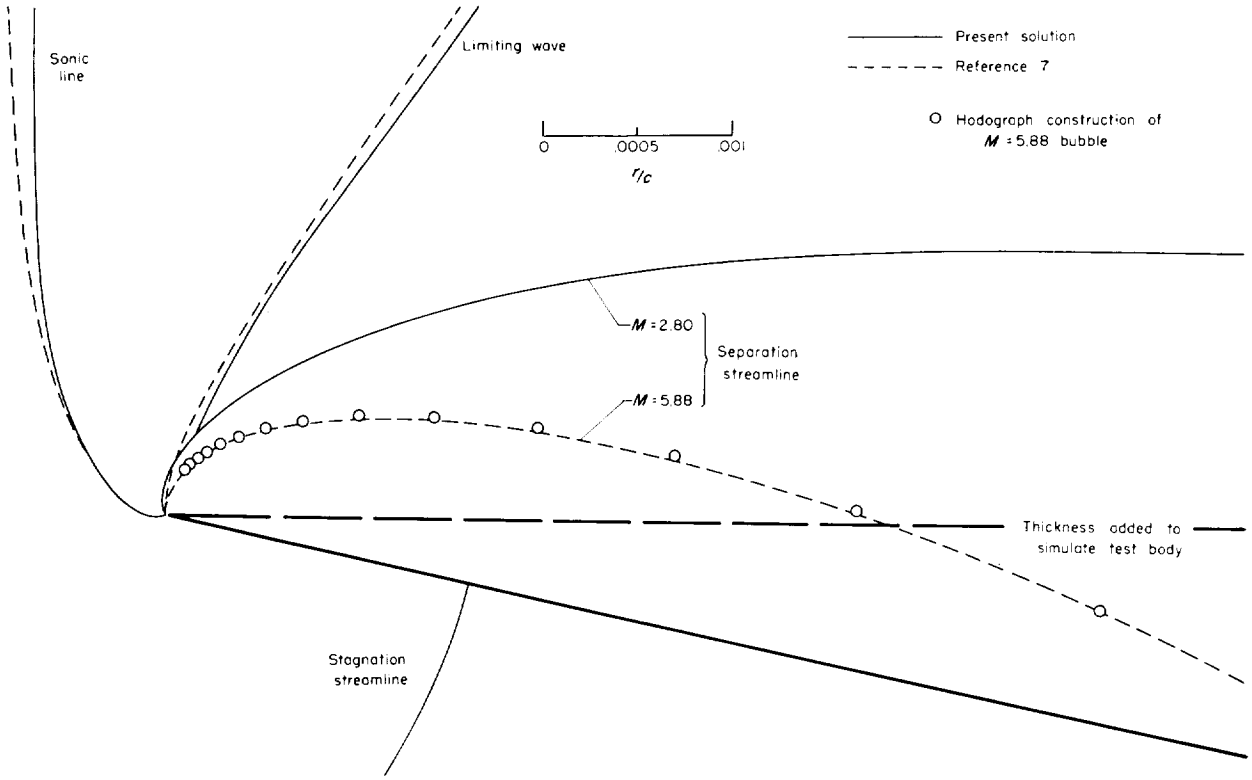

(b) Region near leading edge.

FIGURE 11.—Concluded.

the intersection angles of the longer bubble. This more fully illuminates the variation of attachment angle with Mach number upstream of attachment for the inviscid solutions (fig. 10).

Despite the rather large differences in bubble sizes, it may be seen from figure 11(a) that the sonic lines and limiting waves are displaced only slightly from one another. The contours of constant Mach number in the subsonic region (not shown) exhibit progressively smaller differences as the Mach number in the field decreases below 1. This is as was expected at the outset of the calculations (see appendix B). The stagnation point is at 0.16 percent of the chord from the leading edge—a value indistinguishable from that for the original calculations.

As is explained in appendix B, the present method of calculating the shape of the separation bubble is different from the method used in reference 7. A comparison between the two methods was effected by using the present method to recompute the bubble corresponding to the bubble boundary Mach number of 5.88. It can be seen from figure 11(b) that the two methods produce solutions in satisfactory agreement.

DISCUSSION

Up to this point, the experimental portion and the theoretical portion of this investigation have been treated separately. A method based on simple known considerations of viscosity has been devised for representing a viscous, mixed flow past a sharp leading edge at a Mach number of unity by an inviscid model. Concurrent wind-tunnel measurements have been carried out with a test body and for flow conditions which approximate those stipulated by the theory. It is now proposed to compare various features of the experimental results with the corresponding features of the theoretical findings without dwelling on the justification for the validity of such a comparison. Suffice it to state that there is no apparent reason on the basis of present knowledge to expect large qualitative differences between the experimental flow in the immediate neighborhood of a body in the close-throat wind tunnel under choked-flow

546395—60——3

conditions and the theoretical unbounded flow past the same body at a Mach number of exactly unity. To be sure, there are numerous reasons, stemming both from experimental shortcomings and theoretical predictions, for expecting quantitative differences between the two flows. However, these differences, it is believed, become small enough in the region of interest near the leading edge that valid conclusions can nevertheless be drawn from the comparisons that will be made.

As a preliminary to these comparisons it is advisable to examine the experimental results from an over-all point of view. To this end figure 12 has been prepared. It shows the experimental flow fields as defined by their density contours for the test range of Reynolds numbers and Mach numbers. The contour plots shown were obtained from faired curves prepared from the data of table I. The shock-wave locations were taken as the locus of points of maximum density gradient and were extrapolated to intersect the surface to provide a convenient measure of bubble length. In most cases shown, whether or not the flow was completely separated from the upper surface, the sonic lines ($\rho/\rho_t=0.634$) tend to approach the leading edge from slightly upstream, which suggests that they touch the leading edge on the underside. The stagnation points indicated are from analysis of the radiographs and are all located 0.56-percent chord from the leading edge.

It is noted that the fields which are characteristic of attached flow are remarkably alike throughout the range of test conditions. The increase in Mach number from 0.705 to 0.737 caused only a slight change in the pattern, including a small but detectable decrease in the distance from the leading edge to the foot of the shock wave, which can be interpreted as a decrease in bubble length from 5½- to 4¾-percent chord. This was inferred in connection with the earlier presentation of figure 8(a). The measured density ratio at the edge of the separation bubble has a value, determined by analysis of all of the data in table I, of 0.165.

There was a slight tendency for the bubble size to decrease (from 6- to 5-percent chord) when the Reynolds number was increased by a factor of about 3 at a constant Mach number (compare plots for $Re=1.0\times10^6$ and $Re=2.7\times10^6$). This relative insensitivity to Reynolds number change is in agreement with the theory of reference 8 for purely laminar attachment. According to reference 8, a change can be expected in attachment conditions if boundary-layer transition were to take place within or upstream of the attachment zone. That the attachment process was definitely all laminar at Reynolds numbers below 3.5×10^6 but was possibly transitional or all turbulent at a Reynolds number of 6.2×10^6 was deduced from examination of the negatives from which the shadowgraphs of figure 7 were made. Corroborative evidence that the attachment at Reynolds numbers less than 3.5×10^6 was all laminar lies in the fact that the average density ratio across the foot of the attachment shock wave for the data shown in figure 12 is 1.65 ± 0.08, a value satisfactorily near the theoretical prediction of 1.63 for a bubble-edge density ratio of 0.165 (ref. 8).

Figure 13 compares selected features of one of the experimentally determined flow patterns with the available corresponding calculated features. Theoretical contours were not obtained for $\rho/\rho_t<0.634$, except on the bubble. For the flow above the body gross differences in density contours are confined principally to the region near the separation bubble. For the theoretical calculations it was assumed that the Mach number on the bubble boundary was 2.80 and the subsequent determination of the bubble shape implied, as shown in figure 10, that this bubble-edge Mach number fulfilled the theoretical requirements for laminar attachment. The experiment, however, yields a value of 2.30 for this Mach number, which corresponds to the average density ratio of 0.165.

One possible reason for the discrepancy may be that the solution found is not unique, and that, in fact, two or more theoretical solutions can be obtained and represented in figure 10. That is, if theoretical, inviscid solutions were available for other values of bubble pressure (or what is the same, the bubble-edge Mach number) they might show in figure 10 other intersections in addition to the one already obtained. If this be true, then selection of the proper solution would have to be made by introducing an additional consideration such as least entropy rise through the attachment-zone shock wave. Because, as can be shown readily by means of the inviscid theory, a decrease in bubble boundary Mach number toward unity produces an increase in bubble length toward infinity, it is evident that a new calculation of the inviscid flow field for a bubble-edge Mach number of 2.30 would produce a longer bubble than that

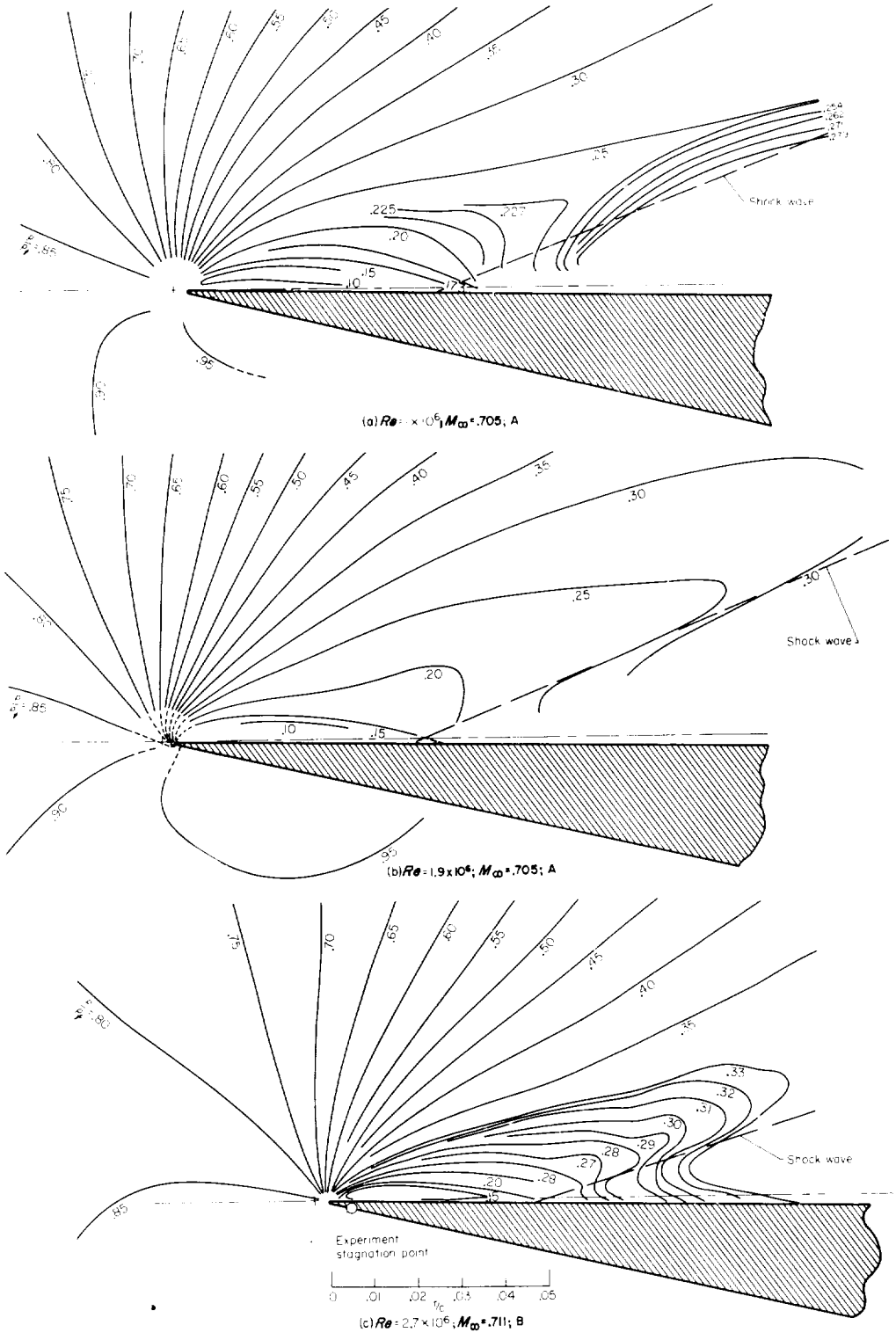

(a) $Re = 1 \times 10^6$; $M_\infty = 0.705$; A
(b) $Re = 1.9 \times 10^6$, $M_\infty = 0.705$; A
(c) $Re = 2.7 \times 10^6$; $M_\infty = 0.711$; B

FIGURE 12.—Experimental density contours for various Mach numbers and Reynolds numbers.

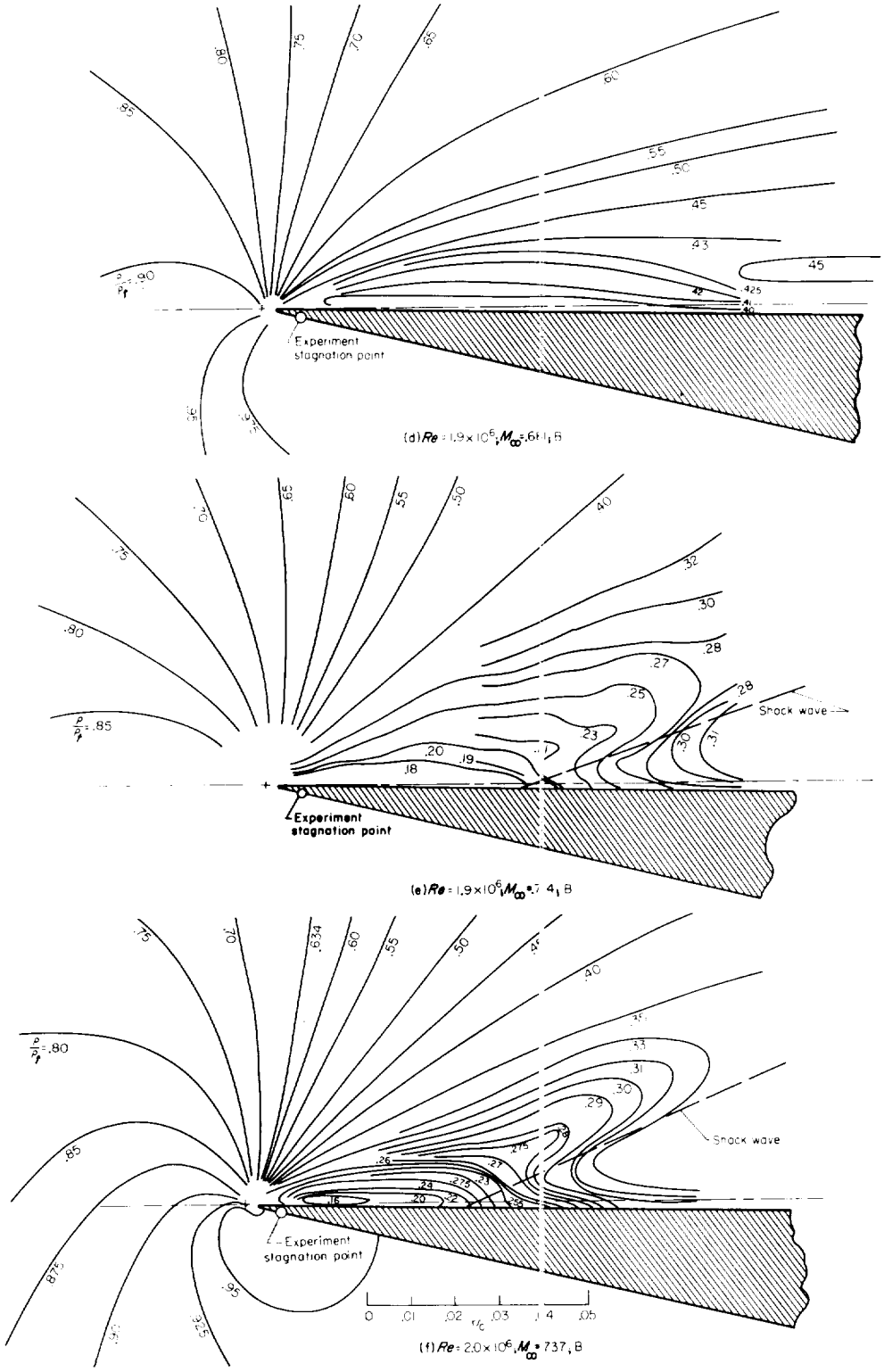

(d) $Re = 1.9\times10^6$; $M_\infty = 0.681$; B
(e) $Re = 1.9\times10^6$; $M_\infty = 0.714$; B
(f) $Re = 2.0\times10^6$; $M_\infty = 0.737$; B

FIGURE 12.—Concluded

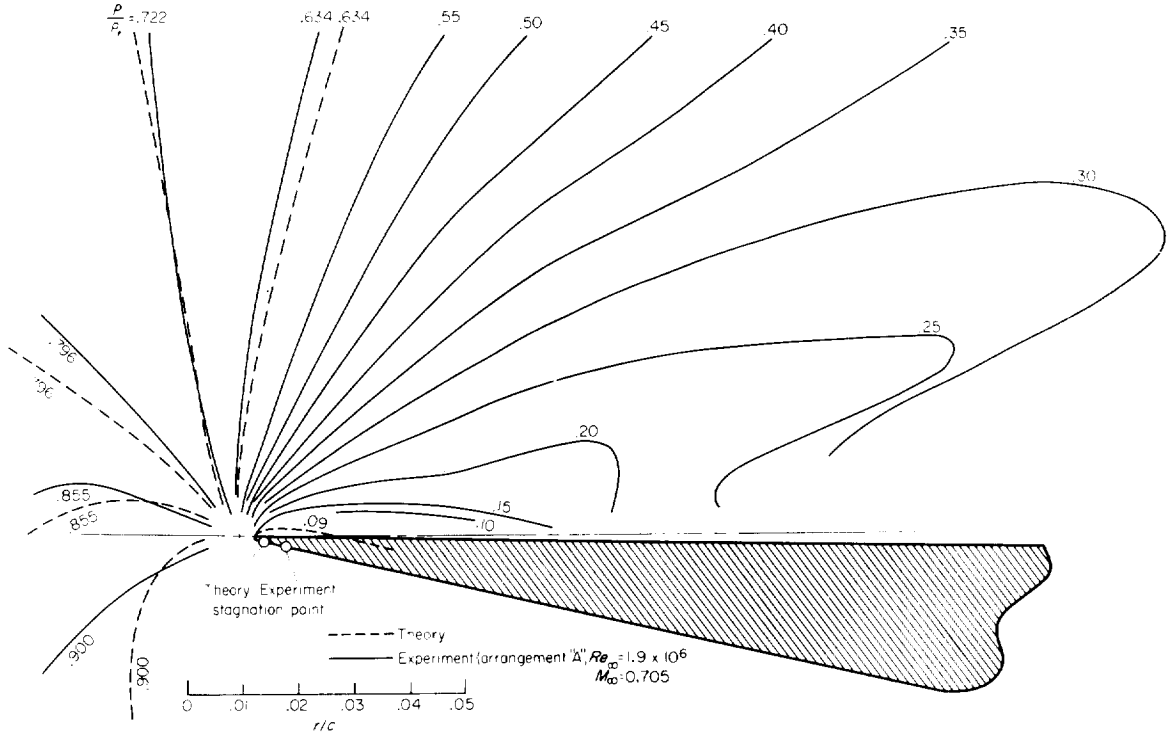

FIGURE 13.- Comparison between theoretical and experimental density contours about leading edge.

shown for a Mach number of 2.80. Thus it appears possible that such a theoretical solution would agree better with the experimentally determined flow field than that given.

Another reason for at least part of the discrepancy between features of the experimental and theoretical separation bubbles stems from a conceptual difficulty which arises when one attempts to reconcile the model for the inviscid flow attachment process with the model for the viscous flow attachment process. The model of the attachment process according to the inviscid theory represents the separated flow by the single distinguishing feature of the Mach number on the bubble boundary, the boundary being at the same time the dividing streamline between a dead-air region within the bubble and the inviscid outer flow. On the other hand, the model of the attachment process according to the viscous theory describes the flow in somewhat more detail. It distinguishes between the dividing streamline which separates the reversed flow inside the bubble from that which proceeds downstream, and the streamline on the bubble edge which delimits the viscid and inviscid portions of the flow (ref. 8). Thus one cannot hope ever to achieve simultaneous agreement between the respective theories as here described and combined in the matter of bubble size and bubble-edge Mach number. If the lengths are to be matched using the dividing streamline as a criterion, the respective Mach numbers thereon can disagree by a large factor because the dividing streamline in the viscous case is located in the midst of the mixing layer. On the other hand, if bubble-edge Mach numbers are to be matched, which was the course pursued here, the respective bubble lengths can disagree by a length the order of the boundary-layer thickness, a dimension which need not be negligible when compared to the bubble length. In view of this discrepancy between the two theoretical models on which the calculations are based, it is to be expected that even though theory and experiment should agree with regard to bubble-edge Mach number they should be expected to disagree with respect to bubble length.

Further possible reasons for the discrepancies between the experimentally determined and the calculated bubbles are two imperfections in the experimental arrangement namely, the finite

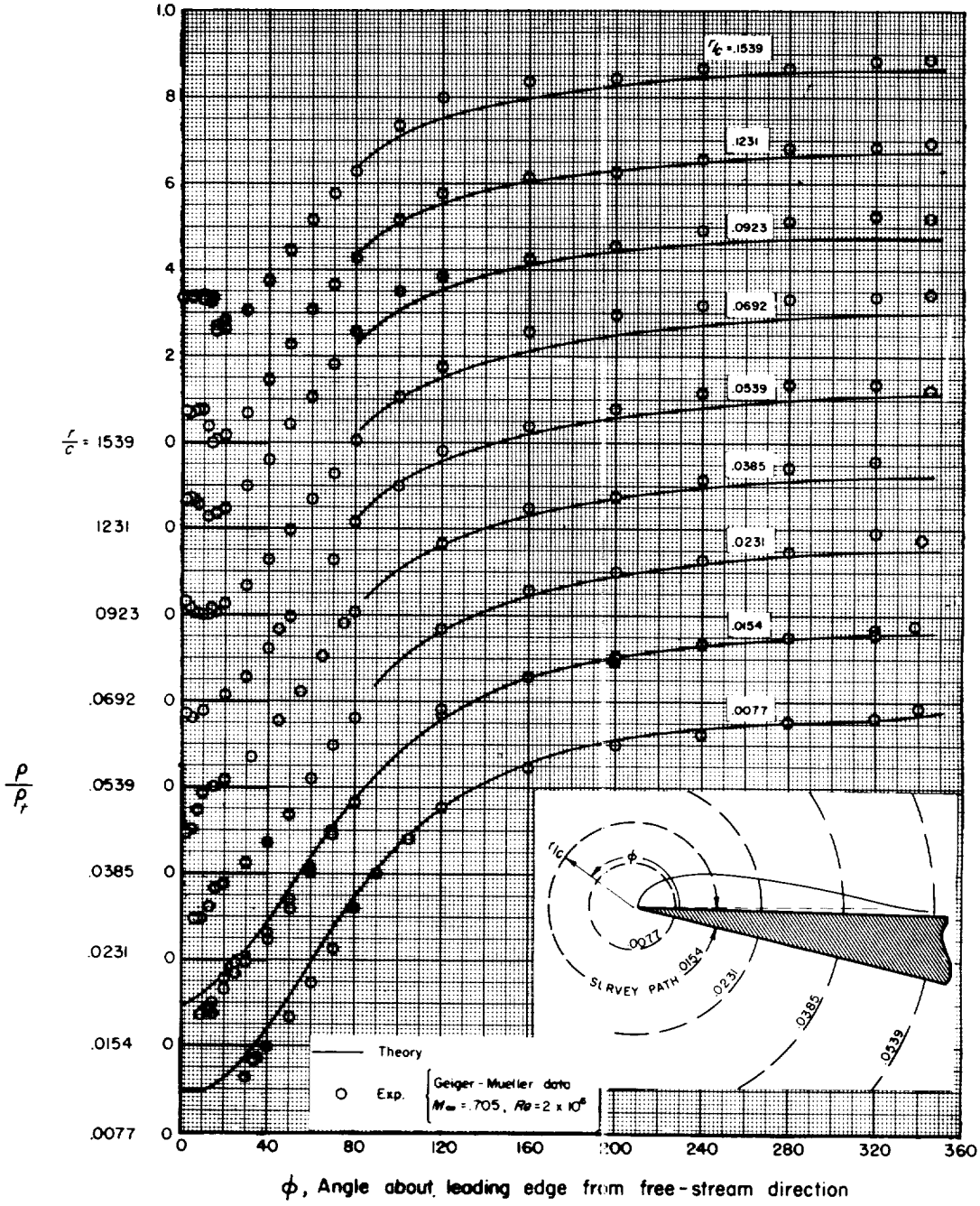

FIGURE 14. Density variation about leading edge at various values of r/c.

thickness of the leading edge and the unsealed gaps at the airfoil tips. Insofar as the effect of leading-edge bluntness is concerned, it is known (refs. 4 and 14) that a sufficiently large nose radius in comparison to the bubble length will suppress completely the formation of a separation bubble. Because in the present case (figs. 2 and 13) the leading-edge radius is small when compared to the bubble length, it is believed that the effect of bluntness on the flow pattern is also small.

The effect of the gaps at the tips has already been discussed insofar as their influence on the two-dimensionality of the flow is concerned. However, in addition to the two-dimensional

effect, the leakage through the gaps would tend to increase the mass flow which had to be scavenged from inside the bubble and would produce an "open" type of mixing process of the kind discussed by Korst, Page, and Childs (ref. 9). Continuity requirements thus would necessitate a somewhat larger bubble than would be necessary if no leakage were present. Fortunately, some indication of the magnitude of this effect can be gained by comparing the bubble length as obtained with densitometer arrangement A with that obtained by means of densitometer arrangement B at substantially identical aerodynamic conditions (figs. 12(b) and 12(e)). It will be recalled that the gaps with arrangement A were 0.001 inch, whereas with arrangement B the gap between one tip and the film surface was 0.008 inch and the gap between the other tip and the membrane over the evacuated tube was about ½ inch. Thus, the leakage with arrangement B was at least eight times that with arrangement A at the one tip and many more than eight times at the other. A comparison of figures 12(b) and 12(e), however, indicates that the bubble length associated with arrangement B is little, if any, different from that associated with arrangement A. Thus one can state that the effects of tip leakage on the bubble length were no greater with arrangement B than they were with arrangement A.

The differences between the experimentally determined and the calculated bubbles aside, attention is next called to detailed density comparisons as depicted in figure 14. These results are plotted in the same form as the distribution of wall pressures in figure 6(a). In this form, the figure can be interpreted as presenting a measure of the agreement between experimental and theoretical densities at fixed locations in the flow field. It may be observed that where comparisons exist, the agreement is, on the whole, quite satisfactory except in the region near the bubble boundary where density ratios are less than 0.230 and local Mach numbers exceed 2.0.

Figure 15 presents a typical comparison of theory with both G–M (Geiger-Mueller) counter data (arrangement A) and radiograph data (arrangement B) for a radius ratio of 0.0154. It can be seen that the radiograph data agree well with theory and the G–M counter data only for the larger angles (i.e., for the subsonic region). The disagreement at the lower angles is not understood.

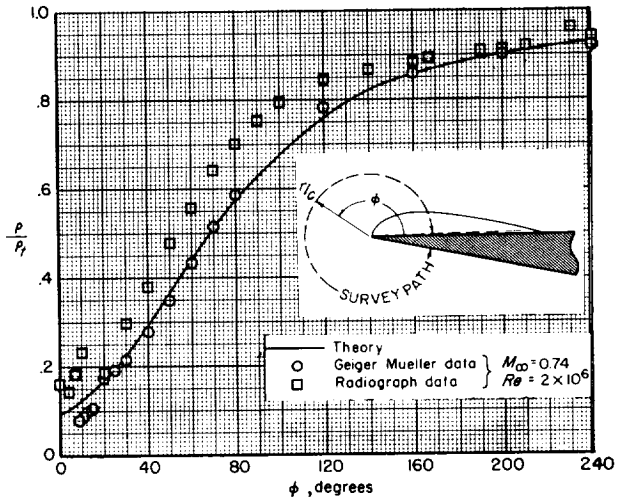

FIGURE 15.—Density variation about leading edge at $r/c = 0.0154$.

Undoubtedly, a large fraction of the discrepancy can be attributed to numerous experimental errors of unknown magnitude (see app. A) which may be expected to be larger for the low densities than for the high densities.

Conditions near the leading edge adjacent to the lower surface are compared with theory in figure 16 wherein pressure coefficient computed for free-

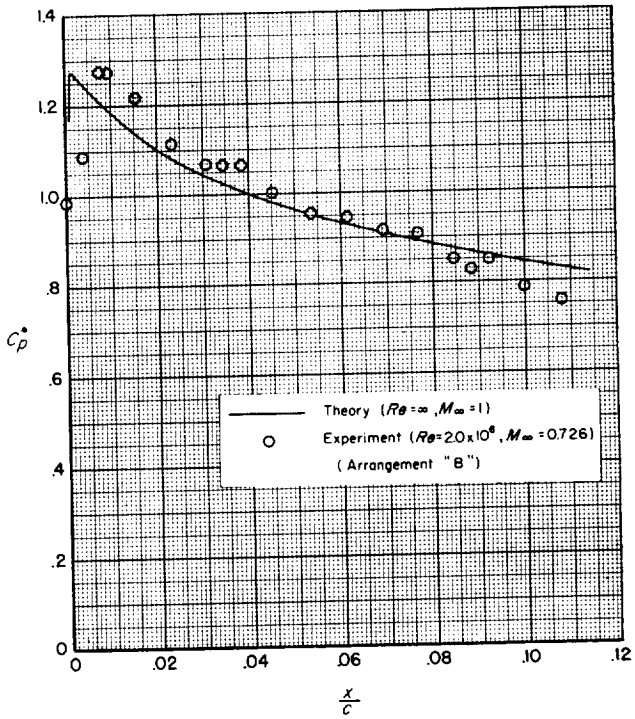

FIGURE 16.—Chordwise pressure distribution on lower surface near leading edge.

stream Mach number of unity is plotted versus dimensionless distance along the lower surface. Except for the discrepancy near the stagnation point, the agreement between theory and experiment is good.

Finally, it is of interest, in view of the experience gained in attempting to calculate the essential features of the flow under study, to speculate upon the mechanisms involved in the process of transonic attachment. Lindsey and Landrum, reference 4, observe that, as the speed is increased, attachment occurs when the supersonic region near the leading edge has grown sufficiently to promote the required decrease in the upwash at the leading edge. Wood, reference 14, hypothesizes that a further factor which may influence the process is the interaction of the terminal shock wave structure with the separated layer, attachment being prevented unless and until the interaction region has moved far enough downstream that its influence cannot be felt at the leading edge. In addition, it is now proposed in this report, for bodies comparable to that under study here, to regard attachment primarily as a natural consequence of a lowering of the pressure in the separated region. The additional mechanism responsible is the combined scavenging action of the boundary layer leaving the trailing edge on the underside of the body and the separated layer leaving the leading edge. As soon as sonic conditions are established at leading and trailing edges, the wake becomes effectively isolated from the subsonic field and the wake pressure then becomes dependent primarily upon conditions established by the pumping action of the respective boundary layers. As the sonic line at the leading edge continues to lengthen with increasing speed, the separated layer over the upper surface is forced to curve more and more toward the upper surface as a result of the impingement of compression wavelets from the sonic line. Meanwhile, the flow on the lower surface at the trailing edge begins to expand around the corner. When the separated layer finally impinges upon the wake from the lower surface, the stage is set for the rapid establishment of the attached flow condition, because it then becomes possible for the pressure in the region between the convergent streams to be much less than the pressure in the downstream wake (refs. 8 and 9). Since the mass flow scavenged by the separated layer greatly exceeds the mass flow reversed by the coalescence of the layers from upper and lower surfaces, the pressure falls rapidly and therefore the length of the separated region must decrease. Equilibrium becomes established when the attachment zone has moved upstream to a position where the mass flow reversed into the bubble is just equal to that scavenged by the separated layer.

CONCLUSIONS

A theoretical and experimental study has been made of a two-dimensional asymmetric transonic flow past a sharp leading edge. The experimental portion of the study yields detailed density distributions as obtained by methods of X-ray densitometry in the zone from 15.4 to within 0.77-percent chord of the leading edge of a 12° wedge. The lower surface was inclined 13° to the air stream in a closed-throat wind tunnel operated near the choking Mach number over a Reynolds number range from 1×10^6 to 3×10^6. From these surveys are determined the locations of the stagnation point, sonic line, boundary of separation bubble on the upper surface, and the value of the local Mach number on the bubble edge. The theoretical portion develops a means for representing an unbounded viscous flow at a free-stream Mach number of 1 by an inviscid flow so chosen by known theoretical considerations of viscosity as to satisfy viscous requirements at a single point in the field. A comparison of the results of these two portions of the study shows that, in general, the essential features of the experimentally determined flow can be predicted by the theoretical model.

Experiment and theory are in agreement with regard to the following specific details:

(1) Values of the density at fixed locations in the flow field in regions of the flow where the local Mach number is 2 or less.

(2) Insensitivity of the flow near the leading edge to changes in Reynolds number.

(3) Values of the pressure coefficient on the lower surface of the airfoil except very near the stagnation point.

The theoretically determined flow field does not agree quantitatively with the experimentally determined flow field in the matters of (a) length of separation bubble, (b) Mach number on bubble edge, and (c) location of stagnation point. One reason offered for this lack of agreement is a possibility that the theoretical solution is not unique and that another solution in better agreement with experiment exists. Another is that the experimental arrangement did not simulate with sufficient accuracy the conditions demanded by theory.

AMES RESEARCH CENTER
NATIONAL AERONAUTICS AND SPACE ADMINISTRATION
MOFFETT FIELD, CALIF., *Aug. 25, 1959*

546395 60 4

APPENDIX A

DESCRIPTION OF X-RAY DENSITOMETER EQUIPMENT, DENSITOMETER OPERATION, AND THE DENSITY DETERMINATION PROCESS

The purposes of this appendix are to describe the X-ray densitometer apparatus, explain how it was operated, and indicate the particular ways air densities were determined by X-ray absorption (ref. 15). In all prior aerodynamic applications of the X-ray densitometer known to the authors (e.g., refs. 12, 16, 17, 18, 19, 20, and 21), less complete surveys than those discussed in this report have been made in simpler flow patterns and these surveys have been accomplished by moving the flow pattern with respect to an immobile X-ray beam or by scanning with a narrow beam with one degree of freedom (ref. 16). It is believed that the present investigation represents the first attempt to deal with the rather difficult problems which accrue when a pattern is surveyed with a narrow beam moved relative to the flow pattern and having more than one degree of freedom. It is further believed that the radiographs produced in the present investigation represent the first from which extensive aerodynamic data for a fairly complex flow field have been obtained. It is felt that the experimental results are of sufficient interest to warrant a rather detailed description of the apparatus evolved for obtaining them and of its operation.

DENSITOMETER APPARATUS

Photographs of densitometer arrangement A installed at the wind tunnel are shown in figures 17 and 18.

X-ray generator.—The structure of the X-ray generator as used in arrangement A is illustrated in figure 4. The drawing, a cross section on the

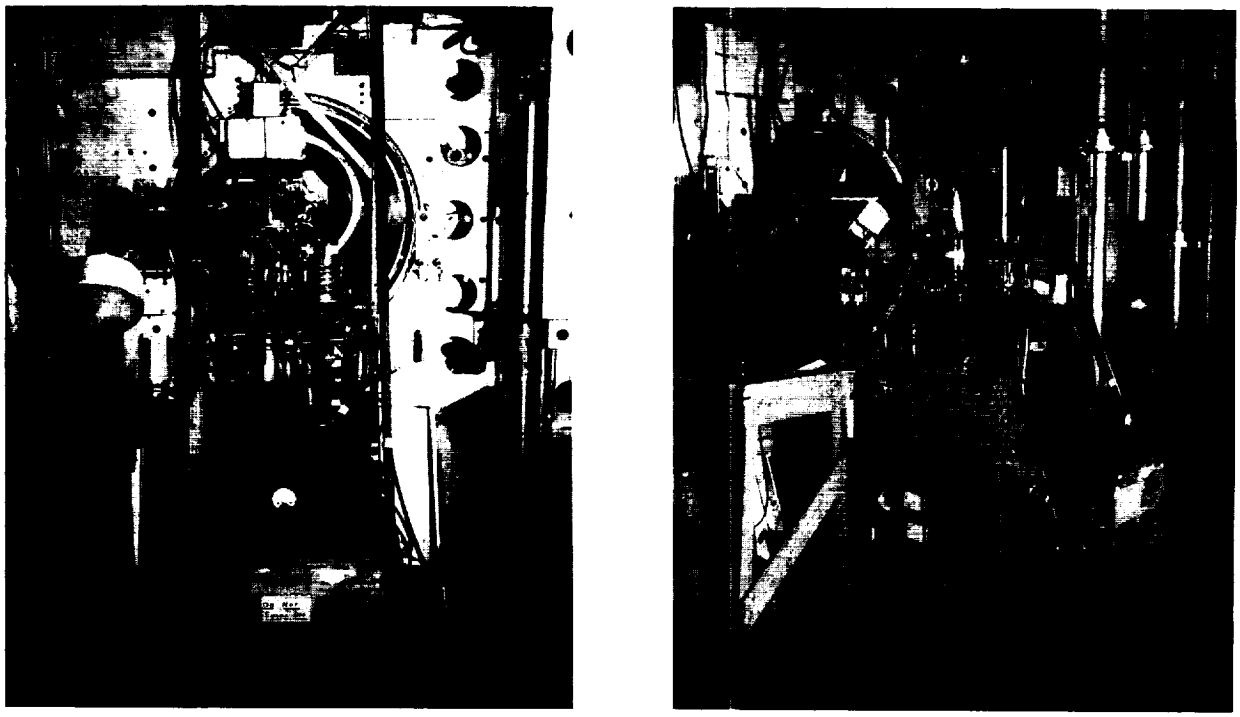

(a) General view normal to tunnel wall.

(b) Three-quarter view.

FIGURE 17.—X-ray densitometer arrangement A from X-ray transmitting side.

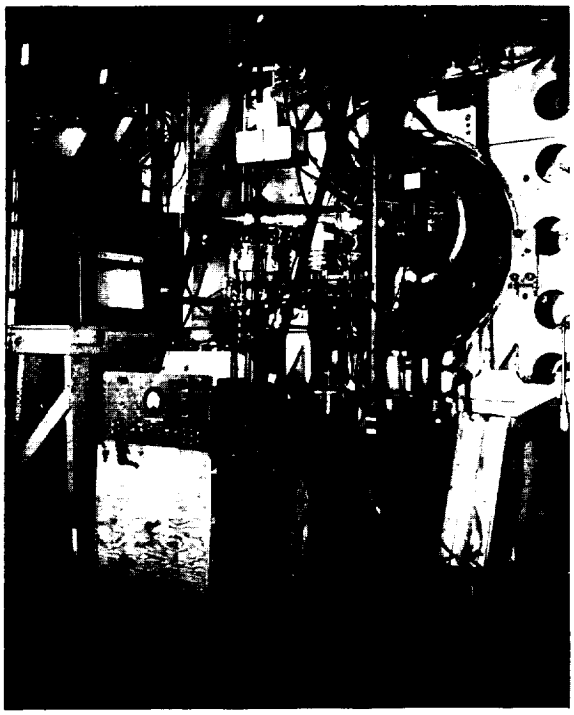

(c) Three-quarter view.

(d) Close-up from same angle as in (c).

FIGURE 17.—Continued.

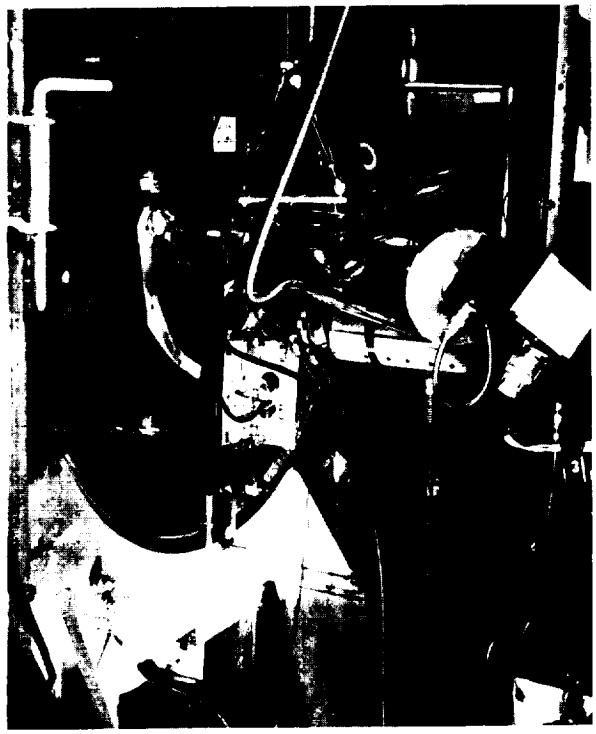

(e) Close-up showing reference chamber, with heat shield, and reference Geiger-Mueller counter.

FIGURE 17.—Concluded.

plane of horizontal symmetry, shows the central cavity of the water-cooled brass housing within which the X-rays are produced, and the two cavity extensions which transmit and shape the tunnel X-ray beam and the reference X-ray beam.

As is shown in figure 4, the 0.050-inch-diameter tungsten target was embedded in a copper stud which in turn was screwed into a tapped hole in the wall of the central cavity. The electron gun consisted of a pancake spiral filament of thoriated tungsten as a source of electrons which was enclosed in a ¾-inch-diameter cylindrical beam-forming electrode of nickel. One filament conductor and the beam-forming electrode were connected electrically, but the gun as a whole was isolated electrically from target potential (ground) by means of stand-off and pass-through glass insulators. The target extended through a hole in the end of the beam-forming electrode and, for maximum X-ray beam intensity for given power input, the end of the target was flush with the inner surface of the end wall of the beam-forming electrode. The plane of the filament

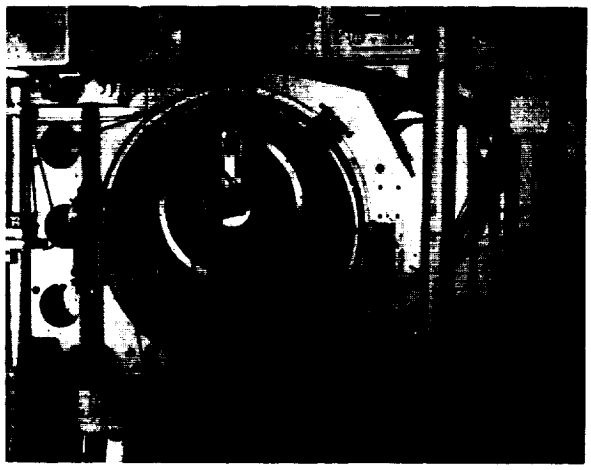

FIGURE 18.—View of tunnel window plate and Geiger-Mueller counter on X-ray receiving side.

spiral was about 0.10 inch from the surface of the target.

Two holes in opposite walls of the nickel cylinder permitted a portion of the X-rays generated at the surface of the target to pass out of the central cavity and into each of the cavity extensions. Each cavity extension was essentially a collimating tube which contained 0.010-inch diameter apertures.

The tube which transmitted the tunnel X-ray beam had two such apertures in order to minimize beam spread, and thus reflection problems; however, the tube transmitting the reference beam had but one. The collimating tubes were adjustable with respect to the X-ray generator housing; their axes could be individually translated while the generator was in operation so as to place each in line with the spot of most intense X-radiation from the target.

The exposed ends of the collimating tubes were equipped with 0.0012-inch-thick cellophane windows. Because cellophane is permeable to the water molecule, and because other small leaks typical of such an enclosure existed, the cavity of the X-ray generator was connected to a conventional, continuously operated vacuum pumping system. The pressure within the cavity was maintained at less than 10^{-5} mm Hg for stable production of X-rays.

The anode-to-cathode potential of the X-ray tube was continuously adjustable in the range 1000 to 7500 volts (direct current) and was regulated to 0.1 percent. The temperature-limited emission current was also regulated and continuously adjustable and could be set at any value within the range 0 to 0.05 amperes. However, at power inputs above 130 watts target melting was experienced.

The X-ray generator as used in arrangement B had no collimating apertures. The entire surface of the X-ray target could be "seen" from each point in the plane of the film except for certain points in the neighborhood of the test body. To prevent incandescence within the X-ray tube from exposing the film to visible light, a supplementary aluminum-coated film of polyethylene terephthalate covered the regular cellophane window of the collimating tube.

X-ray beam positioning and support.—For arrangement A, the X-ray generator was linked to the wind-tunnel wall in such a manner that the 0.010-inch-diameter X-ray beam which crossed the test section could be made to describe a cylinder about the virtual leading edge of the test body (fig. 2). The radius of the beam path was established by the eccentricity of a hole in a cylindrical bushing of steel. This hole carried the collimating tube of the X-ray generator, and the bushing; in turn was mated with a precision bore in the test body support plate.

A number of bushings with various values of eccentricity were provided. Their lengths were such that their ends were flush with the wind-tunnel air stream and such that the window on the end of the collimating tube was $\frac{1}{32}$ inch from the air stream. The X-ray beam passed into the air stream through 0.020-inch-diameter apertures in the ends of the bushings. The test body lacked 0.001 inch at each tip of completely spanning the test section and thus provided clearance between bushings and tips.

Rotation of a bushing about its axis caused the X-ray beam to orbit about the leading edge of the test body. Rotation of the X-ray generator about the collimating tube axis was prohibited by the arrangement of the vacuum pumps and interconnecting vacuum pump lines; however, the X-ray generator had freedom to translate as demanded by the eccentricity of a given bushing. A protractor arm, with vernier, attached to each gear-and-crank driven bushing allowed measurement of rotation angles with an error of ± 1 minute of arc. A system of friction locks allowed at any angle immobilization of bushing with

respect to support plate and collimating tube with respect to bushing.

The support plate on the opposite side of the wind tunnel carried similar bushings. These bushings on the X-ray-detection side of the wind tunnel had 0.004-inch-diameter apertures at radii corresponding to those taken by the axis of the 0.010-inch-diameter X-ray beam. The window of the Geiger-Mueller quantum counter immediately behind this 0.004-inch aperture was about $\frac{1}{32}$ inch from the wind-tunnel air stream. Alinement of the support plates and construction of corresponding pairs of bushings was such that the central portion of the 0.010-inch-diameter X-ray beam impinged on the 0.004-inch-diameter aperture over the G–M counter window when the protractors were set at the same nominal value of angle, ϕ.

It need hardly be stated that the machine work required to accomplish all this was of the highest quality and precision. Most of the fits between critical moving surfaces met tolerance limits of ± 0.0001 inch.

The chamber traversed by the reference X-ray beam was a 2.75-inch inside-diameter aluminum cylinder. This tube was cantilevered from the reference collimating tube on the X-ray generator and had provisions for mounting a quantum counter at the free end. The distance bwtween the cellophane windows on the collimating tube and the quantum counter was the same as the distance between corresponding elements in the path of the tunnel X-ray beam. The cross-section area of the X-ray beam which entered the reference G–M tube was established by adjustable slits just ahead of the G–M counter window. The reference chamber was provided with pressure orifices and iron-constantan thermocouples so that the reference density could be determined. A controllable pressure regulator was used to adjust the pressure of the dry air in the reference chamber.

For arrangement B, as is shown in figure 3(b), distortion of the radiographs due to divergence of the X-ray beam was minimized by making the distance between source and photographic emulsion large as compared to the width of the wind-tunnel test section. A brass tube through which the X-rays passed connected source and wind tunnel. The end of the fairly flexible tube passed through a rigid supporting yoke which both immobilized and provided for alinement of the X-ray generator with respect to the test body in the wind tunnel. This tube was evacuated to a pressure of 10^{-3} inches Hg to reduce absorption losses along the propagation path between X-ray source and wind-tunnel air stream. The wind-tunnel air stream was separated from the evacuated tube by a 2-inch-diameter (0.001 inch thick) membrane of polyethylene terephthalate. This material is relatively unaffected by weak 2.5 Å X-radiation and has excellent mechanical strength characteristics. However, the relatively high pressure in the wind-tunnel test section caused the membrane to sag into the tube, thus producing a $\frac{1}{2}$-inch (maximum) gap at the airfoil tip.

X-ray detection. The quantum counter systems used in arrangement A were identical in design to those described in reference 12. They included argon-filled Geiger-Mueller tubes with a quenching admixture of ethyl alcohol at an absolute pressure of about 4 inches Hg. The end-mounted windows were of 0.0012-inch-thick cellophane. External quenching and shaping circuits were used in conjunction with the G–M tubes so that all output pulses were the same size and shape and so that the resolving time of the combination would be less than the sum of the dead time and recovery time of the tubes when in a passive circuit. The pulse outputs of the shaping circuits were accumulated and displayed on commercially available scale-of-ten gas tube electronic counters. An electrically operated interval timer with a least count of one second simultaneously activated and deactivated the two electronic counters which collected the outputs of the tunnel and the refere ce quantum counter systems.

The X-ray film used with arrangement B was a standard, double-emulsion, cut film. All film used in the present investigation was taken from the same manufacturer's lot and was cut into 2-inch-diameter circles. The film was held in a shallow cavity in the wind-tunnel wall opposite the plastic membrane by means of a vacuum chuck so that the emulsion surface was recessed 0.008 inch. The film was exposed to the rays from the continuously operated X-ray source by means of a magnetically operated metallic shutter within the evacuated tube.

The instrument used for analysis of the radiographs is one which is used primarily for the analysis of spectrographs. It consists of (1) an enclosure which contains the retractable pickup head, a

stable vacuum photomultiplier tube and a projection screen, (2) a fixed base which encloses a 6 volt, 108 watt projection lamp which, by means of a lens and mirror, projects parallel light vertically through the plane of the film, and (3) a movable bed which supports the film-holder and permits motion in the plane of the film.

The pickup head has a 0.004-inch-diameter circular aperture and is provided with a retracting mechanism for use when projection of the film on the screen is desired. In its extended position, the face of the pickup head is parallel with the plane of the film and is adjusted vertically such that a very thin air gap exists between the pickup and the film. This air gap is provided to prevent damage to the film by scratching.

Parallel light is projected through the film from below and enters the 0.004-inch-diameter aperture. A prism within the pickup turns this transmitted light into a light-tight tube which in turn relays the light to the sensitive element of the multiplier tube. The output from the multiplier tube resulting from this incident light is displayed on an electronic voltmeter. This same signal is also sent to the chart drive servo of an electronic recording potentiometer.

The film holder constructed for the 2-inch-diameter film discs allowed rotation in the plane of the film about the disc center and had an angular positioning accuracy of $\pm 0.08°$. Sidewise motion of the movable densitometer bed was measured with two standard dial indicators, each with a maximum of 1-inch travel and a least count of 0.001 inch. Also mounted on the movable bed was a linear transducer which was sensitive to relative motion between the bed and the rigid pickup head enclosure. The resulting signal from this transducer was sent to the pen drive servo of the potentiometer, and thus a continuous trace of output from the photomultiplier tube versus linear displacement across the surface of the film could be displayed on the recording paper. Calibration of the linear motion transducer was accomplished with the aid of the dial indicators.

A calibration of the photomultiplier tube with respect to film density was obtained in the following manner: Several films were exposed with no flow in the wind tunnel and with the air density known in each case. These films were successively placed in the densitometer and an average voltage reading for each film was obtained. A graph was then made of voltage as a function of air density. The voltages were put into dimensionless form by referencing each reading to the voltage as obtained on the image of the test body. This procedure accounts in part for differences in film density which are not due to differences in air density.

OPERATION OF X-RAY DENSITOMETER

Experiments with densitometer on test stand.— The X-ray densitometer in arrangement A was operated for an extended period of time on a specially constructed stand which simulated the test section of the wind tunnel. Techniques for certain operations which were to be performed during the wind-tunnel tests were initially developed on this stand.

Stability of X-ray production: Of first concern was the production and maintenance of a stable source of X-rays. With the present equipment, stable X-ray production could be achieved by continuous operation at a given X-ray voltage and X-ray emission current after elapse of a 24-hour period. Stability was judged to exist when repeated samples of quantum counts over arbitrary but identical time intervals had standard deviations indistinguishable from those of Poisson statistics (refs. 22, 23, and 24). Counting rates of about 8,000 quanta per minute were achieved for density-path lengths of one atmosphere-foot with 2.3 Å radiation through a 0.004-inch-diameter aperture over the counter tube window.

Movement of X-ray beam: Tests were made with the stable X-ray source to determine the effects of beam movement on the intensity received on the opposite side of the wind tunnel. Random variations in repeatability of a given setting due to clearances between mating parts and nonreproducible strains in the positioning mechanism were reduced until they were equal to or less than the variations due to counting statistics. Residual misalinements caused the apparent intensity of the X-ray beam which crossed the wind tunnel to vary in a cyclic manner as the X-ray generator was orbited about the axis through the projected leading edge of the test body. This variation changed a small but detectable amount over periods of months as a result of creep of metal and slippage of hold-down bolts; the change being most rapid immediately following realinement of the support plates. The apparent intensity variation due to these beam-aiming aberrations was handled as a calibration which was repeated with

sufficient frequency that the drift effect was accounted for with negligible uncertainty.

Geiger-Mueller quantum counters: A third series of no-flow experiments was concerned with the efficiency, reliability, and resolving time of the G–M counters used with densitometer arrangement A. Because of slight physical differences among individual counters it was a practical impossibility to obtain identical intensity indications from a group of them in a radiation field known to be unvarying. Moreover, the G–M counters had characteristic curves which depended both upon the internal concentration of water vapor and upon age (total number of quanta counted). In the face of these complications, coupled with the additional fact that the counters missed counts owing to finite resolving time, it was a difficult and time-consuming task to obtain reliable estimates of the intensity of the X-ray beams.

Because it was desired to use G–M counters in pairs, it became necessary to determine the ratio of the efficiencies of each pair of counters which happened to be employed during any given period of time. Successive exposures of the pair to the constant source of X-rays for equal intervals of time provided the necessary information. It was the more frequent practice, however, to interchange counters between the reference X-ray beam and the tunnel X-ray beam and to deduce the counter efficiency ratio from the successive pairs of ratios of tunnel intensity to reference intensity so obtained.

Because moisture affects their operation, and moreover because water vapor diffuses freely through the cellophane windows used on the G–M counters, the intensity indications were dependent on environmental changes of humidity. To minimize this influence, the counters were stored in a desiccator. When in use, the counter windows were exposed to the somewhat less dry air in the wind tunnel, except for the brief intervals of time required to effect the interchange of pairs of counters or to replace those which had become inoperative. To account for the small changes in intensity indications incident to these operations and to the aging of the counters with use, it was the practice to carry out the interchange experiment periodically and thus to establish the variation with time of the ratio of Geiger-Mueller counter efficiencies.

Resolving time of a G-M quantum counting system is the time interval immediately following the registration of a quantum during which the system is paralyzed. During a finite time interval, therefore, the system can receive and record events for some fraction of this interval which depends upon the number of events detected. Thus, the resolving time must be known if output is to be rendered proportional to input for a wide range of inputs. The resolving times of the counting systems used with the apparatus described were determined by use of a cathode ray oscilloscope with a triggered sweep circuit. The method of measurement was similar to that described in reference 25. Because of the characteristics of the vacuum-tube quenching circuits coupled to the G–M counters, the resolving times were less than they would have been had the quench circuits not been used. However, their use made the resolving times definite decreasing functions of the increment of anode voltage on the G–M counter above that at the threshold of Geiger counting. Resolving times from 300 microseconds near threshold to 70 microseconds near runaway were measured. For most of the tests in the wind tunnel, the most probable value of resolving time representative of both counter systems is 133 μsec, with a range of uncertainty between 190 and 100 μsec.

Experiments with densitometer in wind tunnel.—The influence of wind-tunnel operation upon the operation of densitometer arrangement A was assessed by calibrations in the empty tunnel. Tests were made to determine the change in aim of the X-ray beam which crossed the test section as a result of relative movement of the wind-tunnel walls. Such shifts as occurred due to operation of the tunnel drive system and variation of pressure and temperature at the test section had an undetectable effect on aim.

Operation of densitometer arrangement A very near the surface of the test body, however, was complicated by the reception of X-rays reflected from the surface of the test body at grazing incidences. Reflections increased the apparent intensity of the tunnel X-ray beam and led to the impression that a decrease in air density had occurred as the surface was approached. Although the reflection effect alone could be handled by calibrations with no flow in the wind tunnel, the deflection of the test body due to flow forces so changed the reflection patterns that precise density determinations with arrangement A very near the body surface were nearly always impossible.

With arrangement B it was possible to position the source of X-rays so that reflections caused negligible intensity increases adjacent to the body surface. The positioning was done by means of intensity surveys with Geiger-Mueller counters. The X-ray source was adjusted so that the spot on the target of most intense radiation was near the axis through the virtual leading edge of the test body. It was possible with optimum alinement to obtain from radiographs values of density right up to the image of the body surface. These values were in doubt, however, because the radiation path was not precisely parallel to a body generator and also because of deflection of the body under aerodynamic load.

DETERMINATION OF AIR DENSITY IN THE FLOW FIELD FROM X-RAY INTENSITY DATA

The experimental procedure for obtaining air densities in the flow field from the G–M counting data was essentially one of matching an intensity measurement of the beam through the flow field with a measurement of the beam intensity through the reference chamber, the density of air in which being determined by measurements of pressure and temperature. This procedure is discussed in the following in terms of the monochromatic X-ray absorption law (Lambert's law). The X-ray beams emerging from the collimating tubes of the densitometer were neither coherent nor monochromatic and thus Lambert's law is not rigorously applicable. It serves, however, fairly well as an approximation (to within 2 percent) to the experimentally observed intensity-density relationship for data taken with the densitometer over density increments equal to about 0.000250 gms/cc (0.000485 slugs/cu ft) and provides the only analytical expression available to work with simply and completely.

The first step in the density measurement consisted of calibrating the mechanical movements of the pair of bushings which carried the transmitting collimating tube (attached to the X-ray generator) and the receiving G–M tube around the projected leading edge of the model. For this calibration the tunnel air was static and the air densities in tunnel and reference chamber were measured and, by adjusting pressure in the reference chamber, made to be equal or nearly equal. Then the value of the ratio of tunnel G–M count rate to reference G–M count rate, Q_c, was determined at each value of angle, φ, for which a density measurement in the flow field was desired. (The notation is given in appendix C.) Before, and for some runs during and after, this calibration the ratio of counting efficiencies of the G–M counters was measured by the interchange of counters described below. From these data, values of the quantities $(A_T/A_R)q$ and $\rho_T-\rho_R=\beta_c\cong 0$ were obtained for each value of φ and this set of corresponding values constitutes the "calibration" for the given pair of bushings. In the simplest, ideal case this would give a value of the ratio of tunnel beam intensity to reference beam intensity for the condition $\rho_T=\rho_R$, which would be matched in the flow field run by adjusting reference pressure and hence reference density, ρ_R, thereby yielding a measurement of the desired flow field density, ρ_T. The flow field density, ρ_T, in this discussion is, of course, the integrated density across the span of the model without discrimination of boundary layer variations.

In practice, for the flow field runs the matching was accomplished by measuring at each φ the ratio of tunnel G–M count rate to reference G–M count rate, Q, for three (and sometimes more) different values of ρ_R, chosen such that the match point determined in the calibration would lie inside the range of values of $(A_T/A_R)q$ thus determined. Measured background count rates were less than the standard deviations of the tunnel and reference count rates in nearly every measurement and they have therefore been ignored. The quantity $(A_T/A_R)_f$ was computed from Q and the ratio of G–M counter efficiencies as measured again specifically for the flow field run (before, after, and, in some cases, during). Judging the values of ρ_R to use in order that the calibration value of $(A_T/A_R)_f$ be bracketed by the values resulting from the flow field measurements was a simple matter of operational experience. For each φ, then, considering the narrow range covered by the values of ρ_R, a straight line was fitted to the $ln[(A_T/A_R)q]$ *vs.* ρ_R data by the least squares method or by a graphical plot. In the use of the least squares method the equation of this line was computed and solved for $\rho_R=\rho_T-\beta_c$ with the match point value of $ln[(A_T/A_R)q]$ from the calibration. The residual density increment, β_c, was added to this result giving ρ_T, the integrated density across the flow field at the position (r, φ).

The above procedure can be described in fuller

detail, and the basis for corrections made to the density measurements for counter resolving time can be explained, by now considering the expressions for Lambert's law and for X-ray beam intensity. The absorption law states that

$$i=i_o e^{-\mu y \rho} \tag{A1}$$

where i_o is the initial intensity, i is the intensity after absorption over a distance y, ρ is the density of absorbing medium, and μ is the mass absorption coefficient, which is a function of wavelength and of the absorbing medium.

Intensity of an X-ray beam in the densitometer detected by a G–M counter is given by

$$i=\frac{N}{\epsilon}\frac{h\nu}{A} \tag{A2}$$

where N is the G–M count rate, ϵ is the G–M efficiency, A is the effective "area" of collimating arrangement, $h\nu$ is the X-ray quantum.

The ratio of G–M counter efficiencies, ϵ_T/ϵ_R, was measured by interchanging counters with respect to X-ray beams detected. Position "one" for the counters is illustrated in the diagram; G_1 denotes counter number 1; G_2, counter number 2.

$$\boxed{G_1} \xleftarrow[i_T]{(T)} \quad i_{oT} \otimes i_{oR} \quad \xrightarrow[i_R]{(R)} \boxed{G_2} \tag{I}$$

The ratio of count rates, $Q_1=N_{T1}/N_{R2}$, was determined for this arrangement. By equation (A2),

$$Q_1=\frac{N_{T1}}{N_{R2}}=\left(\frac{i_T \epsilon_1 A_T}{h\nu}\right)\left(\frac{h\nu}{i_R \epsilon_2 A_R}\right)=\frac{i_T}{i_R}\frac{\epsilon_1}{\epsilon_2}\frac{A_T}{A_R}$$

Next the counter positions were interchanged.

$$\boxed{G_2} \xleftarrow[i_T]{(T)} \quad \otimes \quad \xrightarrow[i_R]{(R)} \boxed{G_1} \tag{II}$$

The ratio Q_2 was determined, and from equation (A2)

$$Q_2=\frac{N_{T2}}{N_{R1}}=\frac{i_T}{i_R}\frac{\epsilon_2}{\epsilon_1}\frac{A_T}{A_R}$$

During this interchange of counters the densitometer was operated under conditions such that i_T/i_R remained constant throughout. Therefore

$$\frac{Q_1}{Q_2}=\left(\frac{\epsilon_1}{\epsilon_2}\right)^2 \tag{A3}$$

and

$$\frac{1}{2}\ln\frac{Q_1}{Q_2}=\ln\frac{\epsilon_1}{\epsilon_2} \tag{A4}$$

All measurements were taken and data were reduced in terms of the ratio of tunnel count rate to reference count rate. Hence, consider the true intensity ratio as given by equation (A1),

$$\frac{i_T}{i_R}=\frac{i_{oT}e^{-\mu y_T \rho_T}}{i_{oR}e^{-\mu y_R \rho_R}}$$

From the geometry of the apparatus, $y_T=y_R=l$ (by design), and thus

$$q=\frac{i_T}{i_R}=q_o e^{-\mu l(\rho_T-\rho_R)}$$

and

$$\ln q=\ln\left(\frac{i_T}{i_R}\right)=-\mu l(\rho_T-\rho_R)+\ln q_o \tag{A5}$$

From equation (A2),

$$q=\frac{i_T}{i_R}=\left(\frac{N_T}{\epsilon_1}\frac{h\nu}{A_T}\right)\left(\frac{\epsilon_2}{N_R}\frac{A_R}{h\nu}\right)=Q\frac{\epsilon_2}{\epsilon_1}\frac{A_R}{A_T} \tag{A6}$$

where $Q=N_T/N_R$ and it is assumed counter number 1 receives the beam through the tunnel, which was the standard practice throughout all runs and calibrations. Combining the above with equations (A4) and (A5) yields

$$\ln Q-\frac{1}{2}\ln\frac{Q_1}{Q_2}-\ln\frac{A_T}{A_R}-\ln q_o=-\mu l(\rho_T-\rho_R) \tag{A7}$$

For the calibration data, equation (A7) becomes

$$\ln Q_c-\frac{1}{2}\ln\frac{Q_{1c}}{Q_{2c}}-\ln\frac{A_T}{A_R}-\ln q_o=-\mu l\beta_c \tag{A8}$$

It can be assumed that $q_o=i_{oT}/i_{oR}$ remained the same for the flow field run and calibration since the X-ray generator was operated continuously under constant conditions with no known changes in the cellophane windows through which the beams passed and no changes in the collimating apertures. Likewise, for any value of φ, A_T/A_R remained constant from calibration to flow field run. Therefore, subtraction of (A8) from (A7) gives

$$\ln\frac{Q}{Q_c}-\frac{1}{2}\ln\left[\left(\frac{Q_1}{Q_2}\right)\left(\frac{Q_{2c}}{Q_{1c}}\right)\right]=-\mu l(\rho_T-\rho_R-\beta_c) \tag{A9}$$

or

$$\ln\left[Q\left(\frac{Q_2}{Q_1}\right)^{1/2}\right]-\ln\left[Q_c\left(\frac{Q_{2c}}{Q_{1c}}\right)^{1/2}\right]=-\mu l(\rho_T-\rho_R-\beta_c) \tag{A10}$$

Equation (A7) rewritten shows the relationship between the measured quantities used as described at the beginning of this section of the appendix to deduce values of density. Thus,

$$\ln\left[Q\left(\frac{Q_2}{Q_1}\right)^{1/2}\right]=(\mu l)\rho_R+\left(\ln\frac{A_T}{A_R}+\ln q_o-\mu l\rho_T\right)$$

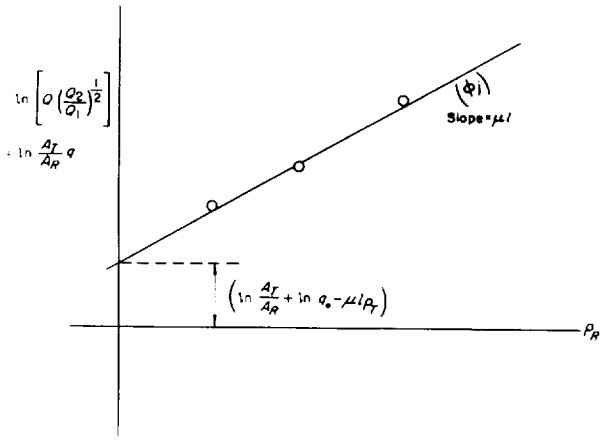

Sketch (a)

it being observed that at any angle, φ, ρ_T is constant (as are A_T/A_R and q_o) and also that from equations (A3) and (A6)

$$Q\left(\frac{Q_2}{Q_1}\right)^{1/2}=\frac{A_T}{A_R}q$$

For each angle, φ, then, in each flow field run a relationship was established as shown in sketch (a). From equation (A10) it is seen that the value for $Q(Q_2/Q_1)^{1/2}$ in the above relation that corresponds to the condition $\rho_R=\rho_T-\beta_c$ is given by

$$\ln\left[Q\left(\frac{Q_2}{Q_1}\right)^{1/2}\right]-\ln\left[Q_c\left(\frac{Q_{2c}}{Q_{1c}}\right)^{1/2}\right]=0$$

that is,

$$\ln\left[Q\left(\frac{Q_2}{Q_1}\right)^{1/2}\right]_{\text{match}}=\ln\left[Q_c\left(\frac{Q_{2c}}{Q_{1c}}\right)^{1/2}\right] \tag{A10a}$$

Time-dependent variations in ϵ_1/ϵ_2 were observed to occur during some runs and calibrations even when ϵ_1/ϵ_2 was computed from count rate data corrected for resolving time. This change in counter efficiencies is attributed to aging effects in the G–M tubes, uncontrollable variations in the water vapor content of the G–M tube gas mixture during measurements and slight variations in the applied voltages (the G–M tube characteristic curves did not possess perfectly flat plateaus and, as mentioned elsewhere, the resolving time was dependent on the G–M tube voltage). Account was taken of this variation wherever possible by recording times of making measurements at each φ and in the data reduction obtaining the value of Q_1/Q_2 for each φ from a plot of Q_1/Q_2 vs. time. (A linear variation in Q_1/Q_2 with time was assumed between measurements taken before, after, and in some instances during a run and/or calibration.) Where insufficient time data existed, but Q_1/Q_2 variations were measured, the foregoing method was approximated by simple interpolation.

Geiger-Mueller counter resolving time corrections were applied to the densities in two ways. Densities from some runs were determined by the above method using count rate data corrected directly for resolving time. The densities from some other runs were measured first as above using uncorrected counting data and then were corrected by the formula deduced below.

The equation relating observed count rate, corrected count rate, and resolving time is (refs. 22, 24, 26, and 27)

$$N'=\frac{N}{1-N\sigma} \tag{A11}$$

where N' is the corrected count rate, N is the observed count rate, and σ is the resolving time. Let other primed symbols denote quantities which are functions of corrected count rates. Thus,

$$Q'=\frac{N'_T}{N'_R}, \qquad Q'_1=\frac{N'_{T1}}{N'_{R2}}, \qquad \text{etc.}$$

From equation (A11) in combination with the definitions and relations already introduced in the preceding discussion, it follows that

$$\left.\begin{aligned} Q'&=Q\,\frac{1-N_R\sigma_2}{1-N_T\sigma_1} \\ \text{and} \\ Q'_1&=Q_1\,(1-N_{R2}\sigma_2)(1-N_{T2}\sigma_2) \\ Q'_2&=Q_2\,(1-N_{R1}\sigma_1)(1-N_{T1}\sigma_1) \end{aligned}\right\} \tag{A12}$$

Consider equation (A10a) to be expressed in terms of Q', Q'_c, Q'_1, Q'_2, Q'_{1c}, Q'_{2c}. Then by substitution in (A10a) from equations (A12), and by algebraic simplification and rearrangement of terms it further follows that for the "matching condition," $\rho_R=\rho_T-\beta_c$,

$$\ln\left[Q\left(\frac{Q_2}{Q_1}\right)^{1/2}\right]=\ln\left[N_T\sigma_2\left(\frac{Q_2}{Q_1}\right)^{1/2}+(Q_c-N_{Tc}\sigma_2)\left(\frac{Q_{2c}}{Q_{1c}}\right)^{1/2}F\right] \quad \text{(A13)}$$

where

$$F=\left[\frac{(1-N_{R1c}\sigma_1)(1-N_{T1c}\sigma_1)(1-N_{R2}\sigma_2)(1-N_{T2}\sigma_2)(1-N_T\sigma_1)^2}{(1-N_{R2c}\sigma_2)(1-N_{T2c}\sigma_2)(1-N_{R1}\sigma_1)(1-N_{T1}\sigma_1)(1-N_{Tc}\sigma_1)^2}\right]^{1/2}$$

and it is observed that $Q_M=N_T/N_R$. Thus equation (A13) gives the value to use in solving for resolving time corrected density from the (uncorrected) $Q(Q_2/Q_1)^{1/2}$ vs. ρ_R relation. A correction term, $\delta\rho_T$ (computed for each φ), which was applied to densities determined using equation (A10a) with the above uncorrected relation, is readily deduced by examination of the plot illustrated in sketch (b) below. Thus $\delta\rho_T=\{\ln[Q(Q_2/Q_1)^{1/2}]_{10}-\ln[Q(Q_2/Q_1)^{1/2}]_{13}\}/a$, where $\ln[Q(Q_2/Q_1)^{1/2}]_{10}$ was determined by equation (A10a) and $\ln[Q(Q_2/Q_1)^{1/2}]_{13}$ by equation (A13). The slope, a, was known from the least squares solution for the line. Computations employing equation (A13) were simplified somewhat by having $\sigma_1=\sigma_2=\sigma$.

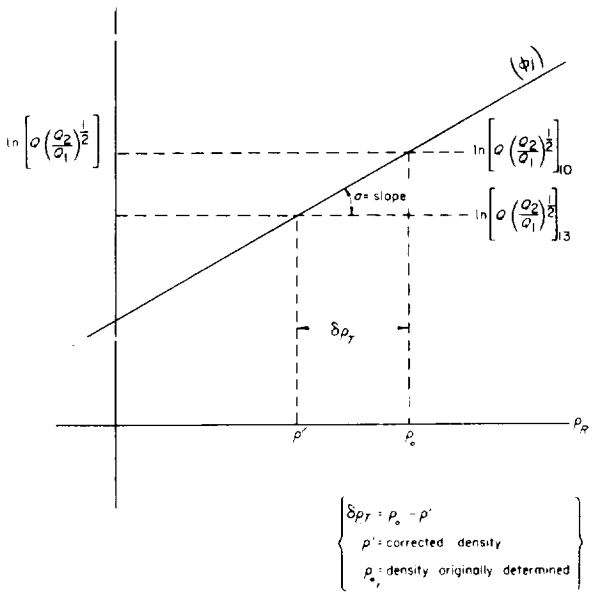

Sketch (b)

DISCUSSION OF ERRORS AND PRECISION OF MEASUREMENTS

The errors encountered in this investigation can be thought of as arising from two separate sources. The first of these is the inability of the experimental arrangement to faithfully simulate two-dimensional flow. The second is the inadequacy of the densitometer to measure exactly the density which exists in the non-two-dimensional environment. These two types of errors are discussed in the following paragraphs.

Non-two-dimensional effects.—The values of density ratio appearing in table I contain systematic errors which arise both from the wind-tunnel wall boundary layers and from the leakage through the clearance gaps at the airfoil tips. The presence of the gaps at the tips, in combination with the side-wall boundary-layer effect, produces the situation illustrated in figure 19. Here are plotted the average density distributions for the smallest (fig. 19(a)) and the largest (fig. 19(b)) values of radius ratio as measured with the densitometer at Mach number 0.705 and Reynolds number 2×10^6 and the corresponding pressure distributions as measured locally on the side walls of the wind tunnel (fig. 6(a)). Also shown are three calculated curves which represent estimates of the stream core density obtained by various means. Remembering that the local pressure distributions on the wall can be considered to be approximate density distributions, one notes that for both values of radius ratio there exist systematic differences between the distributions as represented by average densities across the span and as represented by local densities on the wind-tunnel wall. As would be expected as a result of the effects of the heating in the side-wall boundary layers the wall density values tend to be lower than the

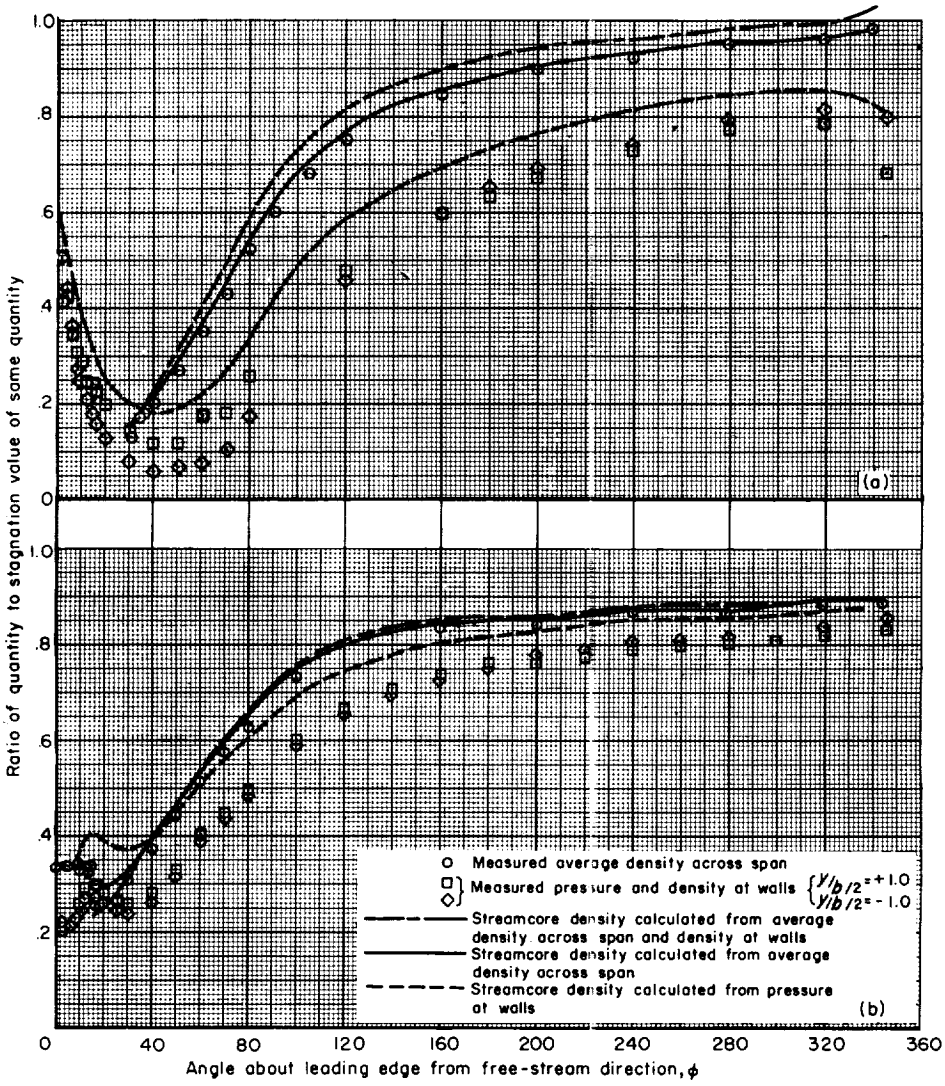

(a) $r/c=0.0077$
(b) $r/c=0.154$

FIGURE 19.—Comparison of density distributions as obtained by densitometer with those obtained from wall pressure distributions.

spanwise average density values. However, very near the upper surface of the body the effect of the leakage tends to overcome this influence and the values of wall density tend to exceed the average values. It can also be expected that the leakage would tend to make the wall density values near the lower surface of the body somewhat lower than they would be as a result of the heating alone. These trends are noted to be much more pronounced for the survey closest to the leading edge, 0.77-percent chord (fig. 19(a)), than they are at the largest survey radius, 15.4-percent chord (fig. 19(b)).

In addition to the data shown in each of figures 19(a) and 19(b), three calculated curves are presented. All of these curves represent estimates of the density in the core of the stream as obtained from the data by methods to be described. The curves cross one another at an angle ϕ of about 40° for both values of radius ratio. The curve which lies lowermost on each of figures 19(a) and 19(b) at angles ϕ greater than 40° (herafter called

the lower curve) is an estimate of the stream core density distribution as calculated from the measured local pressure distributions on the side walls. The lower curve for each value of radius ratio was obtained from an average of the measured pressure distributions on both tunnel walls by the relationships

$$\frac{p_w}{p_t}=\frac{p_c}{p_t}=\left(\frac{\rho_c}{\rho_t}\right)^{\gamma} \tag{A14}$$

where the subscripts w and c refer to wall and stream core values, respectively. The first equality in equations (A14) assumes that boundary layers and gaps have no effect on the spanwise distribution characteristic of ideal conditions on a two-dimensional airfoil. The second equality states that the pressure and density in the stream core are isentropically related.

The middle curves in each of figures 19(a) and 19(b) were computed from the densitometer data with the aid of the following equation:

$$\bar{\rho}=\frac{2}{b}\left(\int_0^{\delta}\rho\,dy+\int_{\delta}^{b/2}\rho_c dy\right) \tag{A15}$$

where $\bar{\rho}$ is the spanwise average density. The density was assumed to vary linearly across the boundary layer from the wall value ρ_w to the core value ρ_c as follows:

$$\rho=\rho_w+(\rho_c-\rho_w)\frac{y}{\delta}, \qquad 0\le y\le\delta \tag{A16}$$

To evaluate the wall density in terms of the core density and stagnation density it was further assumed that the walls were insulated, and that the static pressure was unvarying across the layer. Thus it follows that

$$\frac{\rho_c}{\rho_w}=1+f\left[\left(\frac{\rho_t}{\rho_c}\right)^{\gamma-1}-1\right] \tag{A17}$$

where f is the temperature recovery factor. Finally, the combination of equations (A15), (A16), and (A17) leads to

$$\frac{\rho_w}{\rho_t}=\frac{\rho_c/\rho_t}{1+f\left[(\rho_t/\rho_c)^{\gamma-1}-1\right]}=\frac{(\bar{\rho}/\rho_t)-(\rho_c/\rho_t)\left|1-(\delta/b)\right|}{\delta/b} \tag{A18}$$

The middle curves in figures 19(a) and 19(b) were evaluated from equation (A18) with the temperature recovery factor f equal to 0.9 and the boundary-layer thickness to airfoil span ratio equal to 1/6. Use of these values assumes that the wall boundary layers are turbulent and have the same thickness in the presence of the airfoil as that measured in the empty wind tunnel (see fig. 5(b)).

The upper curve in each of figures 19(a) and 19(b) was calculated by the use of equations (A15) and (A16). However, in this case the measured values of both wall density and average density across the span were used in the evaluation. Again the ratio of δ/b was taken to be 1/6.

The discrepancies between the stream core densities calculated by the foregoing three methods are attributed to the effects of leakage through the gaps at the airfoil tips. They are seen to be much greater for the smaller radius ratio of 0.0077 (fig. 19(a)) than they are for the large radius ratio of 0.154 (fig. 19(b)). From the nature of the assumptions made for calculating each of the three curves and from their relative positions in figures 19(a) and 19(b) it can be reasoned that the effect of the gaps at the airfoil tips on the average density distributions is small compared to the effects of the wall boundary layers. In other words, the spanwise distribution of static pressure is constant over the span except within a small fraction of the boundary-layer thickness from the wall. It can further be reasoned that the density distributions obtained with the densitometer are lower than the density distributions characteristic of the stream core almost everywhere in the flow field explored. Moreover, it can be inferred that the true values of the stream core density must lie somewhere between the middle curve and the upper curve in each of figures 19(a) and 19(b). Thus it can be seen by comparing the densitometer data with these two curves that nowhere in the flow field is the maximum discrepancy greater than about 10 percent.

Geiger-Mueller counter data.—The precision with which the flow field density measurements were made can most readily and directly be estimated from the least squares calculation of the best straight line fitting the $(\rho_R,\ \ln[Q(Q_2/Q_1)^{1/2}])$ data from which density was determined at each ϕ (sketch (a)). The standard deviation in ρ was

computed for a representative sample of data points from the relation (ref. 23)

$$s_M = s_{\rho_R} \sqrt{\frac{k\left(\sum_1^k \xi_j^2 - 2\xi_M \sum_1^k \xi_j + k\xi_M^2\right)}{(k-1)\left[k\sum_1^k \xi_j^2 - \left(\sum_1^k \xi_j\right)^2\right]}}$$

where

$s_M = s(\rho_R)_M$ = standard deviation in ρ_{RM}

s_{ρ_R} = standard deviation in the measured values, $\rho_{R,j}$, with respect to the least squares line

$$= \sqrt{\frac{\sum_1^k [\rho_{R,j} - (m + n\xi_j)]^2}{k-1}}$$

$\rho_{RM} = m + n\xi_M$

m = intercept

n = slope of least squares line

k = number of pairs of measured values of ξ_j, $\rho_{R,j}$

For purposes of this calculation ρ_R has been taken as the dependent variable; $\ln[Q(Q_2/Q_1)^{1/2}]$ has been taken as ξ; the quantity $\xi_M = \ln[Q(Q_2/Q_1)^{1/2}]_c$, the value measured in the calibration; and the total uncertainty is (assumed to be) associated with the dependent variable, ρ_R.

An uncertainty in ρ due to the uncertainty in the measured value of counter resolving time, σ, used to correct for resolving time losses in count rates, must also be accounted for. A single, most probable value of σ was used for all resolving time corrections. A plot of values of σ versus counter anode voltage above threshold for a sample of various combinations of Geiger tubes and counter circuits typical of those used in the density measurements was made from which a most probable single value of σ and the extreme variations in this quantity could be determined. Calculations of density for a sample of data points were made with extreme values of σ as well as the most probable value. From the results of these calculations and a familiarity with the effect of the resolving time correction on density for various experimental conditions encountered (i.e., the value of $(Q_1/Q_2)-1$, the values of Q and Q_c, the magnitudes of the count rates, etc.) and the distribution of these conditions throughout the flow fields runs, a guess was made of the value of a contribution, $s\sigma$, to the standard deviation in ρ, due to the uncertainty in σ.

The independent quantities, s_σ and s_M, were combined to give an estimate of the standard deviation in the measured value of ρ equal to $\sqrt{s_\sigma^2 + s_M^2}$. Results of computations for various density measurements showed probable errors in ρ ranging from 3.8×10^{-6} to 1.72×10^{-6} for densities in the range 110×10^{-6} gm/cc to 930×10^{-6} gm/cc. Hence percentage probable errors of 3.5 percent for densities in the neighborhood of 110×10^{-6} gm/cc to 0.2 percent for densities in the neighborhood of 930×10^{-6} gm/cc were encountered.

Several sources of random error were present in the measurements made for the determination of density and contributed to the experimental uncertainty therein. The most significant was the normal statistical fluctuation in count rates (see refs. 22, 23, 24), the errors due to which propagate through the quantity $\ln[Q(Q_2/Q_1)^{1/2}]$. Also included were experimental errors in reading reference chamber temperature and in regulating and reading reference chamber pressure. Random errors in reference temperature and pressure were, of course, propagated to error in the experimental values of ρ_R through the relation $\rho = (\text{constant})(p/T)$.

The maximum experimental error likely in the measurements of T_R was about 0.2 percent while the maximum in p_R was about 1 percent, with this maximum error in p_R occurring for small values of p_R. For most values of p_R the experimental error in p_R was considerably less than 1 percent. Likewise, then, the experimental error in ρ_R is about 1 percent or slightly greater for the smallest values of ρ_R measured and less than 1 percent for all others, being as low as 0.2 percent, approximately, for the largest values.

An expression for the standard deviation in the quantity $\xi = \ln[Q(Q_2/Q_1)^{1/2}]$ can be derived from the

rule for propagation of independent errors and the expression for standard deviation in count rate, N. Thus, if s is the standard deviation,

$$s_\xi = \sqrt{\left(\frac{\partial \xi}{\partial Q}\right)^2 s_Q^2 + \left(\frac{\partial \xi}{\partial Q_1}\right)^2 s_{Q_1}^2 + \left(\frac{\partial \xi}{\partial Q_2}\right)^2 s_{Q_2}^2}$$

and

$$s_{N_T} = \sqrt{\frac{N_T}{t}}, \quad s_{N_{T1}} = \sqrt{\frac{N_{T1}}{t_1}}, \quad s_{N_{T2}} = \sqrt{\frac{N_{T2}}{t_2}}, \quad \text{etc.}$$

where t is the counting interval. The resulting equation is

$$s_\xi = \sqrt{\frac{1}{t}\left(\frac{1}{N_T} + \frac{1}{N_R}\right) + \frac{1}{4t_1}\left(\frac{1}{N_{T1}} + \frac{1}{N_{R2}}\right) + \frac{1}{4t_2}\left(\frac{1}{N_{T2}} + \frac{1}{N_{R1}}\right)} \tag{A19}$$

The deduction of the above expression for s_ξ assumes uncorrected count rates or, if the count rates are corrected for resolving time, that any error due to error in σ may be neglected and that $\sqrt{N}/t$ is a correct expression for the standard deviation of a corrected count rate, N. The latter is a sufficiently good approximation for purposes of this discussion (however, see ref. 24 for a theoretical refinement) and the assumption of no appreciable variation in σ is valid over the period of time which was required to make the measurements for any single density determination during a flow field run. Thus the above expression for s_ξ may be useful in checking the estimate of the precision of the density determinations at each φ made in terms of the least squares line for ρ_R vs. $\ln[Q(Q_2/Q_1)^{1/2}]$. (As already indicated, the effect of the uncertainty in σ on the over-all estimate of precision of the density determinations has been accounted for independently.)

A sample calculation for the density determination at $\varphi = 40°$, $r/c = 0.0692$, $M_\infty = 0.705$, $Re_\infty = 1.06 \times 10^6$ shows the following. The value of s_{ρ_R} computed for this sample from the least squares data is 2.15×10^{-6}. The value of s_ξ computed from equation (A19) is 6.84×10^{-3}. Putting this in the same units as s_{ρ_R} and using the (previously stated) assumption that all the experimental error has been concentrated in ρ_R (in the manner of the example treated on p. 62 of ref. 23), we may solve for a term $\sqrt{s_{\rho_R}^2 - n^2 s_\xi^2}$, the contribution to s_{ρ_R} directly due to the experimental error in the ρ_R measurements themselves. In the sample considered here this gives a value equal to 1.37×10^{-6}, or 0.68 percent of ρ. This accords well with the independently estimated (limits of) experimental error in the measured values of ρ_R.

The time variation of the counter efficiency ratio, $(\epsilon_1/\epsilon_2) = \sqrt{Q_1/Q_2}$, during a run could be considered to constitute a source of systematic error in density. For most of the G–M counter data, corrections for this were made (as noted following sketch (a)) by determining Q_1/Q_2 before, after, and, in some cases, during flow field runs and calibrations, making a plot of Q_1/Q_2 versus time, observing the time of the density measurements and using the corresponding value of Q_1/Q_2 in (either) computing (or correcting) density. It can be stated that such drifts in Q_1/Q_2 would lead to errors in density varying over a set of data from 0 to 10 or 12 percent, and that the corrections which were applied account for these errors at least approximately. The accuracy with which the Q_1/Q_2 versus time relation is known varies, unfortunately, by an unknown amount with different sets of data (tunnel runs), and it was not possible to ascertain with precision how good the corrections are for such systematic errors as are due to drift in Q_1/Q_2.

For the particular set of densities (and hence ρ/ρ_t) for which $M_\infty = 0.705$, $Re_\infty = 1.92 \times 10^6$, $r/c = 0.0923$, it is strongly suspected, from an independent determination of flow field density at the last point in the tunnel run, that systematic errors most likely due to drift in Q_1/Q_2 exist for which corrections were not directly made owing to the absence of a proper measure of the terminal value of Q_1/Q_2. The value of density at $\varphi = 2°$ is quite probably low by about 9 percent and all other densities are low by decreasing (but only approxi-

mately estimable) percentages for the other, increasing values of φ from 4° to 345°. At φ =345° this systematic error is undoubtedly less than 1 per cent, probably less than 0.5 percent.

A few other sets of data in which there may exist some residual systematic errors arising from this source and for which corrections could not be determined are those for which $Re_\infty = 1.92\times10^6$, $M_\infty = 0.705\pm0.006$, $r/c=0.0539$ (p. 46); $Re_\infty = 1.92\times10^6$, $M_\infty = 0.705\pm0.003$, $r/c=0.1231$ (p. 45); $Re_\infty = 1.93\times10^6$, $M_\infty = 0.705\pm0.003$, $r/c=0.0385$, $p_t=14.79$ (p. 47); $Re_\infty = 1.92\times10^6$, $M_\infty = 0.705\pm0.003$, $r/c=0.0385$, $p_t=14.71$ (p. 47).

A condition that it was considered should be fulfilled for the determination of densities by the method described in this report is that $ln[Q(Q_2/Q_1)^{1/2}]_M$ should be independent of ρ. A separate experiment was run to check the extent to which this condition was met. It was found that an approximately linear variation of about 5.5 percent occurred in $ln[Q(Q_2/Q_1)^{1/2}]_M$ over a range of densities from 0.0001 to 0.0014 gm/cc when the counting data used were corrected with moderate accuracy for resolving time. A variation of about 9 percent occurred over the same density range when the counting data used were corrected for resolving time with approximately the same uncertainty as that attending the resolving time corrections applied to the flow field data. (The variation was 12 percent for the case where uncorrected counting data were used.) It may be concluded that the condition stated above was probably fulfilled with good accuracy for some of the flow field runs and with just moderate accuracy for others. The distribution over all the flow field runs of a discrepancy in fulfillment of this condition is not known, however, inasmuch as the distributions of σ_T and σ_R about the most probable value, $\sigma=133\mu$ sec, are not known (although the limits of uncertainty were ascertained and a guess was made of the value of s_σ).

Variations in stagnation density, ρ_t, are considered to have had a relatively negligible effect on the precision and accuracy of the flow field density determinations. The probable error of an individual measurement of ρ_t estimated for a low-density flow field run showing maximum variation in observed stagnation pressure is 0.15 percent.

A further check was made for the standard deviation in the calibration quantity, $\xi_M=ln[Q(Q_2/Q_1)^{1/2}]_c$. For a sample, typical run the standard deviation was computed from the measured individual deviations of plotted points from the faired curve through them for the calibration relation, ξ_M vs. φ. The value was also computed from equation (A19) for this sample of data. The value of $s_{\xi M}$ deduced from the plotted data in this sample was 6.18×10^{-3} and that calculated from equation (A19) was 8.29×10^{-3}. Agreement should be expected since it can be correctly assumed that error in φ is relatively negligible here with only ξ_M subject to error and furthermore that this error should be due just to the compounded count rate statistical errors. Since errors due to mechanical sources (in the bushings) were normally small by comparison, departure from this agreement would have to be explained by inadequate correction for Q_1/Q_2 drift during calibration.

Radiograph data.—Errors in determining air densities from radiographs were many and principally of unknown magnitude. The following list includes all known sources of errors, their nature, and estimates of their magnitudes.

Source	*Nature*	*Probable error*
Exposure time	Random	±1 percent
X-ray beam divergence	Systematic	Negligible
X-ray beam path-length difference through sagging membrane	Systematic	Unknown but probably negligible
Differences in film speed	Random	Unknown but probably negligible since all film was from one mfg. lot
Taper in film base	Systematic	±3-percent density variation in 1-inch radius
Instabilities of photomultiplier tube and light source	Random	Unknown but probably small for a single uninterrupted series of density measurements
Mechanical positioning:		
(a) Absolute location	Random	±0.16-percent chord
(b) Relative locations	Random	±0.02-percent chord
Scratches, dust particles and finite grain size of photographic emulsion	Random	Led to density traces which varied ±2½ percent of the median

APPENDIX B

THEORETICAL CALCULATIONS

By means of the procedures indicated in reference 7, another solution for the problem of a flat plate at angle of attack of 13° and free-stream Mach number 1 corresponding to a different separation bubble pressure has been obtained. The value of the pressure chosen corresponds to a Mach number of 2.80 on the separation streamline. Since this pressure exceeds the maximum theoretical value permissible for expansion to the limiting wave at the leading edge, the flow in the subsonic portion of the field is dependent upon the assigned value. The procedure for solving this particular problem numerically in the hodograph plane was not discussed in reference 7; therefore, a brief summary of the method of solution is presented here. In the following discussion, knowledge of the methods established in reference 7 for the flat plate problem is assumed.

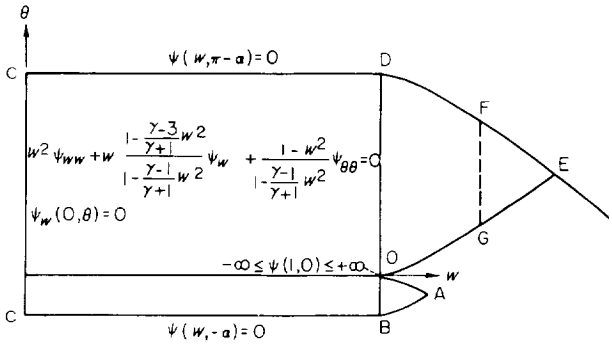

Sketch (c)

METHOD OF SOLUTION IN HODOGRAPH PLANE

The boundary-value problem in the hodograph plane for the inviscid irrotational flow about a flat plate at angle of attack α and free-stream Mach number 1 is as shown in sketch (c). (The notation is defined in appendix C.) Polar coordinates w, θ have been drawn here in rectangular form in conformance with the presentation in reference 7. Sketch (d) shows the corresponding flow in the physical plane. The stream function $\psi(w,\theta)$ is specified as zero on the boundary ABCDE and is required to satisfy the proper singularity at the free-stream point 0. Conditions on the limiting characteristics OE and OA are unspecified except that no singularity propogates along them. This

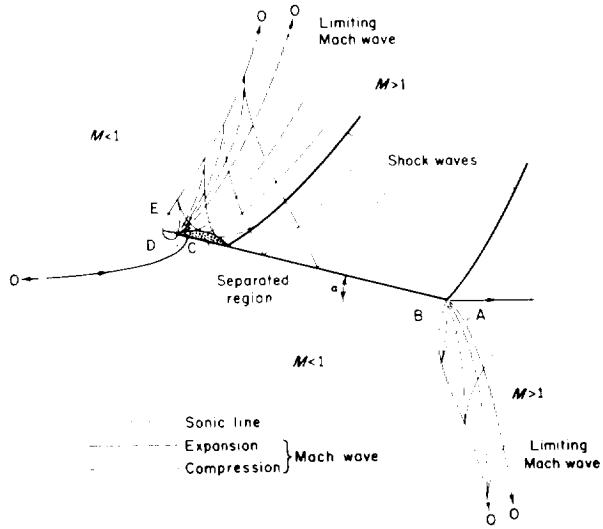

Sketch (d)

is the problem as was formulated in reference 7 for which the bubble pressure is equal to or less than that required for expansion of the flow about the leading edge to the limiting wave OE. For the pressure chosen in reference 7, the bubble trace in the hodograph appears as a line w=constant starting at point E. For an even lower pressure, the corresponding trace w=constant emanates from the leading-edge characteristic at a point to the right of point E in sketch (c), and the solution in the region OABCDEO is entirely independent of this pressure. On the other hand, for a bubble pressure greater than that associated with point E, the trace of the bubble between the leading edge and the limiting wave appears as shown by the broken line FG, and the entire solution depends upon the value chosen. This latter case is the type which is considered here.

For purposes of illustrating the procedure followed in obtaining a solution, let $\psi^\circ(w,\theta)$ represent the solution obtained in reference 7 for the region

OABCDEO of sketch (c). Next, let $\psi(w,\theta)$ be the desired solution within the region OABCDFGO. These two problems differ only in the requirement that $\psi(w,\theta)$ is specified as zero on the new boundary FG. A straightforward application of the methods of reference 7 would result in the desired solution $\psi(w,\theta)$. However, a procedure which produced the same result with much less time and effort has been used and is described in the following paragraphs.

The classical procedure for solving linear boundary-value problems involving a singularity is to obtain a singular solution which satisfies simple boundary conditions and to superpose a nonsingular solution such that the result satisfies both the singularity and the remaining boundary conditions. An analogous procedure can be followed

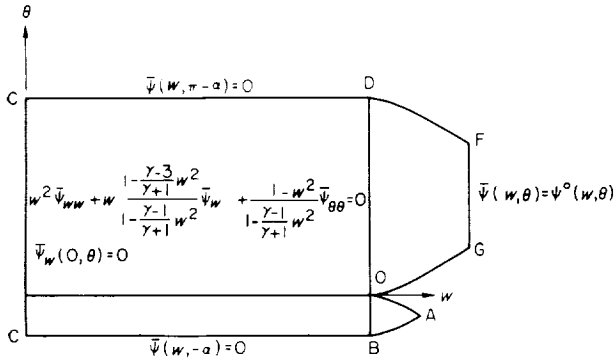

Sketch (e)

in the present case. Since $\psi^\circ(w,\theta)$ and $\psi(w,\theta)$ must both satisfy the same free-stream singularity, the desired result can be obtained by superpostion of $\psi^\circ(w,\theta)$ and the solution to a properly posed nonsingular boundary-value problem. To this end, consider a problem as presented in sketch (e). This problem for $\bar{\psi}(w,\theta)$ has the same boundaries as the problem for $\psi^\circ(w,\theta)$ (see sketch (c)) except for the foreshortened supersonic region which is now limited by the boundary FG; $\bar{\psi}$ is regular at the free-stream point $w=1, \theta=0$. It is thus seen that superposition of $\psi^\circ(w,\theta)$ and $\bar{\psi}(w,\theta)$ will result in the solution $\psi(w,\theta)$ provided the values $\psi(w,\theta)$ along FG are specified as $\psi^\circ(w,\theta)$. The relationship can be written as

$$\psi(w,\theta)=\psi^\circ(w,\theta)-\bar{\psi}(w,\theta)$$

where $\psi^\circ(w,\theta)$ and $\bar{\psi}(w,\theta)$ are solutions to the problems presented in sketches (c) and (d), respectively. The contribution of the present effort is therefore restricted to providing a numerical solution to the problem for $\bar{\psi}(w,\theta)$. It will be recalled that the solution given in reference 7 was obtained by superposition of two independent solutions (each containing a required part of the free-stream singularity) in such a manner as to satisfy the condition that the stagnation streamline has its branch point at zero velocity. In the present case, however, it is assumed that $\bar{\psi}(w,\theta)\ll\psi^\circ(w,\theta)$ for $w \ll 1$ such that the stagnation streamline $\psi(w,\theta)=0$ is coincident (within limits of numerical accuracy) with $\psi^\circ(w,\theta)=0$ for $w \to 0$. This assumption means physically that even though the whole subsonic field is altered by a change in bubble pressure, the effect is expected to be quite negligible at the stagnation point for reasonably small changes in pressure. This assumption was checked numerically in the hodograph upon completion of the solution $\bar{\psi}(w,\theta)$ and was found to be justified.

In the preceding discussion, the solution $\psi(w,\theta)$ is described in terms of the differential equation and boundary conditions as shown in sketches (c) and (e). However, the numerical solution for $\bar{\psi}(w,\theta)$ was actually obtained by first transforming the differential equation into a form resembling Tricomi's equation (see eq. (7) of ref. 7) and then solving this equation in the major portion of the hodograph. Details of this procedure are presented in reference 7.

The detailed numerical procedures used for obtaining $\bar{\psi}(w,\theta)$ are almost identical to those devised for the solution $\psi^\circ(w,\theta)$. Some computational advantages were realized as a result of the absence of the free-stream singularity. More important, however, was the fact that the largest values of $\bar{\psi}$ were concentrated in the supersonic region near the boundary FG. This condition led to rapid convergence of the relaxation process in the subsonic region ($w<1$).

The stream function is tabulated in table II.

TRANSFORMATION TO PHYSICAL PLANE

The procedures used for transformation of the solution $\psi(w,\theta)$ to the physical plane are those indicated on page 43 of reference 7. The image of the plate, the lines of constant w, and the characteristics were all obtained by straightforward application of the transformation equations as there presented. For the present problem

an additional computation was performed to permit construction of the complete separation bubble in the hodograph. This was done by

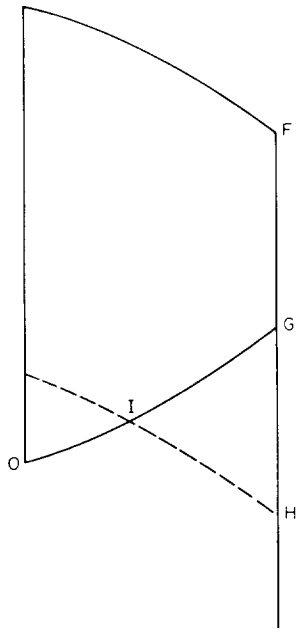

Sketch (f)

application of the computational procedures developed for the interdependent portion of the supersonic region (region DFGO of sketch (e)). In this manner, the solution $\psi(w,\theta)$ was continued into a triangular region GHI as is shown in sketch (f). The shape of the bubble in the physical plane was then found by integration of the appropriate functions along the boundary FGH. The characteristic HI was chosen sufficiently close to point 0 to insure that the bubble trace in the physical plane would intersect the surface of the plate. In this manner, use of the method of characteristics for the bubble construction was eliminated. A check on the accuracy of the present method was obtained by calculating the bubble of reference 7 and comparing with the results of the characteristics construction. The agreement between the results of the two methods was found to be excellent (see fig. 11(b)).

The results of the transformations are presented in figures 11 and 13 through 16. Discussion of these results is presented in the main body of the report.

APPENDIX C

NOTATION

a slope of ξ vs. ρ_R line $=\frac{1}{n}$

A area of collimating aperture

b span of test body

c chord of test body, 6½ in.

C_p pressure coefficient, $\frac{p-p_\infty}{(1/2)\rho_\infty V_\infty^2}$

C_p^* pressure coefficient at free-stream Mach number unity

f temperature recovery factor

F dimensionless function (see eq. (A13))

h Planck's constant

H humidity

i X-ray beam intensity

k number of pairs of measured values (ρ_R, ξ) in a density determination by Geiger-Mueller counter data

l X-ray beam path length

m intercept of the line ρ_R vs. ξ

M Mach number

n slope of the line ρ_R vs. ξ

N count rate

p pressure

p_c pressure in core of stream

p_t total pressure

p_w pressure on wind-tunnel wall

p_t' boundary-layer total pressure

q beam intensity ratio, $\frac{i_T}{i_R}$

Q ratio of count rates

r scalar distance or radius measured from projected leading edge

Re Reynolds number

s standard deviation

s_M $s(\rho_R)_M$

s_σ contribution to standard deviation in density due to uncertainty in σ

t time or counting interval

T absolute temperature

v speed of flow

V photodensitometer output voltage

V_m photodensitometer reference output voltage

w speed of flow (dimensionless through division by critical speed)

x scalar distance

y scalar distance

z scalar distance

α angle of attack

β_c calibration density increment, $(\rho_T-\rho_R)_c$

γ ratio of specific heats (1.405 in theoretical calculations)

δ boundary-layer thickness

ϵ counting efficiency of Geiger-Mueller counters

θ inclination of flow measured counterclockwise from the freestream direction

μ mass absorption coefficient

ν frequency

ξ $\ln\left[Q\left(\frac{Q_2}{Q_1}\right)^{1/2}\right]$

ρ air density

ρ_c density in core of stream

ρ_t stagnation or total density

ρ_w density at wind-tunnel wall

σ counter resolving time

φ polar coordinate angle about the projected leading edge

ψ stream function

$\bar{\psi}$ stream function representing solution to problem as defined in sketch (e)

ψ° stream function representing solution obtained in reference 7

SUBSCRIPTS

c calibration data

j general index

M "match point" value

o original or initial value

R reference chamber

T tunnel test section

∞ stream condition at reference point in wind tunnel

$_1$ on N (for counter interchange test) or ϵ or σ denotes Geiger-Mueller counter number 1

$_2$ on N (for counter interchange test) or ϵ or σ denotes Geiger-Mueller counter number 2

$_1$ on Q or t denotes first counter arrangement in counter interchange

$_2$ on Q or t denotes second counter arrangement in counter interchange

Subscript on s (where not otherwise defined) denotes quantity for which s is the standard deviation

No subscript on Q or t denotes tunnel run data

SUPERSCRIPT

$(')$ new or corrected quantity

REFERENCES

1. Lindsey, W. F., Daley, Bernard N., and Humphreys, Milton D.: The Flow and Force Characteristics of Supersonic Airfoils at High Subsonic Speeds. NACA TN 1211, 1947.
2. Holder, D. W., Tomlinson, R. C., and Rogers, E. W. E.: Preliminary Experiments on Blunt-Nosed Plates in Supersonic Airstreams. A.R.C. F.M. 1367, June 9, 1949.
3. Maccoll, J. W., and Codd, J.: Theoretical Investigations of the Flow Around Various Bodies in the Sonic Region of Velocities. Theo. Res. Rep. No. 17145, Armament Res. Dept. British Ministry of Supply. A.R.C. 9315, Sept. 1945.
4. Lindsey, Walter F., and Landrum, Emma Jean: Compilation of Information on the Transonic Attachment of Flows at the Leading Edges of Airfoils. NACA TN 4204, 1958.
5. Wood, George P.: Experiments on Transonic Flow Around Wedges. NACA TN 2829, 1952.
6. Guderley, Gottfried: The Flow Over a Flat Plate With a Small Angle of Attack at Mach Number 1. Jour. Aero. Sci., vol. 21, no. 4, April 1954, pp. 261–274.
7. Vincenti, Walter G., Wagoner, Cleo B., and Fisher, Newman H., Jr.: Calculations of the Flow Over an Inclined Flat Plate at Free-Stream Mach Number 1. NACA TN 3723, 1956.
8. Chapman, Dean R., Kuehn, Donald M., and Larson, Howard K.: Investigation of Separated Flows in Supersonic and Subsonic Streams With Emphasis on the Effect of Transition. NACA TN 3869, 1957, pp. 22–29.
9. Korst, H. H., Page, R. H., and Childs, M. E.: A Theory for Base Pressures in Transonic and Supersonic Flow. Univ. of Ill. Eng. Experiment Stn. Mech. Eng. Dept. TN 392–L, March 1955.
10. Marschner, Bernard W.: The Flow Over a Body in a Choked Wind Tunnel and in a Sonic Free Jet. Jour. Aero. Sci., vol. 23, no. 4, April 1956, pp. 368–376.
11. Guderley, K. Gottfried: The Flat Plate With an Angle of Attack in a Choked Wind Tunnel. Jour. Aero. Sci., vol. 22, no. 12, Dec. 1955, pp. 844–866.
12. Dimeff, John, Hallett, Ralph K., Jr., and Hansen, C. Frederick: X-ray Instrumentation for Density Measurements in a Supersonic Flow Field. NACA TN 2845, 1952.
13. Sproull, Wayne T.: X-rays in Practice. McGraw-Hill Book Co., Inc., First edition, 1946.
14. Wood, George P., and Gooderum, Paul B.: A Factor Affecting Transonic Leading Edge Flow Separation. NACA TN 3804, 1956.
15. Compton, A. H., and Allison, S. K.: X-rays in Theory and Experiment. D. Van Nostrand Co., Inc., N.Y., 1935.
16. Weltman, Ruth N., and Kuhns, Perry W.: Density Profiles of Subsonic Boundary Layers on a Flat Plate Determined by X-ray and Pressure Measurements. NACA TN 3098, 1954.
17. Weltman, Ruth N., Fairweather, Steven, and Papke, Daryl: Application of X-ray Absorption to Measurement of Small Air Density Gradients. NACA TN 2406, 1951.
18. Winkler, Eva M.: Density Measurements in Supersonic Flow by Means of the X-ray Absorption Method. Jour. of Appl. Physics, vol. 22, no. 2, Feb. 1951, pp. 201–202.
19. Kistiakowsky, G. B., and Kydd, P. H.: The Measurement of Density Changes in Gaseous Detonations. ONR Chemistry Division, reprint: Second ONR Symposium on Detonations, Feb. 9–11, 1955, Washington, D.C., p. 69.
20. Physical Measurements in Gas Dynamics and Combustion. High Speed Aerodynamics and Jet Propulsion, vol. IX, Princeton, pp. 97–107.
21. Nothwang, George J.: An Evaluation of Four Experimental Methods for Measuring Mean Properties of a Supersonic Turbulent Boundary Layer. NACA TN 3721, 1956.
22. Friedlander, Gerhart, and Kennedy, Joseph W.: Introduction to Radiochemistry. Ch. 10, John Wiley and Sons.
23. Beers, Y.: Introduction to the Theory of Error. Addison-Wesley Publishing Company, Inc., 1953.
24. Campbell, L. L.: Standard Deviation of Dead Time Correction in Counters. Canadian Journal of Physics, vol. 34, no. 9, Sept. 1956.
25. Stever, H. G.: The Discharge Mechanism of Fast G–M Counters from the Deadtime Experiment. Physical Review, vol. 61, Jan. 1 and 15, 1942.
26. Feller, W.: On Probability Problems in the Theory of Counters. Courant Anniversary Volume, 1948. Interscience Publishers, pp. 105–115.
27. Beers, Y.: A Precision Method of Measuring Geiger Counter Resolving Times. Review of Scientific Instruments, vol. 13, Feb. 1942.

TABLE I.- TABULATION OF DATA FROM DENSITOMETER

(a) Arrangement A

$M_\infty = 0.705 \pm 0.003$; $r/c = 0.1539$			
$Re_\infty = 1.92 \times 10^6$ $H \leq 0.00025$ $\rho_t = 0.002133$ slugs/cu ft $p_t = 14.71$ lb/sq in.		$Re_\infty = 1.04 \times 10^6$ $H \leq 0.00045$ $\rho_t = 0.001136$ slugs/cu ft $p_t = 7.376$ lb/sq in.	
Flow field		Flow field	
$(\rho/\rho_t)_{measured}$	φ, deg	$(\rho/\rho_t)_{measured}$	φ, deg
0.3329	0	0.2869	0
.3365	5	.3159	5
.3310	10	.3142	10
.3319	12	.3142	12
.3256	14	.2613	14
		.2561	15
.2601	16	.2493	16
.2646	20	.2596	20
.3065	30	.3091	30
.3751	40	.3654	40
.4429	50	.4389	50
.5147	60	.5089	60
.5793	70	.5840	70
.6293	80	.6446	80
.7330	100	.6882	100
.7994	120	.7787	120
.8376	160	.8350	160
.8439	200	.8590	200
		.8931	240
.8685	280	.8982	280
.8812	320	.9024	320
.8885	345	.9153	345

$Re_\infty = 2.0 \pm 0.1 \times 10^6$; $r/c = 0.1539$			
$M_\infty = 0.708$ $H \leq 0.00021$ $\rho_t = 0.002135$ slugs/cu ft $p_t = 14.73$ lb/sq in.		$M_\infty = 0.737$ $H \leq 0.00021$ $\rho_t = 0.002135$ slugs/cu ft $p_t = 14.73$ lb/sq in.	
Flow field		Flow field	
$(\rho/\rho_t)_{measured}$	φ, deg	$(\rho/\rho_t)_{measured}$	φ, deg
0.3377	4	0.3647	4
.3400	5	.3686	5
.3410	10	.3669	10
.3318	12	.3433	12
.3324	14	.3655	14
.2724	16	.3698	16
.2857	20	.2913	20
.9316	340	.9158	340
.9234	341	.9051	341
.9244	342	.9003	342
.9289	343	.9067	343
.9353	344	.9235	344
$M_\infty = 0.707$ $H \leq 0.00022$ $\rho_t = 0.002137$ slugs/cu ft $p_t = 14.74$ lb/sq in.		$M_\infty = 0.737$ $H \leq 0.00022$ $\rho_t = 0.002137$ slugs/cu ft $p_t = 14.74$ lb/sq in.	
.2799	20	.2908	20
.3241	30	.3330	30
.3908	40	.3971	40
.4556	50	.4592	50
.5254	60	.5299	60
.5867	70	.5931	70
.6364	80	.6378	80
.7091	100	.7066	100
.7548	120	.7501	120
.8097	160	.7974	160
.8463	200	.8318	200
.8694	240	.8558	240
.8893	280	.8759	280
.9070	320	.8899	320
[a].9155	[a]345	.8995	345

[a] $H = 0.0004$.

TABLE I. TABULATION OF DATA FROM DENSITOMETER – Continued

(a) Arrangement A– Continued

$M_\infty = 0.705 \pm 0.003$; $t/c = 0.1231$

$Re_\infty = 1.92 \times 10^6$, $H \leq 0.0004$, $\rho_t = 0.002140$ slugs/cu ft, $p_t = 14.77$ lb/sq in.		$Re_\infty = 1.06 \times 10^6$, $H \leq 0.00027$, $\rho_t = 0.001153$ slugs/cu ft, $p_t = 7.484$ lb/sq in.	
Flow field		Flow field	
$(\rho/\rho_t)_{measured}$	φ, deg	$(\rho/\rho_t)_{measured}$	φ, deg
		0.2808	0
0.2715	2	.3150	2
.2680	4	.3169	4
		.3221	5
.2709	6	.3240	6
.2729	8	.3170	8
		.3128	9
.2736	10	.3162	10
		.2859	11
.2362	12	.2644	12
.2001	14	.2560	14
.2058	16	.2511	16
.2158	20	.2818	20
		.7359	100
		$Re_\infty = 1.05 \times 10^6$, $H = 0.00035$, $\rho_t = 0.001143$ slugs/cu ft, $p_t = 7.421$ lb/sq in.	
		.2562	20
.2679	30	.3167	30
.3473	40	.3737	40
		.4187	45
.4282	50	.4547	50
.5094	60	.5366	60
[a] .5654	[a] 70	.5923	70
[a] .6275	[a] 80	.6368	80
.7174	100	.7319	100
.7758	120	.7956	120
		.8431	160
$Re_\infty = 1.91 \times 10^6$, $0.0004 \leq H \leq 0.0008$, $\rho_t = 0.002138$ slugs/cu ft, $p_t = 14.72$ lb/sq in.		$Re_\infty = 1.04 \times 10^6$, $H = 0.00035$, $\rho_t = 0.001143$ slugs/cu ft, $p_t = 7.406$ lb/sq in.	
[b] .7450	[b] 120		
[b] .8140	[b] 160		
.8249	200	.8579	200
.8593	240	.8915	240
.8811	280	.9248	280
.8829	320	.9326	320
.8929	345	.9334	345
.2659	0		
.2904	5		
.2895	10		
.2341	20		

[a] $H = 0.0005$
[b] $H = 0.0012$

$M_\infty = 0.705 \pm 0.004$; $t/c = 0.0923$

$Re_\infty = 1.92 \times 10^6$, $H \leq 0.00025$, $\rho_t = 0.002133$ slugs/cu ft, $p_t = 14.71$ lb/sq in.		$Re_\infty = 1.04 \times 10^6$, $0.0003 \leq H \leq 0.00065$, $\rho_t = 0.001138$ slugs/cu ft, $p_t = 7.388$ lb/sq in.	
Flow field		Flow field	
$(\rho/\rho_t)_{measured}$	φ, deg	$(\rho/\rho_t)_{measured}$	φ, deg
0.2666	2	0.2847	[a] 2
.2695	4	.2834	[a] 4
.2684	6	.2615	[a] 6
.2561	8	.2356	[a] 8
		.2268	[a] 10
.2280	12	.2206	[a] 12
.2348	16	.2367	16
.2468	20	.2450	20
.2977	30	.2916	30
.3585	40	.3587	40
$Re_\infty = 1.92 \times 10^6$, $H \leq 0.00037$, $\rho_t = 0.002140$ slugs/cu ft, $p_t = 14.76$ lb/sq in.			
.4421	50	.4477	50
.5031	60	.5156	60
.5803	70	.5760	70
.6569	80	.6428	80
.7489	100	.7407	100
.7820	120		
.8258	160		
.8574	200		
.8928	240		
.9118	280		
.9258	320		
.9214	345		

[a] $H = 0.0003$

TABLE I.--TABULATION OF DATA FROM DENSITOMETER--Continued

(a) Arrangement A Continued

$M_\infty = 0.705 \pm 0.003$; $r/c = 0.0692$

$Re_\infty = 1.93 \times 10^6$ $H \leq 0.00032$ $\rho_t = 0.002135$ slugs/cu ft $p_t = 14.75$ lb/sq in.		$Re_\infty = 1.06 \times 10^6$ $H \leq 0.0004$ $\rho_t = 0.001147$ slugs/cu ft $p_t = 7.449$ lb/sq in.	
Flow field		Flow field	
$(\rho/\rho_t)_{measured}$	φ, deg	$(\rho/\rho_t)_{measured}$	φ, deg
		0.1714	0
		.1736	1
0.2305	2	.2123	2
.2153	4	.2059	4
.2027	6	.2120	6
.2025	8	.2062	8
.2023	10	.2097	10
.2003	12	.2167	12
.2166	14	.2240	14
.2088	16	.2238	16
.2250	20	.2402	20
.2691	30	.2930	30
.3271	40	.3485	40
		.3889	45
.3974	50	.4216	50
.4677	60	.4862	60
.5289	70	.5500	70
.6026	80	.6153	80
.7048	100	.7158	100
.7740	120	.7846	120
$Re_\infty = 1.93 \times 10^6$ $0.0005 \leq H \leq 0.0009$ $\rho_t = 0.002132$ slugs/cu ft $p_t = 14.69$ lb/sq in.			
.2227	0	.1714	0
.2193	5		
.2279	10	.2097	10
.2554	20	.2402	20
.4017	45	.3889	45
.6170	80	.6153	80
.7919	120	.7845	120
		.8273	140
.8545	160	.8583	160
		.8762	180
.8962	200	.8782	200
		.9014	220
.9190	240	.9000	240
		.9068	260
.9318	280	.9179	280
		.9171	300
.9378	320	.9298	320
.9458	345	.9525	345
$Re_\infty = 1.92 \times 10^6$ $H = 0.0006$ $\rho_t = 0.002132$ slugs/cu ft $p_t = 14.69$ lb/sq in.			
.6121	80		
$Re_\infty = 1.93 \times 10^6$ $H = 0.00065$ $\rho_t = 0.002144$ slugs/cu ft $p_t = 14.79$ lb/sq in.			
.8391	160		
.9054	240		
.9290	320		

$M_\infty = 0.705 \pm 0.006$; $r/c = 0.0539$

$Re_\infty = 1.92 \times 10^6$ $0.0007 \leq H \leq 0.0015$ $\rho_t = 0.002140$ slugs/cu ft $p_t = 14.76$ lb/sq in.		$Re_\infty = 1.05 \times 10^6$ $0.00023 \leq H \leq 0.00048$ $\rho_t = 0.001148$ slugs/cu ft $p_t = 7.459$ lb/sq in.	
Flow field		Flow field	
$(\rho/\rho_t)_{measured}$	φ, deg	$(\rho/\rho_t)_{measured}$	φ, deg
		0.1223	359.75
		.1272	0
		.1247	0.5
		.1218	1
		.1230	1.5
		.1205	2
0.1699	2.5	.1205	2.5
		.1164	3
		.1529	4
.1601	5	.1691	5
		.1729	6
		.1747	8
.1774	10	.1867	10
		.1852	12
		.1957	14
		.1930	16
.2114	20	.2208	20
		.2766	30
		.3276	40
.3666	45	.3608	45
		.3883	50
		.4659	60
		[a] .5220	[a] 70
.6133	80	[a] .5941	[a] 80
.7805	120		
.8392	160		
.8784	200		
.9181	240		
.9346	280		
.9371	320		
.9223	345		

[a] $I = 0.00065$

TABLE I. TABULATION OF DATA FROM DENSITOMETER Continued

(a) Arrangement A– Continued

$Re_\infty = 2.0 \pm 0.1_\infty \times 10^6$; $t/c = 0.0539$

$M_\infty = 0.704$ $H \leq 0.0004$ $\rho_t = 0.002139$ slugs/cu ft $p_t = 14.75$ lb/sq in.		$M_\infty = 0.735$ $H \leq 0.0004$ $\rho_t = 0.002139$ slugs/cu ft $p_t = 14.75$ lb/sq in.	
Flow field		Flow field	
$(\rho/\rho_t)_{measured}$	φ, deg	$(\rho/\rho_t)_{measured}$	φ, deg
0.1400	2	0.2372	2
.1583	2.5	.2372	2.5
.1722	5	.2188	5
.1712	6	.2121	6
.1785	8	.2044	8
.1732	10	.1967	10
.2552	30	.2720	30
.3201	40	.3361	40
.3947	50	.4054	50
.5281	70	.5398	70
.5987	80	.6119	80
.6996	100	.7116	100
.7720	120	.7721	120
.8363	160	.8287	160
.8688	200	.8588	200
$M_\infty = 0.706$ $H \leq 0.00047$ $\rho_t = 0.002141$ slugs/cu ft $p_t = 14.77$ lb/sq in.		$M_\infty = 0.736$ $H \leq 0.00032$ $\rho_t = 0.002141$ slugs/cu ft $p_t = 14.77$ lb/sq in.	
.8982	240	.8953	240
.9430	280	.9261	280
.9491	320	.9387	320
.9693	345	.9512	345

$M_\infty = 0.705 \pm 0.003$; $t/c = 0.0385$

$Re_\infty = 1.92 \times 10^6$ $0.0004 \leq H \leq 0.0008$ $\rho_t = 0.002138$ slugs/cu ft $p_t = 14.74$ lb/sq in.		$Re_\infty = 1.05 \times 10^6$ $H \leq 0.0003$ $\rho_t = 0.001148$ slugs/cu ft $p_t = 7.450$ lb/sq in.	
Flow field		Flow field	
$(\rho/\rho_t)_{measured}$	φ, deg	$(\rho/\rho_t)_{measured}$	φ, deg
		0.1072	0
		.1094	.25
		.0930	.5
		.0965	1
		.1046	1.5
		.0948	2
0.0913	2.5	.0835	2.5
		.0779	3
		.0751	4
.1011	5	.0818	5
$Re_\infty = 1.92 \times 10^6$ $H \leq 0.00065$ $\rho_t = 0.002132$ slugs/cu ft $p_t = 14.69$ lb/sq in.			
0.0914	5		
		.0804	6
.1466	7.5	.1199	7.5
$Re_\infty = 1.93 \times 10^6$ $0.00047 \leq H \leq 0.0006$ $\rho_t = 0.002144$ slugs/cu ft $p_t = 14.79$ lb/sq in.			
		.1478	10
0.1979	15	.1707	15
.2147	20	.2079	20
.2680	32	.2524	32
.3531	45	.3503	45
.4210	55	.3983	55
$Re_\infty = 1.92 \times 10^6$ $0.00037 \leq H \leq 0.00075$ $\rho_t = 0.002131$ slugs/cu ft $p_t = 14.71$ lb/sq in.			
0.1871	10		
.5063	65	.4923	65
.5798	75	.5385	75
.6064	80	.5745	80
.7627	120	.7665	120
.8487	160	.8568	160
.8736	200	.8680	200
.9130	240	.8987	240
.9410	280	.9364	280
.9580	320	.9457	320
		.9464	340

TABLE I.—TABULATION OF DATA FROM DENSITOMETER—Continued

(a) Arrangement A—Continued

$M_\infty = 0.705 \pm 0.003$; $r/c = 0.0231$

$Re_\infty = 1.92 \times 10^6$; $H \leq 0.0009$; $\rho_t = 0.002135$ slugs/cu ft; $p_t = 14.72$ lb/sq in.		$Re_\infty = 1.05 \times 10^6$; $H \leq 0.00045$; $\rho_t = 0.001150$ slugs/cu ft; $p_t = 7.466$ lb/sq in.	
Flow field		Flow field	
$(\rho/\rho_t)_{measured}$	φ, deg	$(\rho/\rho_t)_{measured}$	φ, deg
0.0928	5.75	0.0771	5.75
.0909	7.5	.0810	7.5
.0926	10	.0776	10
.1216	13	.0918	13
.1658	16	.1414	16
.1635	16.5	.1537	16.5
.1656	17	.1588	17
		$Re_\infty = 1.05 \times 10^6$; $H \leq 0.0003$; $\rho_t = 0.001145$ slugs/cu ft; $p_t = 7.433$ lb/sq in.	
		.1457	17
.1765	20	.1556	20
.2224	30	.1967	30
.2712	40	.2489	40
.3346	50	.3186	50
.4187	60	.3960	60
.4984	70	.4572	70
.5589	80	.5394	80
		.6036	90
.7681	120		
.8539	160		
.8997	200		
.9279	240		
.9494	280		
.9916	320		
.9760	341		
$Re_\infty = 1.92 \times 10^6$; $H \leq 0.0007$; $\rho_t = 0.002134$ slugs/cu ft; $p_t = 14.71$ lb/sq in.			
.2324	30		
.2763	40		
.3402	50		
.4298	60		
.5243	70		
.5633	80		

$M_\infty = 0.705 \pm 0.003$; $r/c = 0.0154$

$Re_\infty = 1.94 \times 10^6$; $H \leq 0.000375$; $\rho_t = 0.002136$ slugs/cu ft; $p_t = 14.74$ lb/sq in.		$Re_\infty = 1.05 \times 10^6$; $H \leq 0.00035$; $\rho_t = 0.001150$ slugs/cu ft; $p_t = 7.468$ lb/sq in.	
Flow field		Flow field	
$(\rho/\rho_t)_{measured}$	φ, deg	$(\rho/\rho_t)_{measured}$	φ, deg
		0.1219	4
		.1255	5
		.1231	6
		.1081	7
		.1069	8
		.0982	9
		.0970	10
		.0906	11
		.0929	12
		.0987	13
		$Re_\infty = 1.05 \times 10^6$; $H \leq 0.00025$; $\rho_t = 0.001145$ slugs/cu ft; $p_t = 7.441$ lb/sq in.	
0.1103	15	.0874	15
.1551	20	.1313	20
		.1684	22
.1853	23	.1739	23
		.1796	24
.1917	25	[a].1723	25
.2009	27	.1779	27
.2079	30	.2056	30
		.2461	40
		$Re_\infty = 1.05 \times 10^6$; $H \leq 0.00031$; $\rho_t = 0.001147$ slugs/cu ft; $p_t = 7.446$ lb/sq in.	
		.1959	25
.2649	40	.2723	40
.3411	50	.3363	50
.4180	60	.4054	60
.5023	70	.4941	70
.5639	80	.5521	80
.7701	120	.7600	120
.8537	160	.8462	160
.8899	200	.8889	200
.9300	240	.9244	240
[b].9525	280	.9420	280
[b].9699	320	.9696	320
[b].9761	338	.9731	338
		.9662	340
		.9641	342
		.9738	344
		.9792	345
		.9318	346
		[a].7546	346.5

[a] $H = 0.0005$

[b] $0.0005 < H < 0.0006$

TABLE I.—TABULATION OF DATA FROM DENSITOMETER Continued

(a) Arrangement A—Concluded

$Re_\infty = 2.0 \pm 0.1 \times 10^6$; $t/c = 0.0154$

$M_\infty = 0.707$ $H \leq 0.00035$ $\rho_t = 0.002142$ slugs/cu ft $p_t = 14.78$ lb/sq in.		$M_\infty = 0.737$ $H \leq 0.00035$ $\rho_t = 0.002142$ slugs/cu ft $p_t = 14.78$ lb/sq in.	
Flow field		Flow field	
$(\rho/\rho_t)_{measured}$	φ, deg	$(\rho/\rho_t)_{measured}$	φ, deg
0.0729	9	0.0787	9
.0781	10.5	.0864	10.5
.0835	12	.0943	12
.0870	13.5	.1147	13.5
.0756	15	.1053	15
.1304	20	.1718	20
.1677	25	.1891	25
.1909	30	.2127	30
.2471	40	.2779	40
.3197	50	.3481	50
.4005	60	.4340	60
.4896	70	.5172	70
.5628	80	.5899	80
.7813	120	.7836	120
.8578	160	.8585	160
.9022	200	.9011	200
.9314	240	.9214	240
[a].9500	280	[a].9428	280
[a].9568	320	[a].9492	320

[a] $H = 0.0005$

NOTE: Values of ρ used above for $M_\infty = 0.707$ are based on the value of ρ at $\varphi = 280°$, $Re_\infty = 1.94 \times 10^6$, table I, p. 48, and measured values of density difference between the different angular settings, φ. Values of ρ used above for $M_\infty = 0.737$ are based on density difference measurements between the different Mach number settings at each angle, φ.

$M_\infty = 0.705 \pm 0.003$; $t/c = 0.0077$

$Re_\infty = 1.98 \times 10^6$ $H \leq 0.00035$ $\rho_t = 0.002135$ slugs/cu ft $p_t = 14.73$ lb/sq in.		$Re_\infty = 1.06 \times 10^6$ $H \leq 0.00025$ $\rho_t = 0.001154$ slugs/cu ft $p_t = 7.490$ lb/sq in.	
Flow field		Flow field	
$(\rho/\rho_t)_{measured}$	φ, deg.	$(\rho/\rho_t)_{measured}$	φ, deg.
		0.3365	7
		.1939	9
		.1290	11
		.0932	13
		.0967	15
		.0876	17
		.0969	19
		.1033	22
		.1031	25
		.3757	60
		$Re_\infty = 1.05 \times 10^6$ $H \leq 0.0004$ $\rho_t = 0.001152$ slugs/cu ft $p_t = 7.476$ lb/sq in.	
		.1178	25
0.1267	30	.1789	30
		.2125	33
.1669	34		
.1691	35	.2140	35
.1718	36		
		.2305	37
.1971	40	.2485	40
.2682	50	.3319	50
.3470	60	.4059	60
.4260	70	.4807	70
.5223	80	.5626	80
.5995	90	.6227	90
.6803	105	.7051	105
.7520	120	.7682	120
.8456	160	.8647	160
.8992	200	.8888	200
.9228	240	.9240	240
.9528	280	.9461	280
.9628	320	.9747	320
.9873	330	.9803	330

TABLE I.—TABULATION OF DATA FROM DENSITOMETER—Continued

(b) Arrangement B: Values obtained in polar coordinates (chord=6.5 in.) Continued

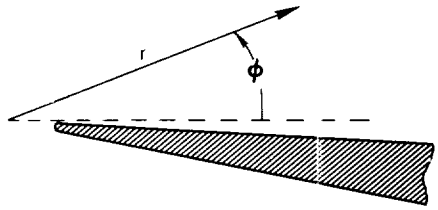

$Re_\infty = 2.7 \times 10^6$; $M_\infty = 0.711$; $\rho_t = 0.002952$ slugs/cu ft; $p_t = 19.93$ lb/sq in.

φ, deg	r/c	ρ/ρ_t	φ, deg	r/c	ρ/ρ_t	φ, deg	r/c	ρ/ρ_t	φ, deg	r/c	ρ/ρ_t
10	0	0.861	60	0.0462	0.564	190	0	0.861	240	0.1077	0.834
	.0154	.117		.0615	.572		.0154	.869		.1231	.819
	.0308	.163		.0769	.579		.0308	.863		.1385	.817
	.0462	.208		.0923	.581		.0462	.851			
	.0615	.235		.1077	.581		.0615	.848	260	0	.839
	.0769	.254		.1231	.577		.0769	.841		.0154	.877
	.0923	.269		.1385	.570		.0923	.843		.0308	.864
	.1077	.353					.1077	.836		.0462	.851
	.1231	.371	80	0	.839		.1231	.829		.0615	.851
	.1385	.387		.0154	.653		.1385	.826		.0769	.836
				.0308	.653					.0923	.825
15	0	.856		.0462	.662	195	0	.856		.1077	.816
	.0077	.309		.0615	.660		.0154	.873		.1231	.809
	.0154	.264		.0769	.668		.0308	.865		.1385	.797
	.0308	.200		.0923	.675		.0462	.864			
	.0462	.236		.1077	.675		.0615	.854	280	0	.841
	.0615	.273		.1231	.675		.0769	.841		.0154	.873
	.0769	.273		.1385	.673		.0923	.848		.0308	.865
	.0923	.283					.1077	.843		.0462	.858
	.1077	.299	100	0	.841		.1231	.836		.0615	.841
	.1231	.323		.0154	.729		.1385	.828		.0769	.828
	.1385	.316		.0308	.733					.0923	.822
				.0462	.735	200	0	.864		.1077	.817
20	0	.864		.0615	.729		.0154	.872		.1231	.814
	.0077	.094		.0769	.735		.0308	.869		.1385	.812
	.0154	.163		.0923	.738		.0462	.863			
	.0308	.230		.1077	.749		.0615	.852	300	0	.848
	.0462	.264		.1231	.748		.0769	.845		.0154	.869
	.0615	.285		.1385	.745		.0923	.838		.0308	.872
	.0769	.301					.1077	.839		.0462	.859
	.0923	.302	120	0	.848		.1231	.833		.0615	.852
	.1077	.311		.0154	.792		.1385	.820		.0769	.849
	.1231	.318		.0308	.786					.0923	.823
	.1385	.313		.0462	.784	210	0	.863		.1077	.817
				.0615	.788		.0154	.869		.1231	.817
30	0	.863		.0769	.786		.0308	.859		.1385	.812
	.0077	.250		.0923	.782		.0462	.856			
	.0154	.254		.1077	.787		.0615	.856	320	0	.832
	.0308	.309		.1231	.792		.0769	.848		.0154	.874
	.0462	.338		.1385	.784		.0923	.843		.0308	.865
	.0615	.357					.1077	.843		.0462	.862
	.0769	.369	140	0	.832		.1231	.838		.0615	.852
	.0923	.371		.0154	.828		.1385	.825		.0769	.834
	.1077	.378		.0308	.815					.0923	.825
	.1231	.369		.0462	.809	220	0	.862		.1077	.820
	.1385	.367		.0615	.802		.0154	.863		.1231	.825
				.0769	.803		.0308	.859		.1385	.820
40	0	.862		.0923	.802		.0462	.849			
	.0154	.345		.1077	.799		.0615	.851	340	0	.824
	.0308	.378		.1231	.803		.0769	.843		.0154	.862
	.0462	.409		.1385	.803		.0923	.841		.0308	.864
	.0615	.424					.1077	.841		.0462	.842
	.0769	.427	160	0	.824		.1231	.821		.0615	.838
	.0923	.433		.0154	.828		.1385	.824		.0769	.823
	.1077	.435		.0308	.826					.0923	.817
	.1231	.437		.0462	.817	230	0	.880		.1077	.811
	.1385	.434		.0615	.803		.0154	.874		.1231	.805
				.0769	.811		.0308	.859		.1385	.803
50	0	.880		.0923	.803		.0462	.861			
	.0077	.471		.1077	.797		.0615	.859	347	0	.887
	.0154	.446		.1231	.804		.0769	.854		.0154	.891
	.0308	.465		.1385	.802		.0923	.848		.0308	.877
	.0462	.485					.1077	.839		.0462	.874
	.0615	.497	167	0	.887		.1231	.822		.0615	.848
	.0769	.507		.0154	.845		.1385	.812		.0769	.841
	.0923	.508		.0308	.848					.0923	.841
	.1077	.511		.0462	.836	240	0	.849		.1077	.841
	.1231	.507		.0615	.833		.0154	.872			
	.1385	.505		.0769	.833		.0308	.862			
60	0	.849		.0923	.833		.0462	.856			
	.0154	.532		.1077	.823		.0615	.851			
	.0308	.541		.1231	.828		.0769	.854			
				.1385	.834		.0923	.838			

TABLE I.—TABULATION OF DATA FROM DENSITOMETER—Concluded

(b) Arrangement B: Values obtained in polar coordinates (chord=6.5 in.)—Continued

$Re_\infty = 1.9 \times 10^6$; $M_\infty = 0.714$; $\rho_t = 0.002127$ slugs/cu ft; $p_t = 14.21$ lb/sq in.

φ, deg	r/c	ρ/ρ_t	φ, deg	r/c	ρ/ρ_t	φ, deg	r/c	ρ/ρ_t	φ, deg	r/c	ρ/ρ_t	φ, deg	r/c	ρ/ρ_t	φ, deg	r/c	ρ/ρ_t
60	0	0.936	80	0.0615	0.624	140	0	0.873	167	0.1077	0.829	260	0	0.928	320	0	0.873
	.0077	.602		.0769	.617		.0154	.845		.1231	.829		.0077	.958		.0154	.987
	.0154	.532		.0923	.610		.0308	.828		.1385	.835		.0154	.961		.0308	.940
	.0308	.520		.1077	.597		.0462	.802					.0308	.957		.0462	.943
	.0462	.520		.1231	.589		.0615	.791	240	0	.936		.0462	.945		.0615	.936
	.0615	.509		.1385	.589		.0769	.778		.0077	.991		.0615	.939		.0769	.933
	.0769	.505					.0923	.767		.0154	.980		.0769	.936		.0923	.938
	.0923	.505	100	0	.867		.1077	.761		.0308	.987		.0923	.933		.1077	.938
	.1077	.505		.0154	.744		.1231	.775		.0462	.977		.1077	.934		.1231	.925
	.1231	.497		.0308	.728		.1385	.753		.0615	.980		.1231	.928			
	.1385	.497		.0462	.716					.0769	.976		.1385	.943	340	0	.911
				.0615	.703	160	0	.911		.0923	.967					.0154	
70	0	.855		.0769	.692		.0154	.908		.1077	.957	280	0	.867		.0308	.977
	.0077	.648		.0923	.688		.0308	.872		.1231	.964		.0154	.952		.0462	.964
	.0154	.630		.1077	.670		.0462	.856		.1385	.954		.0308	.940		.0615	.952
	.0308	.574		.1231	.658		.0615	.848					.0462	.928		.0769	.948
	.0462	.579		.1385	.648		.0769	.835	250	0	.855		.0615	.945		.0923	.944
	.0615	.569					.0923	.828		.0077	.921		.0769	.944		.1077	.914
	.0769	.563	120	0	.884		.1077	.808		.0154	.939		.0923	.950		.1231	.910
	.0923	.563		.0154	.794		.1231	.812		.0308	.934		.1077	.955			
	.1077	.555		.0308	.778		.1385	.812		.0462	.938		.1231	.940	347	0	.925
	.1231	.543		.0462	.760					.0615	.946					.0154	
	.1385	.537		.0615	.748	167	0	.925		.0769	.943	300	0	.884		.0308	
				.0769	.736		.0154	.900		.0923	.921		.0154	.957		.0462	.991
80	0	.928		.0923	.724		.0308	.888		.1077	.913		.0308	.925		.0615	.961
	.0077	.686		.1077	.717		.0462	.868		.1231	.916		.0462	.930		.0769	.957
	.0154	.655		.1231	.709		.0615	.862		.1385	.930		.0615	.934		.0923	.944
	.0308	.639		.1385	.688		.0769	.850					.0769	.952		.1077	.934
	.0462	.628					.0923	.835					.0923	.940			
													.1077	.939			
													.1231	.930			

$Re_\infty = 1.4 \times 10^6$; $M_\infty = 0.717$; $\rho_t = 0.001582$ slugs/cu ft; $p_t = 10.00$ lb/sq in.

10	0	.929	40	0	.950	100	0	.898	190	0	.929	220	0	.950	280	0	.898
	.0154	.077		.0077	.426		.0154	.748		.0154	.933		.0154	.964		.0154	.968
	.0308	.092		.0154	.355		.0308	.742		.0308	.917		.0308	.964		.0308	.965
	.0462	.144		.0308	.340		.0462	.734		.0462	.908		.0462	.947		.0462	.957
	.0615	.178		.0462	.355		.0615	.734		.0615	.903		.0615	.944		.0615	.949
	.0769	.202		.0615	.373		.0769	.734		.0769	.879		.0769	.931		.0769	.947
	.0923	.226		.0769	.393		.0923	.733		.0923	.861		.0923	.918		.0923	.947
	.1077	.259		.0923	.408		.1077	.729		.1077	.851		.1077	.914		.1077	.944
	.1231	.305		.1077	.396		.1231	.748		.1231	.866		.1231	.922		.1231	.947
	.1385	.340		.1231	.396		.1385	.754		.1385	.903		.1385	.957		.1385	.957
				.1385	.403												
15	0	.931				120	0	.911	195	0	.931	230	0	.926	300	0	.911
	.0077	.178	50	0	.926		.0154	.826		.0154	.937		.0154	.958		.0154	.989
	.0154	.073		.0154	.464		.0308	.815		.0308	.921		.0308	.954		.0308	.979
	.0308	.144		.0308	.426		.0462	.798		.0462	.918		.0462	.950		.0462	.982
	.0462	.178		.0462	.439		.0615	.790		.0615	.907		.0615	.954		.0615	.979
	.0615	.226		.0615	.439		.0769	.784		.0769	.880		.0769	.947		.0769	.974
	.0769	.244		.0769	.454		.0923	.784		.0923	.880		.0923	.950		.0923	.956
	.0923	.259		.0923	.481		.1077	.786		.1077	.865		.1077	.922		.1077	.957
	.1077	.259		.1077	.474		.1231	.786		.1231	.868		.1231	.912		.1231	.965
	.1231	.272		.1231	.472		.1385	.811		.1385	.907		.1385	.997		.1385	.982
	.1385	.283		.1385	.479												
						140	0	.925	200	0	.929	240	0	.929	320	0	.925
	0	.929	60	0	.929		.0154	.878		.0154	.922		.0154	.947		.0154	-----
20	.0154	.139		.0154	.529		.0308	.875		.0308	.921		.0308	.944		.0308	-----
	.0308	.139		.0308	.496		.0462	.850		.0462	.912		.0462	.940		.0462	.982
	.0462	.184		.0462	.501		.0615	.833		.0615	.907		.0615	.942		.0615	1.000
	.0615	.223		.0615	.508		.0769	.822		.0769	.889		.0769	.935		.0769	.982
	.0769	.256		.0769	.529		.0923	.815		.0923	.878		.0923	.922		.0923	.958
	.0923	.263		.0923	.534		.1077	.811		.1077	.871		.1077	.922		.1077	.964
	.1077	.269		.1077	.534		.1231	.829		.1231	.866		.1231	.929		.1231	.954
	.1231	.273		.1231	.542		.1385	.851		.1385	.903		.1385	.961		.1385	.965
	.1385	.277		.1385	.535												
						160	0	.949	210	0	.937	260	0	.971	340	0	.949
30	0	.937	80	0	.971		.0154	.889		.0154	.947		.0154	.982		.0154	-----
	.0077	.311		.0154	.660		.0308	.883		.0308	.933		.0308	.968		.0308	-----
	.0154	.242		.0308	.645		.0462	.854		.0462	.918		.0462	.961		.0462	.986
	.0308	.247		.0462	.649		.0615	.844		.0615	.914		.0615	.956		.0615	-----
	.0462	.255		.0615	.671		.0769	.834		.0769	.911		.0769	.958		.0769	.981
	.0615	.300		.0769	.678		.0923	.826		.0923	.900		.0923	.968		.0923	.981
	.0769	.323		.0923	.713		.1077	.825		.1077	.882		.1077	.968		.1077	.968
	.0923	.329		.1077	.678		.1231	.834		.1231	.886		.1231	.967		.1231	.965
	.1077	.329		.1231	.660		.1385	.859		.1385	.933		.1385	.995		.1385	.992
	.1231	.325		.1385	.667												
	.1385	.332															

TABLE I. TABULATION OF DATA FROM DENSITOMETER Continued

(b) Arrangement B: Values obtained in polar coordinates (chord=6.5 in.) Continued

$Pr_\infty = 2.0 \times 10^6$; $M_\infty = 0.737$; $\rho_t = 0.002126$ slugs/cu ft; $p_t = 14.22$ lb/sq in.

φ, deg	r/c	p/p_t	φ, deg	r/c	p/p_t	φ, deg	r/c	p/p_t	φ, deg	r/c	p/p_t	φ, deg	r/c	p/p_t	φ, deg	r/c	p/p_t
−1	0.0077	0.186	4	0.1077	0.411	10	0	0.961	80	0	0.895	190	0.0462	0.876	260	0	0.895
	.0154	.186		.1231	.441		.0154	.232		.0154	.701		.0615	.872		.0154	.943
	.0231	.195		.1385	.448		.0308	.204		.0308	.672		.0769	.872		.0308	.923
	.0308	.203					.0462	.249		.0462	.661		.0923	.872		.0462	.918
	.0462	.226	5	.0115	.186		.0615	.284		.0615	.652		.1077	.872		.0615	.923
	.0615	.288		.0138	.176		.0769	.332		.0769	.652		.1231	.876		.0769	.925
	.0769	.320		.0154	.176		.0923	.381		.0923	.645		.1385	.879		.0923	.923
	.0923	.332		.0192	.176		.1077	.416		.1077	.661					.1077	.916
	.1077	.344		.0231	.176		.1231	.447		.1231	.667	200	0	.948		.1231	.914
	.1231	.370		.0308	.218								.0077	.925		.1385	.914
	.1385	.398		.0462	.249	20	0	.948	90	0	.894		.0154	.907			
				.0615	.292		.0154	.186		.0154	.757		.0308	.885	270	0	.894
0	.0077	.218		.0769	.353		.0308	.268		.0308	.723		.0462	.876		.0154	.955
	.0092	.176		.0769	.350		.0462	.284		.0462	.704		.0615	.868		.0308	.934
	.0123	.161		.0923	.388		.0615	.296		.0615	.710		.0769	.862		.0462	.930
	.0154	.161		.1077	.415		.0769	.303		.0769	.691		.0923	.862		.0615	.929
	.0192	.176		.1231	.455		.0923	.312		.0923	.693		.1077	.862		.0769	.922
	.0231	.176		.1385	.452		.1077	.320		.1077	.699		.1231	.866		.0923	.916
	.0308	.176					.1231	.328		.1231	.704		.1385	.855		.1077	.923
	.0462	.218	6	.0092	.226											.1231	.931
	.0615	.293		.0108	.195	30	0	.956	100	0	.925	210	0	.956			
	.0923	.344		.0138	.175		.0077	.264		.0154	.796		.0077	.939	280	0	.925
	.1077	.369		.0154	.175		.0115	.282		.0308	.757		.0154	.922		.0154	.961
	.1231	.398		.0192	.175		.0154	.299		.0462	.736		.0308	.902		.0308	.933
	.1385	.434		.0231	.195		.0308	.345		.0615	.729		.0462	.900		.0462	.928
				.0269	.218		.0462	.358		.0769	.710		.0615	.896		.0615	.919
1	0	.186		.0308	.226		.0615	.369		.0923	.710		.0769	.889		.0769	.931
	.0038	.195		.0385	.238		.0769	.375		.1077	.723		.0923	.888		.0923	.928
	.0077	.211		.0462	.254		.0923	.381		.1231	.732		.1077	.881		.1077	.920
	.0092	.218		.0615	.289		.1077	.383					.1231	.888		.1231	.920
	.0115	.195		.0769	.346		.1231	.388	120	0	.916					.1385	.920
	.0154	.186		.0923	.391					.0154	.845	220	0				
	.0231	.176		.1077	.417	40	0			.0308	.820		.0077		300	0	.916
	.0308	.176		.1231	.458		.0077	.384		.0462	.799		.0154			.0154	.980
	.0462	.226		.1385	.452		.0154	.380		.0615	.780		.0308	.989		.0308	.944
	.0615	.293		.1485	.432		.0308	.400		.0769	.765		.0462	.992		.0462	.936
	.0769	.336					.0462	.409		.0923	.749		.0615	.985		.0615	.933
	.0923	.356	7	.0092	.250		.0615	.419		.1077	.749		.0769	.982		.0769	.927
	.1077	.381		.0108	.211		.0769	.423		.1231	.754		.0923	.975		.0923	.927
	.1231	.419		.0123	.195		.0923	.426					.1077	.972		.1077	.912
	.1385	.434		.0138	.186		.1077	.432	140	0	.920		.1231	.973		.1231	.907
				.0154	.186		.1231	.444		.0154	.868					.1385	.888
2	.0077	.195		.0192	.186					.0308	.845	230	0	.959			
	.0115	.186		.0231	.203	50	0	.959		.0462	.822		.0154	.965	320	0	.920
	.0154	.176		.0269	.226		.0154	.480		.0615	.799		.0308	.938		.0154	.987
	.0308	.162		.0308	.232		.0308	.487		.0769	.789		.0462	.940		.0308	.950
	.0462	.226		.0385	.244		.0462	.488		.0923	.792		.0615	.940		.0462	.931
	.0615	.284		.0462	.254		.0615	.490		.1077	.792		.0769	.943		.0615	.921
	.0769	.339		.0538	.268		.0769	.489		.1231	.796		.0923	.921		.0769	.916
	.0923	.363		.0615	.284		.0923	.489					.1077	.921		.0923	.916
	.1077	.388		.0769	.328		.1077	.500	160	0	.926		.1231	.925		.1077	.907
	.1231	.430		.0923	.384		.1231	.515		.0154	.887					.1231	.897
	.1385	.443		.1077	.419					.0308	.863	240	0	.918		.1385	.887
				.1231	.453	60	0	.918		.0462	.839		.0154	.946			
3	.0077	.244		.1385	.450		.0154	.559		.0615	.822		.0308	.910	340	0	.926
	.0092	.202					.0308	.541		.0769	.815		.0462	.908		.0154	.987
	.0108	.176	8	.0092	.278		.0462	.537		.0923	.820		.0615	.902		.0308	.952
	.0154	.146		.0100	.254		.0615	.537		.1077	.812		.0769	.904		.0462	.932
	.0308	.176		.0108	.244		.0769	.532		.1231	.812		.0923	.914		.0615	.915
	.0462	.232		.0123	.232		.0923	.537					.1077	.904		.0769	.906
	.0615	.292		.0154	.226		.1077	.543	167	0	.920		.1231	.904		.0923	.892
	.0769	.346		.0192	.218		.1231	.550		.0154	.892		.1385	.907		.1077	.881
	.1077	.375		.0231	.218					.0308	.868					.1231	.865
	.1231	.444		.0308	.238	70	0	.865		.0462	.846	250	0	.865			
				.0462	.254		.0154	.642		.0615	.828		.0154	.939	347	0	.920
4	.0092	.211		.0615	.272		.0308	.614		.0769	.822		.0308	.918		.0154	.984
	.0108	.176		.0769	.300		.0462	.600		.0923	.822		.0462	.914		.0308	.944
	.0154	.146		.0923	.332		.0615	.596		.1077	.822		.0615	.912		.0462	.922
	.0308	.186		.1077	.398		.0769	.596		.1231	.822		.0769	.911		.0615	.908
	.0462	.232		.1231	.436		.0923	.593					.0923	.911		.0769	.898
	.0615	.284		.1385	.464		.1077	.594	190	0	.961		.1077	.908		.0923	.884
	.0769	.350					.1154	.594		.0154	.910		.1231	.908		.1077	.858
	.0923	.382					.1231	.596		.0308	.890		.1385	.908			

TABLE I.—TABULATION OF DATA FROM DENSITOMETER—Continued

(b) Arrangement B: Values obtained in polar coordinates (chord = 6.5 in.)—Continued

$Re_\infty = 1.9 \times 10^6$; $M_\infty = 0.681$; $\rho_t = 0.002123$ slugs/cu ft; $p_t = 14.21$ lb/sq in.

φ, deg	r/c	ρ/ρ_t	φ, deg	r/c	ρ/ρ_t	φ, deg	r/c	ρ/ρ_t	φ, deg	r/c	ρ/ρ_t	φ, deg	r/c	ρ/ρ_t
0	0	0.974	20	0.0769	0.475	40	0.0462	0.593	135	0.0615	0.860	230	0.1231	0.867
	.0615	.413		.0923	.500		.0615	.601		.0769	.861		.1385	.870
	.0769	.411		.1077	.525		.0769	.605		.0923	.861			
	.0923	.418		.1231	.545		.0923	.615		.1077	.864	240	0	.903
	.1077	.430					.1077	.613		.1231	.861		.0077	.961
	.1231	.436	22	0	.952		.1231	.617					.0154	.959
	.1385	.444		.0077	.570		.1385	.619	150	0	.938		.0308	.946
				.0154	.462					.0154	.904		.0462	.926
2	0	.954		.0308	.459	45	0	.930		.0308	.875		.0615	.913
	.0154	.405		.0462	.473		.0077	.611		.0462	.866		.0769	.897
	.0308	.393		.0615	.498		.0154	.588		.0615	.861		.0923	.886
	.0462	.402		.0769	.523		.0308	.597		.0769	.861		.1077	.884
	.0615	.410		.0923	.552		.0462	.601		.0923	.860		.1231	.880
	.0769	.417		.1077	.573		.0615	.606		.1077	.864		.1385	.880
	.0923	.430		.1231	.578		.0769	.611		.1231	.872			
	.1077	.442		.1385	.594		.0923	.613				255	0	.901
							.1077	.611	165	0	.922		.0077	.985
4	0	.959	24	0	.962		.1231	.614		.0154	.906		.0154	.980
	.0154	.395		.0077	.621		.1385	.633		.0308	.900		.0308	.959
	.0308	.399		.0154	.462					.0462	.874		.0462	.941
	.0462	.415		.0308	.452	50	0	.915		.0615	.877		.0615	.924
	.0615	.422		.0462	.491		.0154	.609		.0769	.866		.0769	.907
	.0769	.428		.0615	.512		.0308	.613		.0923	.866		.0923	.901
	.0923	.442		.0769	.545		.0462	.615		.1077	.836		.1077	.897
	.1077	.450		.0923	.564		.0615	.619					.1231	.885
	.1231	.453		.1077	.573		.0769	.622	180	0	.971		.1385	.893
	.1385	.455		.1231	.584		.0923	.621		.0154	.983			
				.1385	.577		.1077	.622		.0308	.960	270	0	.928
8	0	------					.1231	.627		.0462	.943		.0154	------
	.0154	.358	26	0	.954		.1385	.633		.0615	.930		.0308	------
	.0308	.405		.0077	.611					.0769	.919		.0462	.995
	.0462	.415		.0154	.469	60	0	.903		.0923	.911		.0615	.981
	.0615	.420		.0308	.469		.0154	.653		.1077	.907		.0769	.977
	.0769	.426		.0462	.507		.0308	.643		.1231	.906		.0923	.970
	.0923	.430		.0615	.543		.0462	.650		.1385	.895		.1077	.960
	.1077	.434		.0769	.561		.0615	.630					.1231	.968
	.1231	.440		.0923	.573		.0769	.655	192	0	.938		.1385	.965
	.1385	.446		.1077	.577		.0923	.652		.0154	.942			
				.1231	.582		.1077	.651		.0308	.928	285	0	.915
12	0	.938		.1385	.594		.1231	.630		.0462	.915		.0154	------
	.0154	.405					.1385	.664		.0615	.897		.0308	.987
	.0308	.416	28	0	.952					.0769	.887		.0462	.968
	.0462	.422		.0077	.615	75	0	.901		.0923	.884		.0615	.958
	.0615	.431		.0154	.487		.0154	.721		.1077	.868		.0769	.965
	.0769	.432		.0308	.497		.0308	.712		.1231	.858		.0923	.956
	.0923	.438		.0462	.537		.0462	.712		.1385	.864		.1077	.953
	.1077	.444		.0615	.564		.0615	.708					.1231	.946
	.1231	.448		.0769	.574		.0769	.715	200	0	.930		.1385	.946
	.1385	.452		.0923	.578		.0923	.708		.0154	.936			
				.1077	.584		.1077	.730		.0308	.928	300	0	.915
14	0	.942		.1231	.592		.1231	.721		.0462	.911		.0154	------
	.0154	.416		.1385	.594		.1385	.721		.0615	.900		.0308	.994
	.0308	.418								.0769	.868		.0462	.989
	.0462	.426	30	0	.958	90	0	.928		.0923	.874		.0615	.980
	.0615	.438		.0154	.488		.0154	.806		.1077	.855		.0769	.970
	.0769	.442		.0308	.523		.0308	.793		.1231	.856		.0923	.969
	.0923	.446		.0462	.564		.0462	.787		.1385	.853		.1077	.966
	.1077	.452		.0615	.572		.0615	.786					.1231	.967
	.1231	.461		.0769	.584		.0769	.795	210	0	.958		.1385	.971
	.1385	.469		.0923	.588		.0923	.804		.0154	.952			
				.1077	.590		.1077	.810		.0308	.939	315	0	.930
16	0	.938		.1231	.593		.1231	.815		.0462	.921		.0154	------
	.0154	.427		.1385	.600					.0615	.928		.0308	.988
	.0308	.428				105	0	.915		.0769	.899		.0462	.975
	.0462	.436	32	0	.952		.0154	.845		.0923	.887		.0615	.977
	.0615	.442		.0154	.489		.0308	.830		.1077	.878		.0769	.972
	.0769	.450		.0308	.542		.0462	.825		.1231	.868		.0923	.977
	.0923	.461		.0462	.579		.0615	.821		.1385	.878		.1077	.960
	.1077	.471		.0615	.588		.0769	.816					.1231	.958
	.1231	.485		.0769	.595		.0923	.818	220	0	.941		.1385	.954
	.1385	.500		.0923	.601		.1077	.835		.0154	.971			
18	0	.924		.1077	.600		.1231	.827		.0308	.934	330	0	.938
	.0154	.385		.1231	.603		.1385	.830		.0462	.924		.0154	------
	.0308	.433		.1385	.615					.0615	.904		.0308	.991
	.0462	.446				120	0	.915		.0769	.901		.0462	.983
	.0615	.452	36	0	.953		.0154	.884		.0923	.878		.0615	.984
	.0769	.461		.0154	.525		.0308	.864		.1077	.872		.0769	.984
	.0923	.481		.0308	.565		.0462	.858		.1231	.862		.0923	.975
	.1077	.496		.0462	.582		.0615	.847		.1385	.862		.1077	.962
	.1231	.514		.0615	.586		.0769	.847					.1231	.958
	.1385	.541		.0769	.593		.0923	.847	230	0	.915		.1385	.954
				.0923	.600		.1077	.847		.0077	.968			
20	0	.930		.1077	.601		.1231	.842		.0154	.952	345	0	.922
	.0154	.438		.1231	.605		.1385	.842		.0308	.940		.0154	------
	.0308	.434		.1385	.608					.0462	.918		.0308	.995
	.0462	.442				135	0	.930		.0615	.907		.0462	.989
	.0615	.457	40	0	.941		.0154	.895		.0769	.893		.0615	.988
				.0154	.574		.0308	.886		.0923	.884		.0769	.987
				.0308	.586		.0462	.868		.1077	.880		.0923	.972
													.1077	.962
													.1231	.962
													.1385	.962

TABLE I. TABULATION OF DATA FROM DENSITOMETER—Continued

(c) Arrangement B: Values obtained in Cartesian coordinates (chord=6.5 in.)

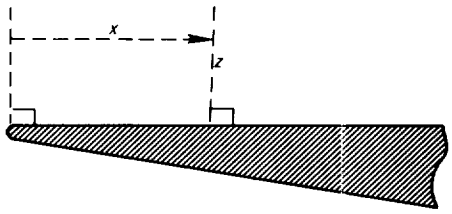

$Re_\infty = 2.7 \times 10^6$; $M_\infty = 0.711$; $\rho_t = 0.002952$ slugs/cu ft; $p_t = 19.93$ lb/sq in.

x/c	z/c	V/V∞	x/c	z/c	V/V∞	x/c	z/c	V/V∞	x/c	z/c	V/V∞
0.0038	0.0008	0.00233	0.0154	0.0038	0.000626	0.0308	0.0052	0.00181	0.0523	0.0005	0.00471
	.0009	.00133		.0040	.000721		.0054	.00192		.0006	.00429
	.0011	.00121		.0042	.000747		.0055	.00194		.0006	.00413
	.0012	.00125		.0043	.000826					.0008	.00400
	.0014	.00163		.0046	.00116	.0346	.0008	.000886		.0009	.00400
	.0015	.00175		.0049	.00147		.0009	.000765		.0011	.00407
	.0018	.00190		.0051	.00172		.0014	.000617		.0012	.00414
	.0022	.00218		.0052	.00110		.0017	.000591		.0015	.00436
				.6054	.00213		.0018	.000591		.0018	.00457
.0054	.0008	.000704					.0022	.000669		.0022	.00464
	.0009	.000573	.0192	.0008	.000504		.0023	.000669		.0023	.00464
	.0011	.000573		.0012	.000513		.0025	.000634		.0025	.00450
	.0015	.000669		.0014	.000478		.0028	.000678		.0028	.00457
	.0017	.000826		.0015	.000460		.0031	.000800		.0034	.00464
	.0020	.000939		.0017	.000460		.0032	.000930		.0037	.00471
	.0022	.00111		.0025	.000521		.0037	.00107		.0040	.00457
	.0026	.00150		.0026	.000539		.0038	.00115		.0040	.00464
	.0028	.00203		.0028	.000547		.0042	.00139		.0043	.00493
				.0029	.000591		.0043	.00143		.0046	.00507
.0062	.0006	.000730		.0031	.000608		.0046	.00154		.0049	.00479
	.0008	.000573		.0034	.000608		.0048	.00165		.0054	.00500
	.0009	.000530		.0035	.000626		.0049	.00172		.0062	.00514
	.0012	.000521		.0037	.000652		.0051	.00176		.0069	.00507
	.0014	.000495		.0038	.000713					.0077	.00536
	.0017	.000547		.0045	.00133	.0385	.0008	.000756		.0085	.00571
	.0018	.000600		.0046	.00154		.0009	.000756		.0092	.00586
	.0020	.000704		.0048	.00178		.0011	.000713		.0100	.00571
	.0022	.000791		.0049	.00183		.0012	.000678		.0108	.00600
	.0023	.000843		.0051	.00200		.0014	.000678		.0115	.00607
	.0026	.00108					.0017	.000721		.0123	.00629
	.0028	.00123	.0231	.0008	.000704		.0022	.000843		.0131	.00643
	.0032	.00211		.0011	.000600		.0023	.000921		.0138	.00714
				.0012	.000547		.0025	.000956		.0146	.00750
.0077	.0008	.000643		.0014	.000547		.0026	.000565		.0154	.00714
	.0009	.000547		.0015	.000539		.0028	.000991		.0162	.00779
	.0011	.000521		.0020	.000495		.0031	.00115		.0169	.00821
	.0017	.000521		.0022	.000469		.0034	.00146		.0177	.00857
	.0020	.000504		.0025	.000530		.0038	.00175			
	.0023	.000521		.0029	.000678		.0040	.00190	.0585	.0005	.00486
	.0025	.000547		.0031	.000686					.0006	.00479
	.0026	.000626		.0032	.000643	.0423	.0008	.000804		.0009	.00500
	.0029	.000721		.0034	.000678		.0009	.000869		.0009	.00507
	.0031	.000852		.0037	.000791		.0011	.000808		.0011	.00529
	.0034	.00123		.0038	.000878		.0015	.000808		.0012	.00564
	.0035	.00160		.0040	.00102		.0017	.000834		.0014	.00536
	.0038	.00223		.0042	.00122		.0018	.000843		.0015	.00550
				.0045	.00148		.0020	.000886		.0018	.00536
.0115	.0008	.000634		.0046	.00167		.0023	.00113		.0022	.00536
	.0009	.000591		.0048	.00185		.0026	.00125		.0025	.00550
	.0011	.000608		.0049	.00190		.0031	.00163		.0028	.00543
	.0012	.000600		.0051	.00197		.0032	.00172		.0031	.00536
	.0014	.000556		.0052	.00207					.0038	.00500
	.0015	.000539				.0462	.0006	.00294		.0046	.00529
	.0017	.000539	.0308	.0008	.000686		.0011	.00307		.0054	.00543
	.0020	.000504		.0009	.000617		.0014	.00287		.0062	.00529
	.0022	.000504		.0011	.000600		.0015	.00309		.0069	.00557
	.0025	.000539		.0012	.000565		.0018	.00309		.0077	.00536
	.0029	.000626		.0015	.000547		.0031	.00400		.0085	.00536
	.0031	.000678		.0018	.000556		.0034	.00407		.0085	.00557
	.0032	.000704		.0020	.000582		.0037	.00421		.0092	.00550
	.0034	.000773		.0023	.000608		.0040	.00429		.0100	.00557
	.0037	.00113		.0025	.000608		.0046	.00429		.0108	.00571
	.0042	.00235		.0026	.000660		.0054	.00457		.0115	.00607
				.0028	.000678		.0077	.00513		.0123	.00643
.0154	.0009	.000565		.0031	.000791		.0092	.00549		.0131	.00643
	.0011	.000513		.0032	.000826		.0100	.00584		.0138	.00657
	.0017	.000478		.0034	.000913		.0108	.00579		.0146	.00679
	.0020	.000513		.0035	.000895		.0115	.00621		.0154	.00679
	.0022	.000521		.0040	.00131		.0123	.00607		.0162	.00750
	.0023	.000539		.0042	.00140		.0126	.00667		.0169	.00757
	.0026	.000539		.0043	.00163		.0131	.00700		.0177	.00786
	.0029	.000521		.0045	.00169		.0138	.00707		.0185	.00807
	.0032	.000539		.0046	.00162		.0146	.00614		.0193	.00879
	.0034	.000582		.0048	.00160		.0154	.00743			
	.0037	.000600		.0051	.00176		.0154	.00757			
							.0162	.00821			

TABLE I.- TABULATION OF DATA FROM DENSITOMETER- Continued

(c) Arrangement B: Values obtained in Cartesian coordinates (chord = 6.5 in.)— Continued

$Re_\infty = 2.7 \times 10^6$; $M_\infty = 0.711$; $\rho_t = 0.002952$ slugs/cu ft; $p_t = 19.93$ lb/sq in.

x/c	z/c	V/V∞	x/c	z/c	V/V∞	x/c	z/c	V/V∞	x/c	z/c	V/V∞
0.0646	0.0005	0.00543	0.769	0.0092	0.0104	0.0892	0.0022	0.0102	0.0954	0.0208	0.0105
	.0009	.00636		.0100	.00942		.0028	.0106		.0215	.0104
	.0012	.00657		.0108	.00871		.0031	.0109		.0223	.0104
	.0015	.00657		.0115	.00806		.0037	.0120		.0231	.0110
	.0018	.00643		.0123	.00806		.0040	.0126		.0238	.0109
	.0022	.00663		.0131	.00735		.0043	.0121		.0246	.0103
	.0025	.00671		.0138	.00735		.0049	.0130		.0254	.0109
	.0028	.00714		.0146	.00697		.0052	.0123		.0262	.0114
	.0031	.00657		.0154	.00735		.0060	.0130		.0269	.0115
	.0034	.00657		.0162	.00761		.0065	.0132		.0277	.0112
	.0037	.00671		.0169	.00787		.0068	.0137		.0285	.0115
	.0040	.00714		.0178	.00774		.0071	.0140		.0292	.0113
	.0043	.00679		.0185	.00839		.0077	.0137		.0308	.0123
	.0046	.00671		.0192	.00826		.0080	.0143		.0315	.0122
	.0054	.00671		.0200	.00858		.0083	.0139		.0323	.0125
	.0069	.00607		.0208	.00826		.0086	.0132		.0331	.0132
	.0077	.00621		.0215	.00877		.0089	.0129		.0338	.0132
	.0085	.00607		.0223	.00903		.0092	.0131		.0346	.0135
	.0092	.00579		.0231	.00910		.0100	.0134		.0354	.0133
	.0100	.00607		.0238	.00916		.0108	.0134		.0362	.0133
	.0108	.00600		.0246	.00981		.0117	.0130		.0369	.0139
	.0115	.00643		.0254	.0105		.0131	.0131		.0377	.0138
	.0123	.00643		.0262	.0101		.0138	.0126		.0385	.0141
	.0131	.00650		.0269	.0111		.0146	.0124		.0400	.0145
	.0138	.00714		.0277	.0111		.0154	.0109		.0415	.0138
	.0154	.00714		.0285	.0112		.0154	.0105		.0423	.0159
	.0169	.00843		.0292	.0105		.0162	.00979		.0431	.0155
	.0177	.00836		.0300	.0105		.0166	.00959		.0438	.0161
	.0192	.00907		.0308	.0127		.0169	.00966		.0446	.0157
							.0177	.00890		.0454	.0168
.0692	.0006	.00742	.0831	.0003	.0101		.0185	.00924			
	.0008	.00710		.0006	.00897		.0192	.00940	.1046	.0003	.0142
	.0009	.00703		.0009	.00869		.0200	.00940		.0005	.0135
	.0011	.00703		.0012	.00924		.0208	.00924		.0006	.0122
	.0014	.00800		.0015	.00910		.0215	.00952		.0008	.0115
	.0015	.00781		.0018	.00979		.0223	.00986		.0009	.0118
	.0022	.00697		.0025	.00952		.0231	.0100		.0012	.0118
	.0028	.00742		.0031	.0110		.0238	.00959		.0015	.0132
	.0031	.00723		.0034	.0102		.0246	.00993		.0018	.0133
	.0034	.00684		.0037	.0113		.0254	.0102		.0023	.0133
	.0037	.00703		.0040	.0109		.0262	.00890		.0031	.0144
	.0040	.00645		.0043	.0112		.0269	.0106		.0038	.0151
	.0043	.00777		.0046	.0112		.0277	.0110		.0046	.0154
	.0046	.00777		.0054	.0117		.0285	.0108		.0054	.0159
	.0062	.00748		.0062	.0121		.0292	.0108		.0062	.0155
	.0069	.00748		.0069	.0123		.0300	.0114		.0074	.0165
	.0077	.00697		.0077	.0123		.0308	.0117		.0077	.0168
	.0085	.00677		.0085	.0126		.0315	.0126		.0085	.0173
	.0092	.00626		.0092	.0122		.0323	.0121		.0092	.0162
	.0100	.00632		.0100	.0120		.0331	.0123		.0100	.0175
	.0108	.00671		.0108	.0117		.0338	.0119		.0108	.0174
	.0115	.00658		.0115	.0111		.0346	.0130		.0115	.0175
	.0138	.00756		.0118	.0109		.0354	.0132		.0123	.0174
	.0138	.00774		.0123	.00966					.0131	.0177
	.0146	.00774		.0131	.00917	.0954	.0006	.0104		.0138	.0181
	.0154	.00806		.0138	.00828		.0012	.0107		.0146	.0182
	.0162	.00781		.0146	.00862		.0015	.0113		.0208	.0175
	.0169	.00877		.0154	.00869		.0023	.0116		.0215	.0164
	.0177	.00908		.0162	.00855		.0028	.0122		.0223	.0147
	.0180	.00852		.0169	.00897		.0031	.0129		.0231	.0133
	.0185	.00819		.0185	.00848		.0038	.0140		.0238	.0129
	.0192	.00852		.0192	.00883		.0046	.0135		.0246	.0125
	.0200	.00939		.0200	.00876		.0054	.0133		.0252	.0124
	.0208	.00968		.0208	.00952		.0062	.0143		.0254	.0123
	.0215	.00955		.0223	.00952		.0069	.0149		.0260	.0122
	.0223	.0100		.0231	.00917		.0077	.0151		.0262	.0123
	.0232	.0109		.0238	.00986		.0085	.0141		.0269	.0124
				.0246	.0100		.0092	.0155		.0277	.0123
.0769	.0005	.00735		.0254	.00966		.0100	.0143		.0286	.0123
	.0011	.00787		.0262	.0105		.0108	.0151		.0292	.0122
	.0012	.00774		.0269	.0101		.0115	.0150		.0292	.0118
	.0015	.00813		.0277	.0116		.0123	.0147		.0308	.0127
	.0022	.00826		.0286	.0108		.0131	.0142		.0338	.0133
	.0025	.00839		.0292	.0116		.0138	.0151		.0354	.0144
	.0028	.00877		.0300	.0116		.0146	.0173		.0369	.0152
	.0031	.00865		.0308	.0121		.0154	.0149		.0385	.0158
	.0038	.00877		.0315	.0116		.0162	.0159		.0400	.0153
	.0046	.00955					.0169	.0141		.0415	.0147
	.0054	.0100	.0892	.0006	.00993		.0177	.0132		.0431	.0151
	.0062	.0101		.0009	.0104		.0185	.0114		.0446	.0153
	.0069	.0102		.0012	.0106		.0192	.0113		.0462	.0157
	.0077	.0103		.0015	.0103		.0192	.0109		.0477	.0171
	.0085	.0105		.0018	.0101		.0200	.0102		.0492	.0177

TABLE I.—TABULATION OF DATA FROM DENSITOMETER—Continued

(c) Arrangement B: Values obtained in Cartesian coordinates (chord = 6.5 in.)—Continued

$Re_\infty = 1.9 \times 10^6$; $M_\infty = 0.714$; $\rho_t = 0.002127$ slugs/cu ft; $p_t = 14.21$ lb/sq in.

x/c	z/c	V/V∞	x/c	z/c	V/V∞	x/c	z/c	V/V∞	x/c	z/c	V/V∞
0.0038	0.0014	0.000519	0.0154	0.0074	0.00130	0.0231	0.0028	0.000280	0.0308	0.0080	0.000683
	.0017	.000441		.0077	.00142		.0031	.000300		.0086	.000775
	.0020	.000421		.0085	.00160		.0034	.000310		.0092	.000775
	.0023	.000460		.0083	.00164		.0037	.000340		.0098	.000836
	.0026	.000568		.0082	.00168		.0040	.000370		.0105	.000877
	.0029	.000656		.0089	.00179		.0043	.000410		.0111	.000908
	.0032	.000803		.0095	.00185		.0046	.000470		.0114	.00121
	.0034	.00111		.0097	.00188		.0049	.000530		.0120	.00126
	.0037	.00139		.0106	.00192		.0052	.000610		.0126	.00136
	.0040	.00178					.0055	.000640		.0132	.00136
	.0043	.00206	.0115	.0008	.0000566		.0058	.000710		.0138	.00139
	.0046	.00237		.0011	.000390		.0062	.000740		.0145	.00146
				.0014	.000314		.0065	.000730		.0151	.00174
.0046	.0012	.000721		.0017	.000285		.0068	.000830			
	.0014	.000461		.0020	.000247		.0069	.00106	.0346	.0009	.000448
	.0017	.000351		.0023	.000257		.0072	.00107		.0012	.000336
	.0020	.000361		.0026	.000295		.0075	.00103		.0015	.000306
	.0023	.000371		.0029	.000361		.0078	.00109		.0018	.000316
	.0026	.000421		.0032	.000333		.0082	.00113		.0022	.000336
	.0029	.000491		.0035	.000352		.0085	.00117		.0025	.000326
	.0032	.000531		.0038	.000352		.0089	.00127		.0028	.000336
	.0035	.000621		.0042	.000419		.0095	.00121		.0031	.000346
	.0038	.000891		.0045	.000542		.0102	.00138		.0034	.000357
	.0040	.00121		.0048	.000742		.0108	.00138		.0037	.000377
	.0043	.00147		.0051	.000819		.0114	.00158		.0040	.000418
	.0045	.00162		.0054	.000885		.0120	.00162		.0043	.000479
	.0049	.00193		.0055	.00124		.0126	.00206		.0046	.000551
	.0052	.00218		.0060	.00152		.0132	.00185		.0049	.000581
	.0055	.00248		.0063	.00162		.0138	.00198		.0052	.000602
				.0066	.00165					.0055	.000642
.0054	.0008	.000673		.0069	.00170	.0269	.0008	.000489		.0058	.000673
	.0009	.000438		.0072	.00189		.0011	.000364		.0062	.000704
	.0012	.000336		.0082	.00193		.0014	.000322		.0065	.000714
	.0015	.000316		.0080	.00198		.0017	.000302		.0068	.000673
	.0017	.000326		.0077	.00204		.0020	.000291		.0071	.000653
	.0020	.000336		.0085	.00210		.0023	.000312		.0074	.000683
	.0023	.000377		.0088	.00217		.0026	.000322		.0077	.000775
	.0026	.000418		.0091	.00233		.0029	.000312		.0080	.000816
	.0029	.000479					.0032	.000302		.0083	.000734
	.0032	.000642	.0192	.0008	.000519		.0035	.000312		.0086	.000693
	.0035	.000887		.0011	.000411		.0038	.000322		.0089	.000714
	.0037	.00122		.0014	.000352		.0042	.000343		.0092	.000806
	.0042	.00140		.0017	.000313		.0045	.000385		.0098	.000846
	.0043	.00151		.0020	.000303		.0048	.000437		.0105	.00100
	.0046	.00163		.0023	.000294		.0051	.000541			
	.0049	.00184		.0026	.000303		.0054	.000593	.0385	.0008	.000663
	.0052	.00208		.0029	.000323		.0057	.000625		.0009	.0005520
	.0055	.00237		.0032	.000343		.0060	.000635		.0012	.000397
				.0035	.000372		.0063	.000593		.0015	.000346
.0077	.0008	.000460		.0038	.000392		.0066	.000614		.0018	.000316
	.0011	.000343		.0042	.000401		.0069	.000729		.0022	.000306
	.0014	.000303		.0045	.000441		.0072	.000750		.0025	.000306
	.0017	.000303		.0048	.000558		.0075	.000781		.0028	.000336
	.0020	.000294		.0051	.000725		.0078	.000812		.0031	.000336
	.0023	.000274		.0054	.000823		.0082	.000906		.0034	.000367
	.0026	.000294		.0057	.000813		.0085	.000895		.0037	.000448
	.0029	.000352		.0060	.000862		.0088	.000947		.0040	.0005520
	.0032	.000460		.0063	.000921		.0091	.000979		.0043	.000571
	.0035	.000597		.0066	.000931		.0100	.00126		.0046	.000602
	.0038	.000784		.0068	.00119		.0103	.00132		.0049	.000581
	.0040	.00108		.0071	.00123		.0108	.00140		.0052	.000602
	.0043	.00123		.0074	.00116		.0114	.00139		.0055	.000642
	.0046	.00139		.0077	.00120		.0120	.00158		.0058	.000663
	.0049	.00150		.0080	.00127		.0126	.00175		.0062	.000744
	.0052	.00174		.0083	.00137		.0132	.00175		.0065	.000755
	.0055	.00194		.0086	.00140		.0138	.00196		.0068	.000724
				.0089	.00143						
.0154	.0008	.000540		.0094	.00149	.0308	.0011	.000438	.0423	.0008	.000714
	.0011	.000400		.0097	.00158		.0014	.000357		.0011	.000459
	.0014	.000340		.0100	.00160		.0017	.000316		.0014	.000397
	.0017	.000330		.0103	.00167		.0020	.000295		.0017	.000336
	.0022	.000320		.0106	.00160		.0023	.000295		.0020	.000316
	.0025	.000290		.0109	.00171		.0026	.000316		.0023	.000326
	.0028	.000310		.0112	.00183		.0029	.000316		.0026	.000357
	.0031	.000310		.0115	.00197		.0032	.000316		.0029	.000397
	.0034	.000310		.0118	.00204		.0035	.000326		.0032	.000479
	.0035	.000320		.0122	.00202		.0038	.000336		.0035	.0005540
	.0038	.000360		.0125	.00206		.0042	.000367		.0038	.0006622
	.0042	.000380		.0128	.00215		.0045	.000418		.0042	.000683
	.0045	.000450		.0131	.00227		.0048	.000479		.0045	.000683
	.0048	.000540		.0134	.00240		.0051	.000479			
	.0051	.000780					.0054	.000510	.0462	.0009	.000561
	.0054	.000900	.0231	.0006	.000530		.0057	.000551		.0012	.000438
	.0057	.000860		.0009	.000370		.0060	.000602		.0015	.000408
	.0060	.000940		.0012	.000320		.0063	.000683		.0018	.000397
	.0062	.00118		.0015	.000310		.0066	.000704		.0022	.000408
	.0065	.00120		.0018	.000300		.0069	.000683		.0025	.000438
	.0071	.00123		.0022	.000280		.0072	.000673		.0028	.000459
	.0066	.00127		.0025	.000280		.0075	.000714		.0031	.0005530
										.0034	.0006553
										.0037	.0006663

TABLE I. TABULATION OF DATA FROM DENSITOMETER—Continued

(c) Arrangement B: Values obtained in Cartesian coordinates (chord = 6.5 in.)—Continued

$Re_\infty = 1.9 \times 10^6$; $M_\infty = 0.714$; $\rho_t = 0.002127$ slugs/cu ft; $p_t = 14.21$ lb/sq in.

x/c	z/c	V/V_m	x/c	z/c	V/V_m	x/c	z/c	V/V_m	x/c	z/c	V/V_m
0.0462	0.0008	0.00135	0.0538	0.0285	0.00234	0.0692	0.0269	0.00218	0.0846	0.0231	0.00162
	.0011	.000630		.0292	.00274		.0285	.00212		.0246	.00185
	.0012	.000446		.0308	.00295		.0308	.00215		.0262	.00169
	.0022	.000400		.0315	.00311		.0315	.00243		.0277	.00169
	.0028	.000446		.0323	.00305		.0323	.00218		.0292	.00218
	.0034	.000569		.0331	.00335		.0346	.00265		.0308	.00212
	.0043	.000661		.0346	.00349		.0354	.00280		.0323	.00218
	.0062	.000769		.0354	.00369		.0362	.00269		.0338	.00208
	.0069	.000861					.0369	.00277		.0354	.00238
	.0077	.000800	.0615	.0009	.000876		.0377	.00274		.0369	.00243
	.0077	.000815		.0011	.000800		.0392	.00292		.0385	.00252
	.0085	.000769		.0014	.000769		.0397	.00326		.0400	.00237
	.0092	.000892		.0022	.00102		.0400	.00342		.0415	.00285
	.0100	.000969		.0025	.00105		.0408	.00343		.0431	.00285
	.0108	.000846		.0028	.00102		.0415	.00326		.0446	.00215
	.0115	.000892		.0032	.000953		.0423	.00323		.0462	.00298
	.0123	.000984		.0037	.00105		.0431	.00369		.0477	.00392
	.0138	.00108		.0046	.00108					.0485	.00349
	.0154	.00134		.0054	.00109	.0769	.0008	.00185		.0492	.00366
	.0162	.00126		.0062	.00106		.0009	.00157		.0492	.00362
	.0169	.00140		.0069	.000923		.0015	.00185		.0523	.00392
	.0185	.00157		.0077	.000969		.0018	.00188			
	.0200	.00162		.0092	.000892		.0022	.00182	.0923	.0011	.00280
	.0208	.00182		.0100	.00100		.0025	.00180		.0015	.00249
	.0215	.00180		.0108	.000969		.0031	.00205		.0018	.00274
	.0223	.00188		.0115	.00106		.0038	.00185		.0022	.00274
	.0231	.00178		.0123	.00105		.0046	.00197		.0025	.00246
	.0238	.00208		.0131	.00108		.0054	.00200		.0028	.00254
	.0246	.00197		.0138	.00103		.0062	.00215		.0031	.00243
	.0254	.00218		.0146	.00108		.0069	.00182		.0037	.00285
	.0269	.00285		.0154	.000969		.0077	.00203		.0040	.00289
	.0277	.00269		.0169	.00124		.0092	.00151		.0043	.00280
	.0285	.00295		.0177	.00157		.0100	.00142		.0046	.00280
	.0292	.00285		.0185	.00142		.0108	.00151		.0054	.00295
	.0300	.00311		.0192	.00149		.0123	.00126		.0062	.00289
	.0323	.00351		.0200	.00142		.0138	.00134		.0069	.00292
				.0208	.00145		.0146	.00131		.0077	.00320
.0500	.0008	.000704		.0215	.00166		.0154	.00120		.0092	.00269
	.0009	.000551		.0223	.00185		.0162	.00146		.0100	.00311
	.0012	.000448		.0231	.00197		.0177	.00135		.0108	.00300
	.0015	.000420		.0238	.00188		.0192	.00145		.0123	.00311
	.0018	.000448		.0246	.00195		.0200	.00129		.0131	.00269
	.0022	.000540		.0254	.00188		.0208	.00166		.0138	.00320
	.0025	.000602		.0269	.00209		.0223	.00174		.0146	.00246
	.0028	.000632		.0277	.00203		.0223	.00158		.0163	.00218
	.0031	.000704		.0285	.00205		.0238	.00166		.0169	.00208
	.0034	.000734		.0292	.00235		.0246	.00157		.0177	.00185
	.0037	.000744		.0300	.00243		.0262	.00174		.0192	.00182
	.0040	.000806		.0308	.00215		.0277	.00185		.0200	.00171
	.0043	.000765		.0315	.00249		.0292	.00200		.0208	.00182
	.0046	.000755		.0323	.00240		.0308	.00200		.0215	.00188
	.0049	.000744		.0331	.00258		.0323	.00234		.0223	.00203
	.0052	.000785		.0338	.00257		.0338	.00228		.0231	.00203
	.0055	.000826		.0346	.00282		.0354	.00277		.0238	.00175
	.0058	.000867		.0369	.00342		.0369	.00246		.0254	.00197
	.0062	.000846		.0377	.00308		.0385	.00274		.0262	.00197
				.0385	.00323		.0400	.00297		.0269	.00182
.0538	.0008	.000753		.0392	.00346		.0408	.00269		.0277	.00189
	.0011	.000476		.0400	.00342		.0415	.00300		.0285	.00191
	.0015	.000400		.0408	.00366		.0431	.00342		.0292	.00197
	.0025	.000630					.0446	.00323		.0300	.00225
	.0031	.000707	.0692	.0008	.00131		.0462	.00362		.0308	.00209
	.0043	.000800		.0009	.00114		.0472	.00351		.0315	.00234
	.0054	.000800		.0015	.00149		.0477	.00320		.0323	.00231
	.0069	.000907		.0018	.00148		.0508	.00397		.0331	.00197
	.0085	.000846		.0022	.00126		.0538	.00435		.0338	.00234
	.0085	.000753		.0025	.00118					.0346	.00249
	.0092	.000800		.0028	.00131	.0846	.0008	.00215		.0354	.00210
	.0100	.00100		.0037	.00131		.0012	.00166		.0362	.00265
	.0108	.00105		.0054	.00151		.0022	.00226		.0369	.00268
	.0123	.000984		.0069	.00131		.0025	.00218		.0377	.00265
	.0131	.00108		.0085	.00118		.0031	.00269		.0385	.00251
	.0138	.000800		.0092	.00123		.0038	.00215		.0392	.00272
	.0146	.00120		.0100	.00111		.0054	.00262		.0408	.00251
	.0154	.00126		.0114	.00111		.0069	.00246		.0415	.00272
	.0162	.00120		.0115	.00105		.0077	.00231		.0408	.00251
	.0169	.00122		.0138	.00135		.0085	.00212		.0415	.00280
	.0177	.00140		.0146	.00134		.0092	.00211		.0423	.00265
	.0192	.00146		.0162	.00138		.0100	.00208		.0431	.00266
	.0200	.00172		.0169	.00138		.0108	.00251		.0438	.00292
	.0208	.00215		.0177	.00151		.0115	.00185		.0446	.00277
	.0215	.00195		.0192	.00138		.0123	.00188		.0454	.00318
	.0223	.00209		.0200	.00166		.0131	.00200		.0462	.00311
	.0231	.00182		.0208	.00160		.0154	.00149		.0477	.00251
	.0238	.00203		.0215	.00180		.0162	.00169		.0492	.00323
	.0254	.00218		.0223	.00166		.0177	.00160		.0508	.00335
	.0262	.00231		.0238	.00194		.0185	.00177		.0523	.00338
	.0269	.00243		.0246	.00169		.0192	.00154		.0538	.00369
	.0277	.00226		.0262	.00188		.0215	.00162		.0554	.00342

TABLE I. –TABULATION OF DATA FROM DENSITOMETER Continued

(c) Arrangement B: Values obtained in Cartesian coordinates (chord =6.5 in.) –Continued

$Re_\infty = 1.9 \times 10^6$; $M_\infty = 0.714$; $\rho_t = 0.002127$ slugs/cu ft; $p_t = 14.21$ lb/sq in.

x/c	z/c	V/V_m	x/c	z/c	V/V_m	x/c	z/c	V/V_m	x/c	z/c	V/V_m
0.0923	0.0569	0.00369	0.1000	0.0077	0.00308	0.1000	0.0231	0.00231	0.1000	0.0431	0.00246
	.0585	.00366		.0085	.00369		.0238	.00203		.0446	.00277
	.0615	.00415		.0092	.00342		.0246	.00200		.0462	.00254
				.0108	.00366		.0254	.00218		.0492	.00331
0.1000	.0009	.00225		.0115	.00342		.0262	.00205		.0523	.00266
	.0012	.00228		.0123	.00335		.0269	.00215		.0538	.00342
	.0022	.00289		.0138	.00285		.0285	.00203		.0554	.00311
	.0025	.00289		.0146	.00312		.0292	.00203		.0569	.00326
	.0028	.00265		.0154	.00318		.0300	.00228		.0585	.00380
	.0037	.00331		.0162	.00349		.0308	.00200		.0631	.00342
	.0040	.00311		.0169	.00312		.0323	.00197		.0646	.00354
	.0043	.00314		.0177	.00342		.0338	.00215		.0677	.00377
	.0046	.00334		.0185	.00265		.0354	.00234		.0692	.00372
	.0054	.00335		.0192	.00258		.0359	.00234			
	.0062	.00326		.0200	.00222		.0385	.00238			
	.0071	.00351		.0215	.00215		.0415	.00289			

TABLE I.—TABULATION OF DATA FROM DENSITOMETER -Continued

(c) Arrangement B: Values obtained in Cartesian coordinates (chord = 6.5 in.)—Continued

$Re_\infty = 1.4 \times 10^6$; $M_\infty = 0.717$; $\rho_t = 0.001532$ slugs/cu ft; $p_t = 10.00$ lb/sq in.

x/c	z/c	V/V_m	x/c	z/c	V/V_m	x/c	z/c	V/V_m	x/c	z/c	V/V_m
0.0031	0.0008	0.000695	0.0123	0.0058	0.000601	0.0308	0.0068	0.000282	0.0462	0.0049	0.000288
	.0009	.000666		.0062	.000659		.0071	.000268		.0062	.000288
	.0011	.000710		.0063	.000652		.0074	.000311		.0074	.000317
	.0012	.000731		.0066	.000717		.0075	.000311		.0077	.000356
	.0014	.000804		.0068	.000746		.0077	.000326		.0080	.000365
	.0015	.000920		.0069	.000826		.0080	.000340		.0083	.000346
	.0017	.00103		.0072	.000934		.0083	.000333		.0086	.000356
	.0018	.00112		.0074	.000971		.0086	.000355		.0089	.000365
	.0020	.00118		.0077	.000971		.0089	.000384		.0092	.000356
	.0022	.00125		.0078	.00100		.0092	.000384		.0095	.000337
	.0023	.00134		.0082	.00100		.0095	.000376		.0098	.000375
	.0025	.00145		.0083	.00101		.0102	.000427		.0102	.000365
	.0026	.00159		.0085	.00106		.0105	.000427		.0105	.000404
	.0028	.00180								.0108	.000375
			.0154	.0008	.000152	.0385	.0008	.000181		.0114	.000423
.0062	.0008	.000644		.0009	.000137		.0009	.000144		.0120	.000404
	.0009	.000246		.0011	.000123		.0012	.000123		.0126	.000462
	.0011	.000188		.0020	.000115		.0014	.000123		.0135	.000462
	.0012	.000173		.0025	.000137		.0015	.000108		.0137	.000471
	.0014	.000159		.0031	.000137		.0018	.000108		.0138	.000500
	.0015	.000166		.0032	.000152		.0022	.000115		.0142	.000490
	.0018	.000173		.0034	.000152		.0028	.000115		.0145	.000490
	.0023	.000195		.0037	.000173		.0031	.000123		.0148	.000538
	.0029	.000268		.0040	.000195		.0043	.000166		.0154	.000567
	.0031	.000297		.0042	.000224		.0046	.000173		.0157	.000558
	.0032	.000340		.0045	.000297		.0049	.000202		.0160	.000558
	.0035	.000492		.0048	.000355		.0052	.000210		.0163	.000548
	.0037	.000586		.0049	.000398		.0058	.000253		.0169	.000548
	.0040	.000753		.0051	.000398		.0062	.000253		.0175	.000567
	.0042	.000818		.0052	.000427		.0068	.000275		.0178	.000606
	.0043	.000855		.0055	.000456		.0071	.000297		.0182	.000606
	.0045	.000920		.0057	.000478		.0074	.000297		.0188	.000663
	.0046	.000942		.0058	.000513		.0077	.000326		.0191	.000692
	.0048	.00100		.0060	.000536		.0080	.000304		.0194	.000683
	.0049	.00104		.0062	.000586		.0086	.000311		.0200	.000654
	.0051	.00111		.0068	.000601		.0092	.000326		.0206	.000750
	.0052	.00122		.0074	.000637		.0095	.000355		.0212	.000788
	.0054	.00130		.0074	.000659		.0098	.000362		.0218	.000846
	.0055	.00144		.0077	.000702					.0222	.000788
	.0057	.00154		.0077	.000739	.0462	.0008	.000152		.0225	.000846
	.0058	.00157		.0080	.000789		.0011	.000108		.0228	.000846
	.0060	.00168		.0083	.000855		.0012	.000101		.0231	.000798
	.0062	.00181		.0086	.000869		.0020	.000115		.0238	.000885
				.0092	.000869		.0023	.000115		.0246	.000980
.0092	.0008	.000239		.0095	.000855		.0026	.000123		.0254	.000962
	.0011	.000159		.0098	.000891		.0028	.000123		.0262	.00105
	.0014	.000137		.0102	.00101		.0029	.000137		.0269	.00114
	.0015	.000137		.0105	.00107		.0031	.000137		.0277	.00108
	.0018	.000144		.0114	.00133		.0034	.000152		.0285	.00115
	.0020	.000137		.0117	.00138		.0037	.000152		.0292	.00121
	.0022	.000130		.0120	.00141		.0038	.000159		.0300	.00132
	.0023	.000130		.0123	.00149		.0040	.000173		.0308	.00138
	.0026	.000166					.0042	.000181		.0315	.00127
	.0028	.000181	.0231	.0008	.000217		.0043	.000188			
	.0029	.000195		.0009	.000173		.0045	.000202	.0523	.0008	.000068
	.0031	.000195		.0014	.000115		.0046	.000239		.0011	.000365
	.0032	.000202		.0015	.000108		.0051	.000268		.0014	.000269
	.0034	.000217		.0022	.000108		.0052	.000275		.0018	.000192
	.0035	.000246		.0028	.000123		.0055	.000268		.0020	.000183
	.0040	.000376		.0031	.000130		.0057	.000289		.0025	.000192
	.0042	.000427		.0040	.000152		.0058	.000289		.0028	.000197
	.0043	.000492		.0043	.000166		.0062	.000297		.0034	.000226
	.0045	.000543		.0046	.000195		.0065	.000268		.0037	.000260
	.0045	.000565		.0049	.000210		.0072	.000289		.0040	.000279
	.0046	.000630		.0055	.000260		.0074	.000282		.0043	.000264
	.0049	.000659		.0058	.000304		.0075	.000282		.0046	.000269
	.0051	.000666		.0062	.000297		.0078	.000340		.0049	.000269
	.0052	.000695		.0065	.000311		.0085	.000384		.0052	.000288
	.0055	.000797		.0068	.000369		.0086	.000355		.0055	.000269
	.0058	.000971		.0071	.000398		.0089	.000326		.0058	.000303
	.0063	.00109		.0074	.000405		.0091	.000333		.0062	.000203
	.0065	.00112		.0077	.000398		.0094	.000384		.0065	.000288
	.0066	.00112		.0080	.000405		.0097	.000333		.0077	.000327
	.0068	.00113		.0086	.000384		.0098	.000326		.0092	.000361
	.0071	.00119		.0089	.000413		.0100	.000326		.0100	.000375
				.0092	.000427		.0102	.000340		.0108	.000380
.0123	.0008	.000282		.0095	.000463		.0106	.000362		.0115	.000380
	.0009	.000195		.0098	.000471		.0108	.000369		.0123	.000389
	.0011	.000166		.0102	.000507		.0109	.000376		.0131	.000409
	.0015	.000137		.0105	.000572		.0111	.000384		.0138	.000457
	.0017	.000130		.0108	.000615		.0112	.000376		.0146	.000452
	.0020	.000130					.0114	.000340		.0162	.000505
	.0022	.000123	.0308	.0008	.000340		.0115	.000347		.0169	.000548
	.0026	.000130		.0009	.000181		.0117	.000340		.0177	.000601
	.0031	.000159		.0011	.000144					.0185	.000620
	.0035	.000166		.0012	.000123	.0462	.0005	.00124		.0192	.000611
	.0038	.000195		.0015	.000108		.0006	.000788		.0200	.000644
	.0042	.000239		.0018	.000101		.0008	.000606		.0208	.000668
	.0045	.000304		.0028	.000115		.0012	.000337		.0215	.000726
	.0048	.000391		.0031	.000115		.0015	.000279		.0223	.000731
	.0051	.000500		.0040	.000137		.0018	.000192		.0231	.000788
	.0052	.000521		.0046	.000159		.0031	.000192		.0238	.000750
	.0054	.000594		.0052	.000224		.0037	.000202		.0254	.000851
	.0055	.000608		.0058	.000246		.0040	.000221		.0262	.000856
	.0057	.000594		.0065	.000282		.0043	.000250		.0269	.000875
							.0046	.000269		.0285	.001000

TABLE I.—TABULATION OF DATA FROM DENSITOMETER—Continued

(c) Arrangement B: Values obtained in Cartesian coordinates (chord=6.5 in.)—Continued

Re_∞=1.4×10^6; M_∞=0.717; ρ_t=0.001532 slugs/cu ft; p_t=10.00 lb/sq in.

x/c	z/c	V/V$_m$	x/c	z/c	V/V$_m$	x/c	z/c	V/V$_m$	x/c	z/c	V/V$_m$
0.585	0.0008	0.000716	0.0646	0.0089	0.000360	0.0708	0.0262	0.000788	0.0769	0.0331	0.000918
	.0009	.000505		.0092	.000394		.0269	.000755		.0338	.000929
	.0012	.000337		.0100	.000365		.0277	.000745		.0346	.000918
	.0015	.000274		.0108	.000365		.0285	.000807		.0354	.000844
	.0017	.000250		.0115	.000389		.0292	.000827		.0362	.00101
	.0018	.000221		.0123	.000384		.0308	.000856			
	.0020	.000216		.0131	.000399		.0315	.000923	.0831	.0012	.000622
	.0025	.000221		.0138	.000399		.0323	.000865		.0014	.000556
	.0028	.000250		.0146	.000427		.0331	.000889		.0015	.000551
	.0031	.000264		.0146	.000451		.0338	.00101		.0017	.000500
	.0034	.000260		.0154	.000442		.0346	.000957		.0018	.000485
	.0037	.000264		.0162	.000500		.0354	.000986		.0020	.000490
	.0040	.000279		.0169	.000514					.0022	.000464
	.0043	.000279		.0177	.000524	.0769	.0011	.000602		.0023	.000485
	.0046	.000274		.0185	.000591		.0014	.000490		.0025	.000469
	.0049	.000288		.0192	.000572		.0015	.000485		.0026	.000520
	.0052	.000312		.0200	.000591		.0017	.000464		.0028	.000500
	.0055	.000308		.0208	.000653		.0020	.000418		.0031	.000485
	.0058	.000312		.0215	.000644		.0022	.000423		.0034	.000520
	.0062	.000308		.0223	.000683		.0023	.000418		.0040	.000582
	.0069	.000327		.0231	.000697		.0025	.000418		.0043	.000536
	.0077	.000317		.0238	.000697		.0028	.000434		.0046	.000541
	.0092	.000351		.0238	.000731		.0031	.000408		.0049	.000587
	.0100	.000361		.0246	.000697		.0034	.000408		.0052	.000520
	.0108	.000361		.0254	.000779		.0037	.000444		.0055	.000536
	.0123	.000413		.0262	.000760		.0040	.000429		.0058	.000577
	.0131	.000418		.0269	.000827		.0043	.000418		.0062	.000520
	.0138	.000452		.0277	.000841		.0046	.000459		.0065	.000551
	.0146	.000466		.0285	.000851		.0049	.000454		.0071	.000561
	.0154	.000462		.0292	.000889		.0055	.000505		.0074	.000577
	.0162	.000486		.0300	.000880		.0062	.000459		.0077	.000531
	.0169	.000548		.0308	.000904		.0065	.000474		.0080	.000561
	.0177	.000577		.0323	.000803		.0068	.000480		.0083	.000546
	.0185	.000577					.0071	.000444		.0086	.000520
	.0192	.000601	.0708	.0011	.000587		.0074	.000469		.0089	.000531
	.0200	.000635		.0015	.000389		.0077	.000459		.0092	.000531
	.0215	.000663		.0018	.000351		.0080	.000469		.0100	.000500
	.0223	.000673		.0020	.000337		.0083	.000449		.0108	.000480
	.0231	.000731		.0022	.000274		.0086	.000454		.0115	.000505
	.0238	.000745		.0023	.000327		.0089	.000459		.0123	.000500
	.0246	.000731		.0025	.000337		.0092	.000500		.0131	.000536
	.0254	.000745		.0028	.000351		.0095	.000464		.0131	.000459
	.0262	.000870		.0034	.000351		.0098	.000464		.0138	.000561
	.0269	.000817		.0037	.000346		.0102	.000459		.0138	.000495
	.0292	.000928		.0043	.000361		.0105	.000439		.0146	.000469
	.0300	.000986		.0046	.000351		.0111	.000459		.0154	.000520
	.0308	.000995		.0049	.000365		.0114	.000444		.0162	.000490
				.0052	.000356		.0123	.000485		.0169	.000505
.0646	.0009	.000716		.0058	.000409		.0131	.000444		.0177	.000546
	.0012	.000413		.0065	.000385		.0138	.000459		.0185	.000561
	.0018	.000312		.0068	.000396		.0146	.000464		.0192	.000561
	.0020	.000293		.0071	.000385		.0154	.000449		.0200	.000587
	.0022	.000274		.0074	.000394		.0162	.000510		.0208	.000607
	.0023	.000278		.0077	.000394		.0169	.000541		.0215	.000673
	.0028	.000278		.0085	.000370		.0177	.000520		.0223	.000653
	.0029	.000288		.0100	.000399		.0192	.000571		.0238	.000663
	.0031	.000298		.0115	.000375		.0208	.000561		.0246	.000694
	.0034	.000298		.0123	.000389		.0208	.000602		.0254	.000699
	.0037	.000302		.0138	.000442		.0215	.000612		.0262	.000735
	.0040	.000278		.0146	.000418		.0215	.000653		.0269	.000714
	.0043	.000307		.0154	.000447		.0231	.000638		.0285	.000755
	.0046	.000307		.0162	.000462		.0238	.000668		.0292	.000796
	.0049	.000312		.0169	.000519		.0246	.000648		.0300	.000740
	.0052	.000317		.0177	.000510		.0254	.000704		.0308	.000827
	.0055	.000331		.0185	.000519		.0262	.000714		.0315	.000883
	.0058	.000355		.0192	.000577		.0269	.000770		.0323	.000867
	.0062	.000331		.0200	.000562		.0277	.000755		.0331	.000969
	.0065	.000326		.0208	.000601		.0285	.000765		.0338	.000959
	.0074	.000384		.0215	.000630		.0292	.000801		.0346	.000974
	.0077	.000346		.0223	.000606		.0300	.000796		.0354	.00100
	.0080	.000384		.0231	.000625		.0308	.000827		.0362	.00101
	.0083	.000346		.0246	.000721		.0315	.000842		.0369	.00104
	.0086	.000350		.0254	.000731		.0323	.000898			

TABLE I.—TABULATION OF DATA FROM DENSITOMETER—Continued

(c) Arrangement B: Values obtained in Cartesian coordinates (chord = 6.5 in.)—Continued

$Re_\infty = 1.4 \times 10^6$; $M_\infty = 0.717$; $\rho_t = 0.001532$ slugs/cu ft; $p_t = 10.00$ lb/sq in. Concluded

x/c	z/c	V/V∞	x/c	z/c	V/V∞	x/c	z/c	V/V∞	x/c	z/c	V/V∞
0.0892	0.0008	0.000755	0.0954	0.0052	0.000695	0.1015	0.0192	0.000665	0.1077	0.0338	0.000791
	.0009	.000643		.0055	.000760		.0200	.000630		.0346	.000786
	.0011	.000592		.0058	.000705		.0208	.000615		.0354	.000827
	.0012	.000571		.0062	.000720		.0215	.000640		.0362	.000765
	.0014	.000551		.0065	.000710		.0223	.000630		.0369	.000786
	.0015	.000541		.0068	.000760		.0231	.000640		.0377	.000878
	.0017	.000520		.0071	.000705		.0238	.000695		.0385	.000857
	.0018	.000531		.0074	.000750		.0246	.000675		.0392	.000832
	.0022	.000526		.0077	.000775		.0254	.000625		.0400	.000847
	.0025	.000551		.0085	.000730		.0262	.000700		.0408	.000883
	.0028	.000515		.0092	.000780		.0269	.000670		.0415	.000929
	.0031	.000592		.0100	.000790		.0277	.000695		.0423	.000929
	.0034	.000556		.0108	.000775		.0285	.000730		.0431	.000980
	.0037	.000602		.0115	.000770		.0292	.000710		.0438	.000980
	.0040	.000597		.0123	.000760		.0300	.000710		.0446	.00102
	.0043	.000612		.0131	.000725		.0308	.000730			
	.0046	.000607		.0138	.000675		.0315	.000770	.1138	.0008	.000939
	.0046	.000612		.0146	.000655		.0323	.000730		.0009	.000837
	.0052	.000628		.0154	.000610		.0331	.000790		.0011	.000730
	.0055	.000638		.0162	.000625		.0338	.000800		.0012	.000730
	.0058	.000638		.0169	.000610		.0346	.000780		.0015	.000796
	.0062	.000653		.0177	.000630		.0354	.000820		.0018	.000801
	.0065	.000628		.0185	.000610		.0362	.000835		.0022	.000806
	.0068	.000658		.0192	.000600		.0369	.000760		.0025	.000816
	.0071	.000658		.0200	.000595		.0377	.000795		.0028	.000852
	.0074	.000653		.0208	.000605		.0385	.000955		.0031	.000869
	.0077	.000673		.0215	.000580		.0392	.000850		.0034	.000816
	.0085	.000653		.0223	.000625		.0400	.000875		.0037	.000888
	.0092	.000638		.0231	.000620		.0408	.000870		.0040	.000944
	.0100	.000653		.0238	.000660		.0415	.000950		.0043	.000959
	.0108	.000602		.0246	.000625		.0423	.000950		.0046	.000939
	.0115	.000571		.0254	.000630		.0431	.000905		.0054	.00112
	.0123	.000617		.0262	.000660		.0438	.000950		.0062	.00115
	.0131	.000556		.0269	.000695					.0069	.00115
	.0138	.000541		.0277	.000700	.1077	.0009	.000862		.0077	.00110
	.0146	.000561		.0285	.000700		.0012	.000791		.0085	.00120
	.0154	.000541		.0292	.000730		.0015	.000714		.0092	.00120
	.0162	.000500		.0300	.000745		.0018	.000704		.0100	.00117
	.0169	.000536		.0308	.000775		.0022	.000735		.0108	.00111
	.0177	.000612		.0315	.000825		.0025	.000684		.0115	.00114
	.0185	.000561		.0323	.000760		.0028	.000745		.0123	.00120
	.0192	.000561		.0331	.000805		.0031	.000816		.0131	.00114
	.0200	.000587		.0338	.000860		.0034	.000740		.0138	.00124
	.0208	.000602		.0346	.000875		.0037	.000791		.0146	.00114
	.0215	.000658		.0354	.000875		.0040	.000878		.0154	.00118
	.0223	.000622		.0362	.000845		.0043	.000862		.0162	.00120
	.0231	.000643		.0369	.000910		.0046	.000847		.0169	.00120
	.0238	.000663		.0377	.000940		.0054	.000872		.0177	.00112
	.0246	.000684					.0062	.000934		.0185	.00115
	.0254	.000673	.1015	.0012	.000715		.0069	.000939		.0192	.00112
	.0262	.000724		.0014	.000710		.0077	.000939		.0200	.00115
	.0269	.000714		.0015	.000710		.0085	.000929		.0208	.00104
	.0291	.000745		.0015	.000700		.0092	.000990		.0215	.000954
	.0285	.000776		.0018	.000650		.0100	.000944		.0223	.000867
	.0292	.000750		.0022	.000675		.0108	.000990		.0231	.000888
	.0300	.000755		.0025	.000645		.0015	.00105		.0237	.000806
	.0308	.000796		.0028	.000675		.0123	.00107		.0254	.000827
	.0315	.000806		.0031	.000655		.0131	.000959		.0262	.000827
	.0323	.000847		.0034	.000700		.0138	.000980		.0269	.000806
	.0331	.000898		.0037	.000675		.0146	.000985		.0277	.000776
	.0338	.000847		.0040	.000735		.0154	.00100		.0285	.000832
	.0346	.000929		.0043	.000705		.0162	.000990		.0292	.000796
	.0354	.000923		.0046	.000770		.0169	.000985		.0300	.000765
	.0369	.000934		.0049	.000780		.0177	.000959		.0308	.000765
	.0377	.000969		.0052	.000760		.0185	.000878		.0315	.000816
				.0055	.000790		.0192	.000821		.0323	.000765
.0954	.0014	.000640		.0058	.000805		.0200	.000714		.0331	.000755
	.0015	.000620		.0062	.000810		.0208	.000750		.0338	.000827
	.0017	.000610		.0060	.000830		.0215	.000714		.0346	.000821
	.0018	.000595		.0077	.000810		.0223	.000730		.0354	.000776
	.0020	.000600		.0085	.000825		.0231	.000689		.0362	.000878
	.0022	.000590		.0092	.000840		.0238	.000704		.0369	.000893
	.0023	.000625		.0100	.000860		.0246	.000735		.0377	.000842
	.0025	.000625		.0108	.000890		.0254	.000704		.0385	.000842
	.0026	.000620		.0115	.000850		.0262	.000719		.0392	.000918
	.0028	.000620		.0123	.000885		.0269	.000714		.0400	.000821
	.0029	.000625		.0131	.000910		.0277	.000714		.0408	.000908
	.0031	.000630		.0138	.000910		.0285	.000730		.0415	.000878
	.0034	.000660		.0146	.000850		.0292	.000765		.0423	.000908
	.0037	.000670		.0154	.000840		.0300	.000724		.0431	.000893
	.0040	.000720		.0162	.000825		.0308	.000740		.0438	.000959
	.0043	.000720		.0169	.000710		.0315	.000816		.0446	.00106
	.0046	.000700		.0177	.000710		.0323	.000765		.0454	.000995
	.0049	.000675		.0185	.000690		.0331	.000776		.0462	.000965

TABLE I.—TABULATION OF DATA FROM DENSITOMETER—Continued

(a) Arrangement B: Values obtained in Cartesian coordinates (chord=6.5 in.)—Continued

$Re_\infty = 2.0 \times 10^6$; $M_\infty = 0.737$; $\rho_1 = 0.002126$ slugs/cu ft; $p_t = 14.22$ lb/sq in.

x/c	z/c	V/V_m	x/c	z/c	V/V_m	x/c	z/c	V/V_m	x/c	z/c	V/V_m
0.0046	0.0008	0.00250	0.0185	0.0105	0.00368	0.0369	0.0025	0.000655	0.0462	0.0100	0.00180
	.0009	.00178		.0108	.00373		.0028	.000745		.0108	.00202
	.0011	.00140		.0111	.00376		.0031	.000936		.0115	.00201
	.0014	.00159		.0114	.00400		.0034	.000909		.0123	.00206
	.0015	.00178		.0117	.00409		.0037	.000982		.0131	.00207
	.0018	.00178		.0120	.00436		.0040	.00102		.0138	.00215
	.0022	.00236		.0123	.00513		.0043	.00100		.0146	.00221
	.0025	.00359		.0126	.00477		.0046	.00103		.0154	.00257
	.0028	.00439		.0129	.00505		.0049	.00111		.0162	.00254
	.0031	.00551		.0132	.00527		.0052	.00107		.0169	.00282
				.0135	.00518		.0055	.00126		.0177	.00254
.0108	.0006	.00190		.0138	.00518		.0058	.00123		.0185	.00299
	.0008	.00107					.0062	.00123		.0192	.00303
	.0009	.000814	.0277	.0006	.00191		.0065	.00127		.0200	.00320
	.0011	.000655		.0008	.000864		.0068	.00129		.0208	.00361
	.0012	.0005566		.0009	.000727		.0071	.00146		.0215	.00361
	.0014	.000522		.0011	.000618		.0074	.00155			
	.0015	.000487		.0012	.000473		.0077	.00136	.0508	.0009	.00137
	.0017	.000442		.0014	.000427		.0080	.00143		.0012	.00115
	.0018	.000363		.0015	.000382		.0083	.00147		.0015	.00117
	.0026	.000354		.0018	.000345		.0086	.00148		.0018	.00130
	.0028	.000381		.0025	.000345		.0089	.00139		.0022	.00140
	.0029	.000434		.0028	.000355		.0092	.00147		.0025	.00144
	.0031	.000469		.0031	.000409		.0092	.00162		.0028	.00143
	.0034	.0005584		.0034	.000464		.0095	.00170		.0031	.00142
	.0037	.000770		.0037	.000609		.0098	.00175		.0034	.00142
	.0040	.000982		.0040	.000682		.0102	.00176		.0037	.00145
	.0043	.00112		.0043	.000773		.0105	.00174		.0040	.00133
	.0046	.00133		.0046	.000845		.0108	.00173		.0043	.00136
	.0049	.00150		.0049	.000927		.0111	.00189		.0046	.00148
	.0052	.00165		.0052	.000945		.0114	.00203		.0049	.00133
	.0055	.00186		.0055	.000991		.0117	.00204		.0052	.00139
	.0058	.00197		.0058	.00103		.0120	.00211		.0055	.00152
	.0062	.00212		.0062	.00115		.0123	.00207		.0058	.00149
	.0065	.00248		.0065	.00121		.0131	.00229		.0062	.00151
	.0068	.00252		.0068	.00136		.0138	.00227		.0065	.00152
	.0071	.00313		.0071	.00147		.0146	.00250		.0068	.00166
	.0074	.00322		.0074	.00139		.0154	.00264		.0071	.00158
	.0077	.00363		.0077	.00144		.0162	.00259		.0074	.00161
	.0080	.00416		.0080	.00162		.0169	.00309		.0077	.00162
	.0083	.00416		.0083	.00162		.0177	.00318		.0080	.00166
	.0086	.00490		.0086	.00171		.0185	.00296		.0083	.00157
				.0089	.00143		.0192	.00318		.0086	.00155
.0185	.0006	.00214		.0092	.00182		.0200	.00311		.0089	.00166
	.0008	.00101		.0095	.00185		.0208	.00386		.0092	.00166
	.0009	.000727		.0098	.00193		.0215	.00382		.0095	.00170
	.0011	.000600		.0102	.00199		.0223	.00423		.0098	.00184
	.0012	.000527		.0105	.00210		.0231	.00418		.0102	.00176
	.0015	.000427		.0108	.00208		.0238	.00441		.0105	.00183
	.0017	.000364		.0111	.00221		.0246	.00464		.0108	.00179
	.0018	.000382		.0114	.00232		.0254	.00482		.0115	.00185
	.0022	.000327		.0117	.00218		.0262	.00491		.0123	.00200
	.0025	.000300		.0120	.00236					.0131	.00198
	.0028	.000382		.0123	.00264	.0462	.0009	.00320		.0138	.00204
	.0031	.000464		.0126	.00268		.0011	.00148		.0146	.00214
	.0034	.000527		.0129	.00259		.0012	.00110		.0154	.00220
	.0037	.000809		.0132	.00268		.0014	.00100		.0162	.00212
	.0040	.000936		.0135	.00273		.0015	.000959		.0169	.00217
	.0043	.000936		.0138	.00277		.0018	.000926		.0177	.00250
	.0046	.00106		.0146	.00291		.0022	.000967		.0185	.00230
	.0049	.00122		.0154	.00314		.0025	.00101		.0192	.00252
	.0052	.00126		.0162	.00332		.0028	.00112		.0200	.00274
	.0055	.00138		.0169	.00372		.0028	.00115		.0208	.00270
	.0058	.00140		.0177	.00376		.0031	.00112		.0215	.00304
	.0062	.00161		.0185	.00318		.0034	.00120		.0223	.00297
	.0065	.00171		.0192	.00455		.0037	.00122		.0231	.00297
	.0068	.00172		.0200	.00455		.0040	.00124		.0238	.00314
	.0071	.00191		.0208	.00500		.0043	.00121		.0238	.00358
	.0074	.00198					.0046	.00128		.0246	.00341
	.0077	.00210	.0369	.0008	.00100		.0049	.00117		.0254	.00319
	.0080	.00229		.0009	.000709		.0052	.00131		.0262	.00354
	.0083	.00245		.0011	.000682		.0055	.00132		.0269	.00384
	.0086	.00255		.0012	.000527		.0058	.00143		.0277	.00376
	.0089	.00264		.0014	.000482		.0062	.00145		.0285	.00389
	.0092	.00291		.0015	.000455		.0069	.00148		.0292	.00407
	.0095	.00304		.0017	.000455		.0077	.00145		.0300	.00425
	.0098	.00331		.0018	.000482		.0085	.00162		.0308	.00451
	.0102	.00341		.0022	.000545		.0092	.00160			

TABLE I.—TABULATION OF DATA FROM DENSITOMETER—Continued

(a) Arrangement B: Values obtained in Cartesian coordinates (chord = 6.5 in.) —Continued

$Re_\infty = 2.0 \times 10^6$; $M_\infty = 0.737$; $\rho_t = 0.002126$ slugs/cu ft; $p_t = 14.22$ lb/sq in.

x/c	z/c	V/V∞	x/c	z/c	V/V∞	x/c	z/c	V/V∞	x/c	z/c	V/V∞
0.0554	0.0006	0.00230	0.0554	0.0252	0.00365	0.0615	0.0040	0.00221	0.0646	0.0055	0.00236
	.0008	.00143		.0254	.00369		.0043	.00221		.0058	.00249
	.0009	.00212		.0262	.00373		.0046	.00214		.0062	.00256
	.0012	.00218					.0054	.00241		.0065	.00241
	.0015	.00158	.0585	.0009	.00190		.0062	.00230		.0068	.00263
	.0018	.00161		.0012	.00189		.0069	.00217		.0071	.00262
	.0022	.00171		.0015	.00188		.0077	.00221		.0071	.00260
	.0025	.00162		.0018	.00203		.0085	.00199		.0074	.00240
	.0028	.00162		.0022	.00202		.0092	.00199		.0077	.00231
	.0031	.00160		.0025	.00192		.0100	.00208		.0080	.00265
	.0034	.00159		.0028	.00199		.0108	.00199		.0083	.00241
	.0037	.00166		.0031	.00202		.0123	.00199		.0086	.00250
	.0040	.00163		.0034	.00205		.0131	.00204		.0089	.00246
	.0043	.00171		.0037	.00214		.0138	.00177		.0092	.00232
	.0046	.00162		.0040	.00219		.0146	.00181		.0095	.00236
	.0046	.00159		.0043	.00211		.0154	.00199		.0102	.00218
	.0049	.00166		.0046	.00205		.0162	.00190		.0105	.00240
	.0052	.00180		.0049	.00228		.0169	.00199		.0111	.00210
	.0055	.00184		.0052	.00221		.0177	.00217		.0114	.00218
	.0058	.00184		.0055	.00218		.0185	.00226		.0117	.00205
	.0062	.00193		.0058	.00230		.0192	.00217		.0120	.00236
	.0065	.00202		.0062	.00204		.0200	.00230		.0123	.00218
	.0068	.00189		.0069	.00217		.0208	.00243		.0126	.00227
	.0071	.00200		.0077	.00199		.0215	.00217		.0129	.00218
	.0074	.00193		.0085	.00195		.0223	.00243		.0132	.00227
	.0077	.00189		.0092	.00208		.0231	.00252		.0135	.00214
	.0080	.00192		.0108	.00208		.0238	.00252		.0138	.00214
	.0083	.00188		.0115	.00191		.0246	.00261		.0142	.00227
	.0089	.00188		.0123	.00208		.0254	.00274		.0145	.00200
	.0092	.00204		.0131	.00243		.0262	.00274		.0148	.00191
	.0095	.00203		.0138	.00221		.0269	.00297		.0151	.00205
	.0098	.00195		.0146	.00212		.0277	.00274		.0154	.00205
	.0098	.00191		.0154	.00221		.0285	.00297		.0157	.00214
	.0102	.00205		.0162	.00230		.0292	.00341		.0160	.00196
	.0105	.00198		.0169	.00230		.0300	.00314		.0163	.00214
	.0108	.00202		.0177	.00243		.0308	.00341		.0166	.00214
	.0111	.00202		.0185	.00252		.0315	.00341		.0169	.00209
	.0114	.00203		.0192	.00260		.0323	.00362		.0172	.00218
	.0117	.00207		.0200	.00253		.0331	.00350		.0175	.00214
	.0120	.00216		.0208	.00266		.0338	.00363		.0178	.00214
	.0123	.00215		.0215	.00279		.0346	.00376		.0182	.00223
	.0126	.00210		.0223	.00279		.0354	.00376		.0185	.00249
	.0129	.00216		.0231	.00292		.0362	.00385		.0191	.00236
	.0132	.00204		.0238	.00288		.0369	.00434		.0194	.00218
	.0135	.00215		.0246	.00319		.0385	.00474		.0197	.00246
	.0138	.00221		.0254	.00319		.0392	.00460		.0200	.00232
	.0142	.00220		.0262	.00327		.0400	.00496		.0203	.00236
	.0145	.00220		.0269	.00341					.0206	.00241
	.0148	.00215		.0277	.00341	.0646	.0006	.00336		.0209	.00245
	.0151	.00246		.0285	.00350		.0008	.00230		.0212	.00236
	.0154	.00230		.0292	.00358		.0009	.00166		.0218	.00236
	.0157	.00250		.0300	.00363		.0011	.00166		.0222	.00250
	.0160	.00234		.0308	.00393		.0012	.00173		.0225	.00233
	.0163	.00250		.0315	.00373		.0014	.00185		.0228	.00246
	.0166	.00250		.0323	.00425		.0015	.00182		.0231	.00255
	.0169	.00246		.0331	.00412		.0017	.00188		.0234	.00264
	.0172	.00246		.0338	.00443		.0018	.00186		.0237	.00236
	.0177	.00246		.0346	.00456		.0022	.00211		.0240	.00250
	.0185	.00250		.0354	.00478		.0023	.00211		.0243	.00277
	.0192	.00279					.0025	.00208		.0246	.00268
	.0200	.00298	.0615	.0008	.00195		.0028	.00210		.0249	.00264
	.0208	.00307		.0009	.00192		.0031	.00230		.0252	.00267
	.0215	.00298		.0012	.00189		.0034	.00209		.0255	.00286
	.0223	.00312		.0015	.00204		.0037	.00210		.0258	.00282
	.0231	.00315		.0018	.00204		.0040	.00210		.0262	.00274
	.0238	.00324		.0022	.00205		.0042	.00220		.0269	.00303
	.0243	.00339		.0025	.00214		.0043	.00235		.0277	.00286
	.0245	.00353		.0028	.00200		.0045	.00238		.0285	.00296
	.0246	.00373		.0031	.00206		.0046	.00232		.0292	.00358
	.0248	.00356		.0034	.00206		.0049	.00226		.0300	.00291
	.0249	.00341		.0037	.00225		.0052	.00234		.0308	.00346
										.0315	.00355
										.0323	.00364

TABLE I.—TABULATION OF DATA FROM DENSITOMETER—Continued

(c) Arrangement B: Values obtained in Cartesian coordinates (chord=6.5 in.)—Continued

$Re_\infty = 2.0 \times 10^6$; $M_\infty = 0.737$; $\rho_t = 0.002126$ slugs/cu ft; $p_t = 14.22$ lb/sq in.

x/c	z/c	V/V∞	x/c	z/c	V/V∞	x/c	z/c	V/V∞	x/c	z/c	V/V∞
0.0692	0.0006	0.00240	0.0738	0.0080	0.00364	0.0785	0.0028	0.00286	0.0831	0.0086	0.00435
	.0008	.00223		.0083	.00373		.0031	.00296		.0092	.00467
	.0009	.00243		.0086	.00368		.0034	.00327		.0100	.00453
	.0012	.00250		.0089	.00368		.0037	.00324		.0108	.00500
	.0015	.00232		.0092	.00364		.0040	.00314		.0115	.00486
	.0018	.00232		.0095	.00371		.0043	.00323		.0123	.00490
	.0022	.00254		.0098	.00377		.0046	.00293		.0131	.00522
	.0025	.00251		.0102	.00373		.0054	.00364		.0138	.00514
	.0028	.00259		.0105	.00336		.0062	.00391		.0146	.00500
	.0031	.00281		.0108	.00359		.0069	.00427		.0154	.00441
	.0034	.00264		.0111	.00359		.0077	.00436		.0162	.00393
	.0037	.00308		.0114	.00364		.0085	.00436		.0169	.00336
	.0040	.00305		.0117	.00309		.0092	.00436		.0185	.00308
	.0043	.00318		.0120	.00350		.0100	.00441		.0192	.00304
	.0046	.00318		.0123	.00291		.0108	.00455		.0200	.00280
	.0054	.00322		.0126	.00336		.0115	.00492		.0208	.00290
	.0062	.00327		.0129	.00282		.0123	.00450		.0223	.00257
	.0069	.00368		.0132	.00273		.0131	.00436		.0231	.00280
	.0077	.00368		.0135	.00282		.0138	.00418		.0238	.00276
	.0085	.00332		.0138	.00277		.0146	.00373		.0246	.00258
	.0092	.00318		.0142	.00264		.0154	.00355		.0254	.00277
	.0100	.00300		.0145	.00264		.0162	.00328		.0262	.00262
	.0108	.00277		.0148	.00241		.0169	.00286		.0269	.00272
	.0115	.00273		.0151	.00259		.0177	.00282		.0277	.00276
	.0123	.00264		.0154	.00259		.0185	.00277		.0285	.00271
	.0131	.00269		.0157	.00246		.0192	.00296		.0292	.00285
	.0138	.00236		.0160	.00246		.0200	.00269		.0315	.00304
	.0146	.00241		.0163	.00233		.0208	.00255		.0323	.00304
	.0154	.00241		.0166	.00255		.0215	.00259		.0331	.00331
	.0162	.00223		.0169	.00236		.0223	.00277		.0338	.00318
	.0169	.00231		.0172	.00241		.0231	.00277		.0346	.00321
	.0177	.00227		.0175	.00246		.0238	.00269		.0354	.00340
	.0185	.00218		.0178	.00232		.0246	.00268		.0362	.00313
	.0192	.00236		.0182	.00241		.0254	.00296		.0369	.00354
	.0200	.00332		.0185	.00224		.0262	.00273		.0377	.00374
	.0208	.00232		.0188	.00232		.0269	.00268		.0385	.00360
	.0215	.00255		.0191	.00246		.0277	.00286			
	.0223	.00255		.0194	.00218		.0285	.00273	.0877	.0012	.00345
	.0231	.00246		.0197	.00218		.0292	.00309		.0015	.00341
	.0238	.00255		.0200	.00236		.0300	.00327		.0018	.00361
	.0246	.00263		.0203	.00250		.0308	.00309		.0022	.00358
	.0254	.00259		.0206	.00241		.0315	.00323		.0025	.00358
	.0262	.00282		.0209	.00206		.0323	.00309		.0028	.00381
	.0277	.00314		.0212	.00223		.0331	.00323		.0031	.00388
	.0285	.00323		.0215	.00232		.0338	.00332		.0038	.00443
	.0292	.00341		.0218	.00241		.0346	.00368		.0046	.00420
	.0308	.00327		.0222	.00250		.0354	.00350		.0054	.00443
	.0315	.00350		.0225	.00236		.0362	.00359		.0062	.00496
	.0323	.00350		.0228	.00250		.0369	.00346		.0069	.00496
	.0331	.00367		.0231	.00242		.0377	.00350		.0077	.00540
	.0338	.00372		.0234	.00236		.0385	.00386		.0177	.00509
	.0346	.00382		.0237	.00236		.0392	.00391		.0185	.00500
	.0354	.00400		.0240	.00255		.0400	.00409		.0192	.00509
	.0362	.00409		.0243	.00228		.0408	.00400		.0200	.00385
	.0369	.00441		.0246	.00242		.0415	.00418		.0208	.00394
	.0377	.00432		.0249	.00245		.0423	.00436		.0215	.00372
	.0385	.00436		.0252	.00250		.0431	.00436		.0223	.00381
	.0392	.00463		.0255	.00259		.0438	.00446		.0231	.00385
	.0400	.00481		.0258	.00246		.0446	.00477		.0238	.00364
	.0408	.00532		.0262	.00255		.0454	.00468		.0246	.00359
	.0415	.00468		.0265	.00367		.0462	.00473		.0254	.00354
	.0423	.00509		.0268	.00259		.0469	.00496		.0262	.00345
	.0431	.00532		.0271	.00273					.0269	.00341
				.0274	.00264	.0831	.0006	.00439		.0277	.00323
.0738	.0009	.00300		.0277	.00277		.0008	.00296		.0285	.00327
	.0011	.00201		.0280	.00286		.0009	.00264		.0292	.00323
	.0012	.00193		.0283	.00273		.0012	.00272		.0300	.00363
	.0014	.00190		.0286	.00277		.0015	.00272		.0308	.00323
	.0018	.00232		.0292	.00277		.0018	.00263		.0315	.00327
	.0022	.00228		.0295	.00291		.0022	.00273		.0323	.00344
	.0025	.00220		.0298	.00269		.0025	.00285		.0331	.00372
	.0028	.00229		.0302	.00305		.0028	.00285		.0338	.00359
	.0031	.00244		.0305	.00277		.0031	.00318		.0346	.00336
	.0034	.00262		.0308	.00305		.0034	.00308		.0354	.00350
	.0037	.00257		.0311	.00318		.0037	.00313		.0362	.00354
	.0040	.00286		.0314	.00314		.0040	.00322		.0369	.00384
	.0043	.00277		.0317	.00318		.0043	.00340		.0377	.00372
	.0046	.00277		.0320	.00323		.0046	.00340		.0385	.00385
	.0049	.00305		.0323	.00323		.0058	.00371		.0392	.00412
	.0052	.00305		.0331	.00346		.0058	.00397		.0400	.00408
	.0055	.00300		.0338	.00300		.0062	.00393		.0408	.00420
	.0058	.00331					.0065	.00388		.0415	.00404
	.0062	.00318	.0785	.0009	.00264		.0068	.00397		.0423	.00412
	.0065	.00346		.0012	.00259		.0071	.00397		.0431	.00407
	.0068	.00327		.0015	.00264		.0074	.00393		.0438	.00450
	.0071	.00345		.0018	.00286		.0077	.00425		.0446	.00439
	.0074	.00332		.0022	.00282		.0080	.00453		.0454	.00465
	.0077	.00364		.0025	.00285		.0083	.00435		.0462	.00509

TABLE I.—TABULATION OF DATA FROM DENSITOMETER—Continued

(c) Arrangement B: Values obtained in Cartesian coordinates (chord = 6.5 in.)—Continued

$Re_\infty = 2.0 \times 10^6$; $M_\infty = 0.737$; $\rho_t = 0.002126$ slugs/cu ft; $p_t = 14.22$ lb/sq in. (Concluded)

x/c	z/c	V/V_m	x/c	z/c	V/V_m	x/c	z/c	V/V_m	x/c	z/c	V/V_m
0.0923	0.0012	0.00290	0.0923	0.0246	0.00346	0.1015	0.0169	0.00688	0.1108	0.0108	0.00746
	.0014	.00279		.0254	.00341		.0177	.00746		.0115	.00759
	.0015	.00266		.0262	.00322		.0185	.00768		.0123	.00782
	.0017	.00271		.0269	.00351		.0192	.00746		.0131	.00764
	.0018	.00280		.0277	.00308		.0200	.00750		.0138	.00782
	.0018	.00284		.0285	.00318		.0208	.00789		.0146	.00764
	.0020	.00308		.0292	.00280		.0215	.00786		.0154	.00850
	.0022	.00299		.0300	.00305		.0223	.00777		.0162	.00805
	.0025	.00312		.0308	.00327		.0231	.00719		.0169	.00841
	.0028	.00318		.0315	.00322		.0238	.00722		.0177	.00818
	.0031	.00294		.0323	.00327		.0246	.00723		.0185	.00836
	.0034	.00326		.0331	.00308		.0254	.00571		.0192	.00864
	.0037	.00346		.0338	.00299		.0262	.00547		.0200	.00827
	.0043	.00369		.0346	.00322		.0269	.00478		.0208	.00782
	.0046	.00378		.0354	.00322		.0277	.00460		.0215	.00814
	.0049	.00407		.0362	.00327		.0285	.00451		.0223	.00877
	.0052	.00434		.0369	.00336		.0292	.00438		.0231	.00818
	.0055	.00421		.0377	.00355		.0300	.00384		.0238	.00827
	.0058	.00406		.0385	.00336		.0308	.00371		.0246	.00764
	.0062	.00453		.0392	.00346		.0315	.00366		.0254	.00800
	.0065	.00453		.0400	.00327		.0323	.00375		.0262	.00782
	.0068	.00458		.0408	.00355		.0331	.00366		.0269	.00796
	.0071	.00444		.0415	.00351		.0338	.00366		.0277	.00782
	.0074	.00467		.0423	.00351		.0346	.00362		.0285	.00714
	.0077	.00495		.0431	.00360		.0354	.00344		.0292	.00627
	.0080	.00500					.0362	.00371		.0300	.00491
	.0083	.00527	.1015	.0009	.00397		.0369	.00380		.0308	.00464
	.0086	.00486		.0011	.00363		.0377	.00348		.0315	.00455
	.0089	.00533		.0012	.00348		.0385	.00357		.0323	.00432
	.0092	.00505		.0014	.00362		.0392	.00344		.0331	.00414
	.0095	.00509		.0015	.00366		.0400	.00357		.0338	.00418
	.0098	.00556		.0018	.00402		.0408	.00362		.0346	.00418
	.0102	.00542		.0022	.00385		.0415	.00335		.0354	.00391
	.0105	.00514		.0025	.00411		.0423	.00357		.0362	.00364
	.0108	.00555		.0028	.00415		.0431	.00357		.0369	.00364
	.0114	.00592		.0031	.00455		.0438	.00362		.0377	.00341
	.0117	.00592		.0034	.00452		.0446	.00380		.0385	.00346
	.0120	.00561		.0037	.00486		.0454	.00384		.0392	.00341
	.0123	.00570		.0040	.00499		.0469	.00384		.0400	.00323
	.0126	.00565		.0043	.00479		.0477	.00397		.0408	.00364
	.0129	.00579		.0046	.00505		.0485	.00402		.0415	.00336
	.0132	.00584		.0049	.00505		.0492	.00388		.0423	.00373
	.0135	.00565		.0052	.00491		.0500	.00380		.0431	.00350
	.0138	.00542		.0055	.00518		.0508	.00408		.0446	.00350
	.0142	.00565		.0058	.00496		.0515	.00429		.0454	.00341
	.0145	.00551		.0062	.00540		.0523	.00411		.0462	.00373
	.0154	.00584		.0065	.00504		.0531	.00438		.0469	.00377
	.0166	.00551		.0068	.00571		.0538	.00455		.0477	.00396
	.0169	.00547		.0071	.00530		.0546	.00446		.0492	.00364
	.0172	.00523		.0074	.00589		.0554	.00429		.0500	.00364
	.0175	.00575		.0077	.00612		.0562	.00480		.0508	.00377
	.0178	.00565		.0080	.00563		.0569	.00491		.0515	.00420
	.0182	.00528		.0083	.00625		.0577	.00473		.0523	.00418
	.0185	.00542		.0086	.00618					.0531	.00427
	.0188	.00547		.0089	.00629	.1108	.0006	.00386		.0538	.00455
	.0191	.00537		.0092	.00617		.0009	.00341		.0546	.00432
	.0194	.00563		.0095	.00638		.0012	.00364		.0554	.00464
	.0197	.00505		.0098	.00643		.0015	.00373		.0562	.00459
	.0200	.00495		.0103	.00625		.0018	.00386		.0569	.00491
	.0203	.00467		.0108	.00674		.0023	.00418		.0577	.00455
	.0206	.00472		.0112	.00692		.0031	.00464		.0585	.00464
	.0209	.00407		.0117	.00709		.0038	.00491		.0600	.00509
	.0212	.00411		.0122	.00781		.0046	.00500		.0608	.00491
	.0215	.00388		.0126	.00737		.0054	.00568		.0615	.00486
	.0218	.00331		.0131	.00772		.0062	.00636		.0623	.00496
	.0222	.00383		.0135	.00720		.0069	.00650		.0631	.00527
	.0225	.00365		.0138	.00746		.0077	.00650		.0638	.00577
	.0228	.00351		.0146	.00754		.0085	.00646		.0646	.00595
	.0231	.00355		.0154	.00763		.0092	.00746		.0654	.00591
	.0238	.00360		.0162	.00808		.0100	.00759		.0662	.00586
										.0669	.00636
										.0677	.00623

TABLE I.—TABULATION OF DATA FROM DENSITOMETER Concluded

(c) Arrangement B: Values obtained in Cartesian coordinates (chord=6.5 in.)—Concluded

$Re_\infty = 1.9 \times 10^6$; $M_\infty = 0.681$; $\rho_t = 0.002123$ slugs cu ft; $p_t = 14.21$ lb/sq in.

x/c	z/c	V/V_m	x/c	z/c	V/V_m	x/c	z/c	V/V_m	x/c	z/c	V/V_m
0.0154	0.0003	0.00849	0.0462	0.0062	0.00780	0.0769	0.0003	0.00746	0.0923	0.0115	0.00898
	.0006	.00746		.0069	.00763		.0006	.00737		.0123	.0100
	.0009	.00737		.0077	.00763		.0009	.00696		.0131	.00992
	.0012	.00703		.0085	.00831		.0012	.00670		.0138	.00992
	.0015	.00720		.0092	.00835		.0015	.00686		.0146	.00941
	.0018	.00695		.0100	.00848		.0018	.00678		.0154	.0100
	.0022	.00703		.0108	.00864		.0022	.00703		.0162	.00983
	.0025	.00703		.0115	.00881		.0025	.00729		.0169	.00932
	.0028	.00746		.0123	.00992		.0028	.00763		.0177	.00915
	.0031	.00788		.0131	.00958		.0031	.00771		.0185	.00992
	.0034	.00771		.0138	.00949		.0038	.00797		.0192	.00958
	.0038	.00907		.0146	.00949		.0046	.00848		.0200	.0102
	.0046	.00924		.0154	.0102		.0054	.00754		.0208	.0101
	.0054	.00848		.0162	.0102		.0062	.00864		.0215	.00992
	.0062	.0103		.0169	.0104		.0069	.00907		.0223	.0106
	.0069	.0111		.0177	.0112		.0077	.00848		.0231	.0110
							.0085	.00907		.0238	.0108
.0308	.0003	.00907	.0615	.0003	.00913		.0092	.00805		.0246	.0110
	.0006	.00678		.0006	.00774		.0100	.00924			
	.0008	.00737		.0009	.00696		.0108	.00848	.1077	.0006	.00746
	.0011	.00610		.0012	.00713		.0115	.00873		.0009	.00814
	.0012	.00644		.0015	.00678		.0123	.00957		.0012	.00814
	.0015	.00619		.0018	.00713		.0131	.00898		.0015	.00763
	.0018	.00661		.0022	.00696		.0138	.00915		.0018	.00788
	.0022	.00585		.0025	.00722		.0146	.00932		.0022	.00814
	.0025	.00661		.0028	.00696		.0154	.00941		.0025	.00805
	.0028	.00695		.0031	.00713		.0162	.0100		.0028	.00831
	.0031	.00712		.0034	.00722		.0169	.00949		.0031	.00864
	.0038	.00729		.0037	.00757		.0177	.00983		.0034	.00864
	.0046	.00737		.0040	.00757		.0185	.0103		.0037	.00831
	.0054	.00803		.0043	.00717		.0192	.0101		.0040	.00873
	.0062	.00831		.0046	.00791		.0200	.0108		.0043	.00881
	.0069	.00907		.0054	.00810					.0046	.00915
	.0077	.00864		.0062	.00800	.0923	.0006	.00805		.0054	.00949
	.0085	.00864		.0069	.00852		.0009	.00763		.0062	.00932
	.0092	.00873		.0077	.00878		.0012	.00746		.0069	.00949
	.0100	.00915		.0085	.00861		.0015	.00763		.0077	.00932
	.0108	.00983		.0092	.00878		.0018	.00754		.0085	.00949
	.0115	.00890		.0100	.00887		.0022	.00822		.0092	.00932
	.0123	.00909		.0108	.00887		.0025	.00771		.0085	.00949
	.0131	.00949		.0115	.00922		.0028	.00809		.0092	.00949
	.0138	.0108		.0123	.00904		.0031	.00848		.0108	.00958
				.0131	.00896		.0034	.00822		.0123	.00941
.0462	.0003	.00873		.0138	.00922		.0037	.00839		.0138	.00983
	.0006	.00695		.0146	.00948		.0040	.00848		.0154	.00983
	.0009	.00695		.0154	.00939		.0043	.00864		.0169	.00958
	.0012	.00686		.0162	.00965		.0046	.00864		.0185	.00966
	.0015	.00695		.0169	.0102		.0054	.00915		.0200	.00966
	.0018	.00627		.0177	.0103		.0062	.00915		.0215	.00958
	.0025	.00694		.0185	.00904		.0069	.00958		.0231	.00983
	.0028	.00729		.0192	.0104		.0077	.00831		.0246	.00992
	.0031	.00754		.0200	.0104		.0085	.00941		.0262	.0110
	.0038	.00746		.0208	.0106		.0092	.00898		.0277	.0108
	.0046	.00729		.0215	.0110		.0100	.00958		.0292	.0119
	.0054	.00780		.0223	.0112		.0108	.00907			

(d) Arrangement B: Film calibration data

V/V_m	$\rho \times 10^3$ slugs/cu f
0.000225	0.2395
.000828	.4287
.00187	.5996
.00540	.7537
.0105	.9285
.0195	1.126
.0535	1.398
.0541	1.398
.0676	1.546
.0752	1.546
.1116	1.698
.164	1.837
.197	1.837
.182	1.999
.190	1.999
.254	2.159
.308	2.303
.314	2.303
.317	2.303

TABLE II. ψ°, $\overline{\psi}$, AND ψ AS FUNCTIONS OF W AND θ ($\gamma = 1.405$)

w	θ	ψ°	$\overline{\psi}$	ψ	w	θ	ψ°	$\overline{\psi}$	ψ	w	θ	ψ°	$\overline{\psi}$	ψ
1.000	2.80	0.067	0.0004	0.0666	0.856	2.80	0.131	0.0008	0.1302	0.724	2.80	0.199	0.0011	0.1979
	2.70	.148	.0007	.1473		2.70	.259	------	------		2.70	.381	------	------
	2.60	.247	.0013	.2457		2.60	.405	.0020	.4030		2.60	.580	.0029	.5771
	2.5	.361	.0017	.3593		2.50	.569	------	------		2.50	.804	------	------
	2.4	.493	.0023	.4907		2.40	.760	.0034	.7566		2.40	1.057	.0048	1.0522
	2.2	.82	.0036	.8164		2.20	1.22	.0054	1.215		2.20	1.67	.0071	1.6626
	2.0	1.25	.0054	1.245		2.00	1.86	.0080	1.852		2.00	2.52	.0108	2.5092
	1.8	1.87	.0078	1.862		1.80	2.79	.0117	2.778		1.80	3.77	.0158	3.7542
	1.6	2.83	.0112	2.819		1.60	4.23	.0183	4.212		1.60	5.7	.0245	5.6755
	1.4	4.49	.0301	4.460		1.40	6.81	.0371	6.773		1.40	9.2	.0415	9.1585
	1.2	7.39	.0818	7.308		1.20	11.8	.0757	11.72		1.20	15.7	.0687	15.631
	1.0	13.7	.1315	13.57		1.00	21.4	.1127	21.29		1.00	28.1	.0950	28.005
	.9	17.8	.1382	17.66		.90	27	.1213	26.88		.90	38	.1035	37.897
	.8	25.5	.1414	25.36		.80	42	.1269	41.87		.80	55	.1099	54.890
	.7	40.0	.1457	39.85		.70	68	.1321	67.87		.70	86	.1153	85.885
	.6	68.5	.1524	68.35		.60	113	.1383	112.9		.60	134	.1207	133.88
	.5	119	.1592	118.8		.50	195	.1462	194.9		.50	222	.1264	221.87
	.45	163	.1691	162.8		.45	270	.1515	269.8		.45	284	.1293	283.87
	.40	225	.1792	224.8		.40	373	.1597	372.8		.40	366	.1326	365.87
	.35	328	.1980	327.8		.35	538	.1692	537.8		.35	481	.1360	480.86
	.30	484	.2164	483.8		.30	799	.1789	798.8		.30	631	.1387	630.86
	.25	758	.2336	757.8		.25	1238	.1880	1238		.25	816	.1399	815.86
	.20	1297	.2506	1297		.20	2182	.1952	2182		.20	1003	.1391	1002.86
	.15	2510	.2653	2510		.15	3768	.1983	3768		.15	1052	.1348	1051.87
	.10	6024	.2814	6024		.10	7389	.1951	7389		.10	579	.1257	578.87
	.05	24002	.3199	24002		.05	12317	.1794	12317		.05	−1015	.1110	−1015.11
	0	------	.1943	------		0	−11502	.1342	−11502		0	−3588	.0914	−3588.09
	−.05	−36439	.0368	−36439		−.05	−28338	.0810	−28338		−.05	−5441	.0692	−5441.07
	−.10	−10675	.0267	−10675		−.10	−15594	.0481	−15594		−.10	−5233	.0478	−5233.05
	−.15	−3974	.0131	−3974		−.15	−7238	.0260	−7238		−.15	−3542	.0281	−3542.03
	−.20	−981	.0035	−981.0		−.20	−2222	.0088	−2222		−.20	−1284	.0098	−1284.01
.963	.45	191	.1619	190.8	.821	.45	285	.1468	284.9	.693	.45	1106	.1230	1105.88
	.40	264	.1750	263.8		.40	395	.1535	394.8		.40	1296	.1253	1295.87
	.35	386	.1914	385.8		.35	557	.1612	556.8		.35	1530	.1275	1529.87
	.30	584	.2075	583.8		.30	814	.1690	813.8		.30	1820	.1289	1819.87
	.25	925	.2230	924.8		.25	1231	.1758	1230		.25	2177	.1289	2176.87
	.20	1581	.2377	1581		.20	1965	.1806	1965		.20	2603	.1269	2602.87
	.15	3137	.2497	3137		.15	3253	.1810	3253		.15	3084	.1218	3083.88
	.10	7768	.2613	7768		.10	5219	.1749	5219		.10	−8	.1129	−8.1129
	.05	33123	.2778	33123		.05	5007	.1575	5007		.05	−1187	.0997	−1187.10
	0	−57233	.1782	−57233		0	−8.348	.1220	−8.47		0	−2746	.0829	−2746.08
	−.05	−49348	.0548	−49348		−.05	−18198	.0808	−18198		−.05	−3822	.0641	−3822.06
	−.10	−13832	.0326	−13832		−.10	−12878	.0504	−12878		−.10	−3727	.0450	−3727.05
	−.15	−5245	.0166	−5245		−.15	−6732	.0279	−6732		−.15	−2614	.0268	−2614.03
	−.20	−1409	.0051	−1409		−.20	−2166	.0094	−2166		−.20	−967	.0094	−967.01
.927	2.80	.098	------	------	.788	2.80	.165	------	------	.662	2.80	.232	------	------
	2.70	.201	------	------		2.70	.320	------	------		2.70	.441	------	------
	2.60	.322	------	------		2.60	.492	------	------		2.60	.672	------	------
	2.50	.461	------	------		2.50	.684	------	------		2.50	.924	------	------
	.90	23.0	.1301	22.87		.90	33	.1124	32.89		.90	40	.0952	39.9048
	.80	34.0	.1346	33.87		.80	49	.1185	48.88		.80	57	.1013	56.8987
	.70	54.6	.1393	54.46		.70	79	.1240	78.88		.70	85	.1063	84.8937
	.60	90.9	.1458	90.75		.60	130	.1299	129.87		.60	129	.1109	128.89
	.50	156	.1535	155.8		.50	1060	.1370	1059.86		.50	194	.1149	193.89
	.45	219	.1591	218.8		.45	1285	.1413	1284.86		.45	237	.1166	236.88
	.40	305	.1704	304.8		.40	1587	.1469	1586.85		.40	287	.1182	286.88
	.35	445	.1843	444.8		.35	2000	.1529	1999.85		.35	341	.1194	340.88
	.30	669	.1983	668.8		.30	2578	.1587	2577.84		.30	397	.1197	396.88
	.25	1061	.2117	1061		.25	3412	.1633	3411.84		.25	428	.1187	427.88
	.20	1836	.2241	1836		.20	4635	.1660	4634.83		.20	389	.1158	388.88
	.15	3648	.2332	3648		.15	6376	.1643	6375.84		.15	185	.1103	184.89
	.10	8956	.2394	8956		.10	8326	.1565	8325.84		.10	−309	.1017	−309.10
	.05	33671	.2391	33671		.05	8033	.1393	8032.86		.05	−1142	.0898	−1142.09
	0	−26878	.1625	−26878		0	1189	.1109	1188.89		0	−2094	.0751	−2094.08
	−.05	−52219	.0688	−52219		−.05	−5597	.0782	−5597.08		−.05	−2714	.0589	−2714.06
	−.10	−16267	.0387	−16267		−.10	−5715	.0508	−5715.05		−.10	−2635	.0419	−2635.04
	−.15	−6377	.0201	−6377		−.15	−3440	.0288	−3440.03		−.15	−1880	.0253	−1880.03
	−.20	−1.803	.0066	−1.810		−.20	−1159	.0099	−1159.01		−.20	−702	.0088	−702.01
.892	.45	245	.1558	244.8	.755	.45	1338	.1354	1337.86	.632	.45	204	.1097	203.89
	.40	343	.1655	342.8		.40	1636	.1398	1635.86		.40	236	.1106	235.89
	.35	497	.1771	496.8		.35	2031	.1445	2030.86		.35	266	.1110	265.89
	.30	746	.1890	745.8		.30	2563	.1486	2562.85		.30	282	.1105	281.89
	.25	1179	.2004	1179		.25	3290	.1513	3289.85		.25	267	.1087	266.89
	.20	2024	.2101	2024		.20	4254	.1522	4253.85		.20	181	.1052	180.89
	.15	3911	.2162	3911		.15	5404	.1490	5403.85		.15	−34	.0996	−34.0996
	.10	8864	.2173	8864		.10	6209	.1402	6208.86		.10	−436	.0913	−436.09
	.05	23679	.2067	23679		.05	5250	.1240	5249.88		.05	−1007	.0807	−1007.08
	0	−16674	.1479	−16674		0	1199	.1007	1198.90		0	−1596	.0679	−1596.07
	−.05	−41930	.0773	−41930		−.05	−2801	.0741	−2801.07		−.05	−1946	.0535	−1946.05
	−.10	−16957	.0442	−16957		−.10	−3601	.0499	−3601.05		−.10	−1860	.0385	−1860.04
	−.15	−7120	.0233	−7120		−.15	−2506	.0288	−2506.03		−.15	−1330	.0231	−1330.02
	−.20	−2094	.0078	−2094		−.20	−896	.0100	−896.01		−.20	−498	.0080	−498.01

TABLE II.—ψ°, $\overline{\psi}$, AND ψ AS FUNCTIONS OF W AND θ (γ=1.405)—Continued

w	θ	ψ°	$\overline{\psi}$	ψ	w	θ	ψ°	$\overline{\psi}$	ψ	w	θ	ψ°	$\overline{\psi}$	ψ
0.604	2.80	0.263	0.0013	0.2617	0.450	0.90	24	0.0632	23.937	1.083	0.075	4326	0.3431	4326
	2.70	.501	------	--------		.80	28	.0662	27.934		.025	16221	.4132	16221
	2.60	.756	.0037	.7523		.70	30	.0679	29.932		−.025	−24993	.0293	−24993
	2.50	1.036	------	--------		.60	29	.0687	28.931		−.075	−7572	.0188	−7572
	2.40	1.349	.0061	1.3429		.50	20	.0680	19.932		−.125	−2775	.0103	−2775
	2.20	2.11	.0093	2.1007		.40	−2	.0659	−2.0659		−.175	−598	.0028	−598.0
	2.00	3.14	.0133	3.1267		.30	−50	.0613	−50.061					
	1.80	4.64	.0192	4.6208		.20	−118	.0547	−118.05	1.138	2.85	0.00208	0	0.00208
	1.60	6.9	.0283	6.8717		.10	−195	.0450	−195.05		2.75	.0418	.0003	.0415
	1.40	10.9	.0426	10.857		0	−235	.0331	−235.03		2.65	.0997	.0005	.0992
	1.20	17.8	.0641	17.736		−.10	−188	.0189	−188.02		2.55	.1716	.0009	.1707
	1.00	30.1	.0798	30.020							2.45	.2560	.0012	.2548
	.90	38	.0866	37.913	.405	2.80	0.351	.0017	0.3493		2.35	.3533	.0017	.3516
	.80	54	.0921	53.908		2.60	.984	.0046	.9794		2.25	.462	.0021	.4599
	.70	76	.0965	75.904		2.40	1.71	.0080	1.702		2.15	.593	.0026	.5904
	.60	108	.1000	107.90		2.20	2.58	.0116	2.568		2.05	.736	.0031	.7329
	.50	150	.1025	149.90		2.00	3.69	.0158	3.674		1.95	.907	.0038	.9032
	.45	168	.1032	167.90		1.80	5.15	.0213	5.129		1.85	1.113	.0045	1.109
	.40	184	.1034	183.90		1.60	7.1	.0283	7.072		1.75	1.355	.0054	1.350
	.35	193	.1032	192.90		1.40	9.7	.0366	9.663		1.65	1.65	.0062	1.644
	.30	184	.1020	183.90		1.20	12.8	.0454	12.755		1.55	2.04	.0078	2.032
	.25	141	.0996	140.90		1.00	16.2	.0533	16.147		1.45	2.56	.0117	2.548
	.20	38	.0959	37.904		.90	16	.0559	15.944		1.35	3.22	.0200	3.200
	.15	−158	.0901	−158.09		.80	16	.0585	15.942		1.25	4.14	.0731	4.067
	.10	−462	.0824	−462.08		.70	15	.0592	14.941		1.15	5.30	.1077	5.192
	.05	−848	.0727	−848.07		.60	10	.0600	9.9400		1.05	7.21	.1200	7.084
	0	−1211	.0614	−1211.06		.50	−1	.0582	−1.0582		.95	9.80	.1483	9.652
	−.05	−1404	.0486	−1404.05		.40	−21	.0563	−21.056		.85	12.7	.1511	12.55
	−.10	−1312	.0350	−1312.04		.30	−54	.0511	−54.051		.75	18.4	.1522	18.25
	−.15	−930	.0208	−930.02		.20	−93	.0457	−93.046		.65	28.0	.1586	27.84
	−.20	−346	.0069	−346.01		.10	−129	.0366	−129.04		.55	48.1	.1657	47.93
						0	−140	.0274	−140.03		.45	83	.1730	82.83
.576	.45	131	.0965	130.90		−.10	−107	.0136	−107.01		.40	114	.1942	113.8
	.40	135	.0963	134.90							.35	155	.2176	154.8
	.35	130	.0954	129.90	.362	.90	9	------	--------		.30	225	.2438	224.8
	.30	106	.0938	105.91		.80	8	------	--------		.25	326	.2664	325.7
	.25	51	.0910	50.909		.70	5	------	--------		.20	516	.2903	515.7
	.20	−53	.0871	−53.087		.60	1	------	--------		.15	871	.3137	870.7
	.15	−217	.0814	−217.08		.50	−13	------	--------		.10	1640	.3496	1640
	.10	−440	.0743	−440.07		.40	−27	------	--------		.05	3801	.4107	3801
	.05	−697	.0655	−697.07		.30	−49	------	--------		−.05	−6630	.0168	−6630
	0	−919	.0553	−919.06		.20	−69	------	--------		−.10	−2114	.0092	−2114
	−.05	−1019	.0437	−1019.04		.10	−83	------	--------		−.15	−526	.0025	−526.0
	−.10	−933	.0315	−933.03		0	−85	------	--------					
	−.15	−644	.0179	−644.02		−.10	−62	------	------	1.179	.375	103	.2118	102.8
	−.20	−236	.0050	−236.01							.325	142	.2361	141.8
					.323	2.80	.355	.0018	.3532		.275	204	.2640	203.7
.550	2.8	.292	------	--------		2.60	.990	.0049	.9851		.225	298	.2879	297.7
	2.7	.555	------	--------		2.40	1.69	.0082	1.682		.175	471	.3144	470.7
	2.6	.835	------	--------		2.20	2.50	.0118	2.488		.125	794	.3508	793.6
	2.5	1.138	------	--------		2.00	3.47	.0158	3.454		.075	1486	.4091	1486
	.90	34.6	.0786	34.521		1.80	4.62	.0206	4.599		−.075	−2185	.0084	−2185
	.80	47.3	.0832	47.217		1.60	5.95	.0262	5.924		−.125	−478	.0023	−478.0
	.70	62.8	.0867	62.713		1.40	7.38	.0322	7.348					
	.60	80.6	.0893	80.511		1.20	8.51	.0381	8.472	1.218	2.80	.00178	0	.00178
	.50	94.2	.0905	94.110		1.00	8.40	.0430	8.357		2.70	.0352	.0002	.0350
	.40	94.0	.0900	93.910		.80	5.12	.0457	5.074		2.60	.0843	.0005	.0838
	.30	46.5	.0867	46.413		.60	−4.40	.0454	−4.445		2.50	.1451	.0008	.1446
	.20	−102	.0797	−102.08		.40	−23.63	.0412	−23.67		2.40	.2173	.0012	.2161
	.10	−394	.0676	−394.07		.20	−48.39	.0323	−48.42		2.30	.2997	.0015	.2982
	0	−697	.0502	−697.05		0	−52.67	.0189	−52.69		2.20	.392	.0019	.3901
	−.10	−670	.0290	−670.03							2.10	.502	.0022	.4998
					.200	2.80	.262	.0016	.2604		2.00	.623	.0027	.6203
.498	2.80	.318	.0015	.3165		2.60	.720	.0045	.7155		1.90	.767	.0034	.7636
	2.60	.900	.0043	.8957		2.40	1.18	.0074	1.173		1.80	.922	.0039	.9181
	2.40	1.58	.0073	1.5727		2.20	1.65	.0104	1.640		1.70	1.139	.0047	1.134
	2.20	2.43	.0108	2.4192		2.00	2.10	.0135	2.087		1.60	1.38	.0054	1.375
	2.00	3.57	.0151	3.5549		1.80	2.48	.0166	2.463		1.50	1.71	.0067	1.703
	1.80	5.16	.0211	5.1389		1.60	2.71	.0197	2.690		1.40	2.14	.0099	2.130
	1.60	7.5	.0294	7.4706		1.40	2.65	.0226	2.627		1.30	2.70	.0465	2.654
	1.40	11.1	.0405	11.060		1.20	2.11	.0250	2.085		1.20	3.48	.0973	3.383
	1.20	16.8	.0536	16.746		1.00	.811	.0264	.785		1.10	4.45	.1293	4.321
	1.00	25.4	.0658	25.334		.80	−1.52	.0265	−1.547		1.00	6.04	.1452	5.895
	.90	30	.0707	29.929		.60	−4.96	.0250	−4.985		.90	8.25	.1632	8.087
	.80	39	.0744	38.926		.40	−8.87	.0216	−8.892		.80	10.8	.1630	10.64
	.70	47	.0771	46.923		.20	−11.35	.0162	−11.37		.70	15.2	.1686	15.03
	.60	51	.0787	50.921		0	−9.255	.0092	−9.264		.60	23.6	.1737	23.43
	.50	51	.0789	50.921							.50	40.5	.1835	40.32
	.40	34	.0772	33.923	1.083	.425	128	.1779	127.8		.40	70	.2051	69.79
	.30	−24	.0732	−24.073		.375	176	.1983	175.8		.35	95	.2296	94.77
	.20	−133	.0660	−133.07		.325	254	.2238	253.8		.30	131	.2556	130.7
	.10	−286	.0552	−286.06		.275	369	.2438	368.8		.25	189	.2843	188.7
	0	−404	.0407	−404.04		.225	579	.2663	578.7		.20	276	.3105	275.7
	−.10	−349	.0236	−349.02		.175	978	.2863	977.7		.15	435	.3486	434.7
						.125	1867	.3073	1867		.10	734	.4056	733.6
											−.10	−443	.0022	−443.0

TABLE II.—ψ°, $\bar{\psi}$, AND ψ AS FUNCTIONS OF W AND θ ($\gamma = 1.405$)—Continued

w	θ	ψ°	$\bar{\psi}$	ψ	w	θ	ψ°	$\bar{\psi}$	ψ	w	θ	ψ°	$\bar{\psi}$	ψ
1.257	0.325	88	0.2469	87.75	1.417	1.95	0.335	0.0017	0.3333	1.575	2.10	0.1052	0.0008	0.1044
	.275	122	.2737	121.7		1.85	.411	.0021	.4089		2.00	.1429	.0010	.1419
	.225	175	.3040	174.7		1.75	.500	.0025	.4975		1.90	.183	.0012	.1818
	.175	256	.3408	255.7		1.65	.608	.0028	.6052		1.80	.231	.0014	.2296
	.125	406	.3977	405.602		1.55	.736	.0033	.7327		1.70	.282	.0017	.2803
						1.45	.890	.0241	.8659		1.60	.339	.0173	.3217
1.292	2.75	0.00156	0	0.00156		1.35	1.10	.0490	1.051		1.50	.411	.0358	.3752
	2.65	.0305	.0002	.0303		1.25	1.38	.0767	1.303		1.40	.494	.0558	.4382
	2.55	.0731	.0005	.0726		1.15	1.73	.1073	1.623		1.30	.593	.0759	.5171
	2.45	.1263	.0008	.1255		1.05	2.23	.1435	2.087		1.20	.729	.0958	.6332
	2.35	.1884	.0011	.1873		.95	2.88	.1631	2.717		1.10	.914	.1153	.7987
	2.25	.2597	.0014	.2583		.85	3.91	.1748	3.735		1.00	1.16	.1393	1.021
	2.15	.339	.0017	.3373		.75	5.35	.1883	5.162		.90	1.52	.1677	1.352
	2.05	.434	.0020	.4320		.65	6.9	.1937	6.706		.80	1.94	.1869	1.753
	1.95	.538	.0025	.5355		.55	10.0	.2104	9.790		.70	2.65	.2055	2.445
	1.85	.659	.0030	.6560		.45	15.6	.2357	15.36		.60	3.65	.2324	3.418
	1.75	.804	.0035	.8005		.35	26.8	.2706	26.53		.50	4.75	.2580	4.492
	1.65	.974	.0042	.9698		.25	48	.3405	47.67		.40	6.91	.3126	6.597
	1.55	1.18	.0048	1.175		.15	------	------	88.69		.30	------	------	10.28
	1.45	1.46	.0058	1.454		.05	------	------	187.6		.20	------	------	18.37
	1.35	1.83	.0341	1.796							.10	------	------	33.62
	1.25	2.31	.0707	2.240	1.470	2.60	.00115	0	.00115		0	------	------	63.08
	1.15	2.97	.1168	2.853		2.50	.0217	.0002	.0215		−.10	------	------	134.80
	1.05	3.80	.1448	3.655		2.40	.0517	.0004	.0513					
	.95	5.17	.1579	5.012		2.30	.0887	.0006	.0881	1.626	2.45	.00087	0	.00087
	.85	7.04	.1710	6.869		2.20	.1313	.0009	.1304		2.35	.0159	.0002	.0157
	.75	9.2	.1749	9.025		2.10	.1795	.0011	.1784		2.25	.0374	.0003	.0371
	.65	13.1	.1795	12.92		2.00	.233	.0014	.2316		2.15	.0634	.0005	.0629
	.55	20.2	.1872	20.01		1.90	.295	.0016	.2934		2.05	.0930	.0007	.0923
	.45	34.8	.2089	34.59		1.80	.361	.0019	.3591		1.95	.1257	.0009	.1248
	.35	60	.2386	59.76		1.70	.439	.0023	.4367		1.85	.161	.0011	.1599
	.30	82	.2653	81.73		1.60	.532	.0026	.5294		1.75	.202	.0013	.2007
	.25	113	.2939	112.7		1.50	.643	.0215	.6215		1.65	.245	.0155	.2295
	.20	163	.3340	162.7		1.40	.780	.0439	.7361		1.55	.295	.0326	.2624
	.15	239	.3886	238.61		1.30	.955	.0679	.8871		1.45	.355	.0509	.3041
	.10	------	------	378.66		1.20	1.20	.0933	1.107		1.35	.427	.0695	.3575
						1.10	1.51	.1206	1.389		1.25	.510	.0877	.4223
1.325	.275	77	.2840	76.716		1.00	1.96	.1518	1.808		1.15	.627	.1049	.5221
	.225	106	.3217	105.678		.90	2.52	.1727	2.347		1.05	.790	.1253	.6647
	.175	153	.3781	152.622		.80	3.42	.1831	3.237		.95	1.005	.1473	.8577
	.125	------	------	223.871		.70	4.70	.1978	4.502		.85	1.31	.1751	1.135
	.075	------	------	354.791		.60	6.2	.2122	5.988		.75	1.68	.2000	1.480
						.50	8.9	.2354	8.665		.65	2.30	.2233	2.077
1.357	2.70	.00140	0	.00140		.40	13.7	.2666	13.43		.55	3.17	.2543	2.916
	2.60	.0270	.0002	.0268		.30	23.8	.3325	23.52		.45	4.19	.3039	3.886
	2.50	.0648	.0004	.0644		.20	------	------	42.65		.35	-- -- --	------	5.6663
	2.40	.1116	.0007	.1109		.10	------	------	79.44		.25	-- -- --	-- -- --	8.9579
	2.30	.1663	.0010	.1653		0	------	------	168.5		.15	-- -- --	-- -- --	16.12
	2.20	.2286	.0013	.2273							.05	------	------	29.74
	2.10	.298	.0016	.2964	1.523	2.55	.00105	0	.00105		−.05	-- -- --	------	55.91
	2.00	.381	.0019	.3791		2.45	.0197	.0002	.0195		−.15	------	------	120.0
	1.90	.470	.0022	.4678		2.35	.0467	.0004	.0463					
	1.80	.574	.0027	.5713		2.25	.0799	.0006	.0793	1.673	2.40	.00079	0	.00079
	1.70	.698	.0031	.6949		2.15	.1179	.0008	.1171		2.30	.0144	.0001	.0143
	1.60	.845	.0037	.8413		2.05	.1606	.0011	.1595		2.20	.0338	.0003	.0335
	1.50	1.03	.0042	1.026		1.95	.208	.0013	.2067		2.10	.0571	.0005	.0566
	1.40	1.26	.0278	1.232		1.85	.261	.0015	.2595		2.00	.0833	.0007	.0826
	1.30	1.59	.0570	1.533		1.75	.321	.0018	.3192		1.90	.1121	.0008	.1113
	1.20	2.00	.0911	1.909		1.65	.387	.0022	.3848		1.80	.143	.0010	.1420
	1.10	2.57	.1321	2.438		1.55	.469	.0192	.4498		1.70	.178	.0140	.1640
	1.00	3.30	.1562	3.144		1.45	.566	.0397	.5263		1.60	.216	.0298	.1862
	.90	4.48	.1656	4.314		1.35	.684	.0615	.6225		1.50	.259	.0468	.2122
	.80	6.13	.1810	5.949		1.25	.837	.0836	.7534		1.40	.311	.0639	.2471
	.70	8.0	.1841	7.816		1.15	1.05	.1063	.9437		1.30	.372	.0811	.2909
	.60	11.5	.1910	11.31		1.05	1.32	.1298	1.1902		1.20	.444	.0971	.3469
	.50	17.7	.2095	17.49		.95	1.73	.1610	1.569		1.10	.546	.1153	.4257
	.40	30.6	.2385	30.36		.85	2.22	.1799	2.040		1.00	.694	.1342	.5598
	.30	54	.2748	53.73		.75	3.02	.1916	2.828		.90	.876	.1564	.7196
	.25	73	.3120	72.69		.65	4.17	.2137	3.956		.80	1.15	.1888	.9612
	.20	101	.3654	100.63		.55	5.5	.2342	5.266		.70	1.47	.2175	1.253
	.10	------	------	210.9		.45	7.8	.2629	7.537		.60	2.02	.2449	1.775
						.35	12.1	.3226	11.78		.50	2.78	.2974	2.483
1.387	.225	68	.3530	67.65		.25	------	------	20.85		.40	------	------	3.3248
						.15	------	------	38.01		.30	------	------	4.8779
1.417	2.65	.00126	0	.00126		.05	------	------	71.01		.20	-- --	------	7.7469
	2.55	.0242	.0002	.0240		−.05	------	------	151.2		.10	------	------	14.15
	2.45	.0577	.0004	.0573							0	------	------	26.16
	2.35	.0992	.0007	.0985	1.575	2.50	.00096	0	.00096		−.10	------	------	49.48
	2.25	.1474	.0009	.1465		2.40	.0718	.0002	.0176		−.20	-- -- --	------	107.2
	2.15	.2020	.0012	.2008		2.30	.0420	.0003	.0417					
	2.05	.263	.0015	.2615		2.20	.0715	.0005	.0710					

TABLE II.—ψ°, $\overline{\psi}$, AND ψ AS FUNCTIONS OF W AND θ ($\gamma = 1.405$) Concluded

W	θ	ψ°	$\overline{\psi}$	ψ	W	θ	ψ°	$\overline{\psi}$	ψ	W	θ	ψ°	$\overline{\psi}$	ψ
1.717	2.35	0.00072	0	0.00072	1.800	2.25	0.00059	0	0.00059	1.878	2.15	0.00049	0	0.00049
	2.25	.0130	0.0001	.0129		2.15	.0105	0.0001	.0104		2.05	.0084	0.0001	.0083
	2.15	.0304	.0003	.0301		2.05	.0243	.0002	.0241		1.95	.0191	.0084	.0107
	2.05	.0511	.0004	.0507		1.95	.0404	.0004	.0400		1.85	.0315	.0187	.0128
	1.95	.0742	.0006	.0736		1.85	.0581	.0103	.0478		1.75	.0447	.0304	.0143
	1.85	.0994	.0008	.0986		1.75	.0770	.0226	.0544		1.65	.0587	.0426	.0161
	1.75	.126	.0127	.1133		1.65	.0996	.0361	.0635		1.55	.0725	.0552	.0173
	1.65	.157	.0272	.1298		1.55	.119	.0502	.0688		1.45	.0884	.0674	.0210
	1.55	.189	.0430	.1460		1.45	.142	.0643	.0777		1.35	.104	.0813	.0227
	1.45	.226	.0592	.1668		1.35	.168	.0779	.0901		1.25	.122	.0953	.0267
	1.35	.270	.0751	.1949		1.25	.199	.0931	.1059		1.15	.144	.1104	.0336
	1.25	.323	.0903	.2327		1.15	.238	.1084	.1296		1.05	.171	.1299	.0411
	1.15	.384	.1074	.2766		1.05	.282	.1250	.1570		.95	.202	.1532	.0488
	1.05	.473	.1245	.3485		.95	.348	.1467	.2013		.85	.249	.1805	.0685
	.95	.600	.1438	.4562		.85	.443	.1735	.2695		.75	.318	.2237	.0943
	.85	.760	.1707	.5893		.75	.556	.2059	.3501		.65	-------	-----	.1174
	.75	.904	.2059	.7881		.65	.736	.2592	.4768		.55	- - - -	- - - -	.1702
	.65	1.28	.2379	1.042		.55	- - -		.6209		.45	- - -	- - -	.2136
	.55	1.75	.2854	1.465		.45	- - -		.9076		.35	-------	- - -	.3493
	.45	- - - -	- - - - - -	2.0744		.35	- - -		1.3081		.25	- - -	- - -	.4932
	.35	- - -	- - - - -	2.8021		.25	- - -		1.7694		.15	- - -	- - - -	.5858
	.25	- - -	- - - -	4.1174		.15	- - -		2.6045		.05	- - -	- - - -	1.0426
	.15	- - -	- - -	6.6546		.05	- - -		4.3034		−.05	- - -	- - -	1.8651
	.05	- - -	- - -	12.20		−.05	- - -		8.4826		−.15	- - -	- - -	3.9603
	−.05	- - -	- - -	22.81		−.15	- - -		16.3557		−.25	- - -	- - -	7.3834
	−.15	- - -	- - -	43.66		−.25	- - -		31.55		−.35	- - -	- - -	14.16
	−.25	- - -	- - -	95.08		−.35	- - -		69.42		−.45	- - -	- - -	31.60
1.758	2.30	.00065	0	.00065	1.839	2.20	.00054	0	.00054	1.914	2.10	.00044		0
	2.20	.0117	.0001	.0116		2.10	.0094	.0001	.0093		2.00	.0075		
	2.10	.0271	.0002	.0269		2.00	.0216	.0002	.0214		1.90	.0171		
	2.00	.0454	.0004	.0450		1.90	.0358	.0093	.0265		1.80	.0279		
	1.90	.0655	.0006	.0649		1.80	.0512	.0206	.0306		1.70	.0394		
	1.80	.0874	.0115	.0759		1.70	.0675	.0332	.0343		1.60	.0513		
	1.70	.110	.0249	.0851		1.60	.0843	.0463	.0380		1.50	.0629		
	1.60	.137	.0396	.0974		1.50	.103	.0597	.0433		1.40	.0762		
	1.50	.164	.0547	.1093		1.40	.123	.0726	.0504		1.30	.0896		
	1.40	.195	.0699	.1251		1.30	.144	.0872	.0568		1.20	.104		
	1.30	.232	.0842	.1478		1.20	.171	.1018	.0692		1.10	.123		
	1.20	.277	.1004	.1766		1.10	.203	.1177	.0853		1.00	.145		
	1.10	.330	.1166	.2134		1.00	.241	.1382	.1028		.90	.171		
	1.00	.405	.1342	.2708		.90	.296	.1629	.1331		.80	.211		
	.90	.516	.1581	.3579		.80	.376	.1924	.1836		.70	- - -	- - - -	
	.80	.651	.1881	.4629		.70	.477	.2398	.2372		.60	- - -	- - -	
	.70	.854	.2258	.6282		.60	- - -	- - -	.3205		.50	- - -	- - -	
	.60	1.11	.2759	.8341		.50	- - -	- - -	.4278		.40	- - -	- - -	
	.50	- - -	- - -	1.1810		.40	- - -	- - -	.6274		.30	- - -	- - -	
	.40	- - -	- - -	1.7031		.30	- - -	- - -	.9380		.20	- - -	- - -	
	.30	- - -	- - -	2.2833		.20	- - -	- - -	1.2925		.10	- - -	- - -	
	.20	- - -	- - -	3.4059		.10	- - -	- - -	1.7954		0	- - -	- - -	
	.10	- - -	- - -	5.5062		0	- - -	- - -	3.2210		−.10	- - -	- - - -	
	0	- - -	- - -	10.31		−.10	- - -	- - -	6.4949		−.20	- - -	- - -	
	−.10	- - -	- - -	19.75		−.20	- - -	- - -	12.6403		−.30	- - -	- - -	
	−.20	- - -	- - -	37.94		−.30	- - -	- - -	24.01		−.40	- - -	- - -	
	−.30	- - -	- - -	83.19		−.40	- - -	- - -	54.33		−.50	- - -	- - -	

U.S. GOVERNMENT PRINTING OFFICE: 1960